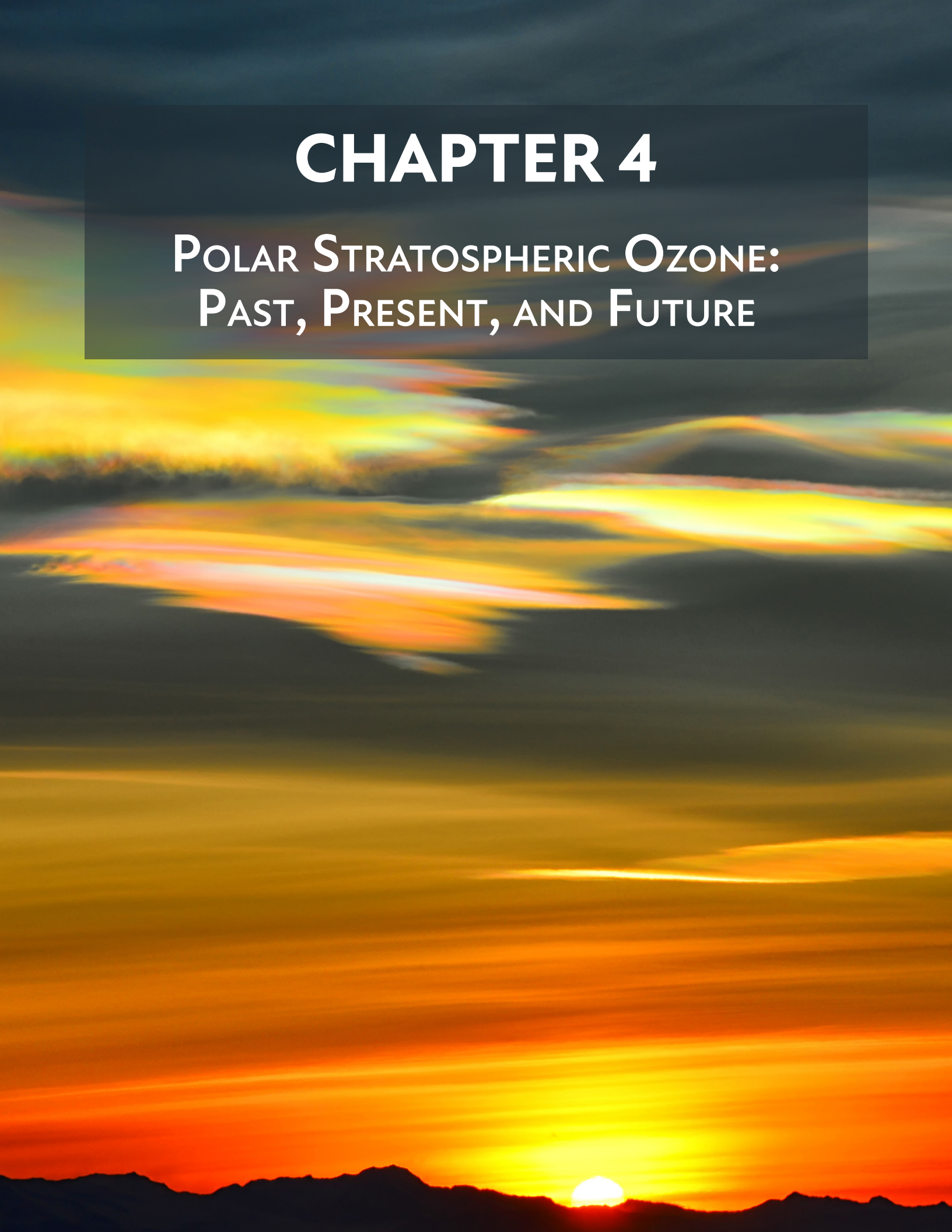

# CHAPTER 4

## Polar Stratospheric Ozone: Past, Present, and Future

*About the cover image:*
*Polar Stratospheric Clouds (PCSs) form in the winter stratosphere at very low temperatures and can become visible with the arrival of sunlight in late winter. Chemical reactions on the surfaces of PSCs release halogen compounds which cause stratospheric ozone depletion in polar regions.*

*Photo credit: Ryan Skorecki, NSF via U.S. Antarctic Program Photo Library*

# CHAPTER 4

## Polar Stratospheric Ozone: Past, Present, and Future


**Lead Authors :** Martyn P. Chipperfield
Michelle L. Santee

**Coauthors :** Simon P. Alexander
A. T. J. de Laat
Doug E. Kinnison
Jayanarayanan Kuttippurath
Ulrike Langematz
Krzysztof Wargan

**Contributing Authors :** Sandip S. Dhomse
Jens-Uwe Grooß
James Keeble
Zachary D. Lawrence
Gloria L. Manney
Rolf Müller
Eric Nash
Paul A. Newman
David A. Plummer
Sarah Safieddine
Ines Tritscher
Peter von der Gathen
Mark Weber
Ingo Wohltmann

**Review Editors :** Susan Solomon
Mark Weber

# CONTENTS

## Chapter 4: Polar Stratospheric Ozone: Past, Present, and Future


SCIENTIFIC SUMMARY 221

4.1 INTRODUCTION 223

4.1.1 Summary of Findings from the Previous Ozone Assessment 223
4.1.2 Scope of Chapter 223

4.2 RECENT POLAR OZONE CHANGES 224

4.2.1 Measurements of Ozone and Related Constituents 224
4.2.2 Evolution of Polar Temperatures and Vortex Characteristics 224
*4.2.2.1 Usage of Reanalyses in Polar Process Studies* 224
*4.2.2.2 Temperatures and PSC Volume* 225
*4.2.2.3 Polar Vortex Breakup Dates* 226
4.2.3 Ozone Depletion in Antarctic Springs (2018–2021) 227
*4.2.3.1 Antarctic Spring 2018: Moderately Large Ozone Hole* 229
*4.2.3.2 Antarctic Spring 2019: Impact of the Strong Minor Sudden Stratospheric Warming* 229
*4.2.3.3 Antarctic Springs 2020 and 2021: Exceptionally Persistent Ozone Holes* 232
4.2.4 Ozone Depletion in Arctic Springs (2018–2021) 233
*4.2.4.1 Arctic Springs 2018, 2019, and 2021: Impacts of Disturbed Polar Vortices* 233
*4.2.4.2 Arctic Spring 2020: Record-Low Arctic Stratospheric Ozone* 234
Box 4-1 What is a 'Polar Vortex' and Why Does it Matter? 236

4.3 UNDERSTANDING OF POLAR OZONE PROCESSES 238

4.3.1 Polar Stratospheric Clouds: Observations and Modeling of PSC Occurence, Extent, and Composition 239
4.3.2 Polar Chemistry: Observations and Modeling 240
*4.3.2.1 Observations* 240
*4.3.2.2 Theoretical Basis and Modeling* 240
4.3.3 Very Short-Lived Halogenated Substances 241
4.3.4 Dynamical Impacts on Polar Ozone 241
*4.3.4.1 Synthesis of the Role of Dynamics in the Last Four Arctic and Antarctic Springs* 241
*4.3.4.2 Predictability of Arctic Spring Ozone* 242
*4.3.4.3 Arctic Winter Variability Under Climate Change* 243
4.3.5 Other Factors Affecting Polar Ozone 244
*4.3.5.1 Solar Variability* 244
*4.3.5.2 Volcanic Eruptions* 245
*4.3.5.3 Wildfire Emissions* 246
*4.3.5.4 Supersonic and Hypersonic Aircraft Emissions* 246
*4.3.5.5 Rocket Emissions* 247

## 4.4 RECOVERY OF POLAR OZONE 247

4.4.1 Polar Ozone Recovery in Previous Assessments 247
4.4.2 Long-Term Antarctic Ozone Trend and Onset of Antarctic Ozone Recovery 248
*4.4.2.1 New Research into Antarctic Ozone Recovery* 248
*4.4.2.2 Recent Antarctic Winters in the Context of Stratospheric Ozone Recovery* 251
4.4.3 Long-Term Arctic Ozone Trend 251
4.4.4 Benefits Achieved by the Montreal Protocol and Its Amendments and Adjustments 251

## 4.5 FUTURE CHANGES IN POLAR OZONE 252

4.5.1 New Ozone Projections from Chemistry-Climate Models 253
4.5.2 Projections of Polar Ozone: Long and Near Term 254
*4.5.2.1 Future Antarctic Spring Total Column Ozone* 254
*4.5.2.2 Future Arctic Spring Total Column Ozone* 255
4.5.3 Factors Controlling Future Polar Ozone 255
*4.5.3.1 Changing Role of ODSs and GHGs* 255
*4.5.3.2 Impact of Noncompliant CFC-11 Production* 256
*4.5.3.3 Dynamical Variability in Arctic Spring* 256
*4.5.3.4 The Role of GHG Scenarios* 257
*4.5.3.5 The Role of VSLS (Bromine and Chlorine)* 259
4.5.4 Uncertainty in Polar Ozone Projections 260
*4.5.4.1 Model Uncertainty* 260
*4.5.4.2 Uncertainty in Ozone Return Dates* 260

## REFERENCES 262

# SCIENTIFIC SUMMARY

*The chemical and dynamical processes controlling polar ozone are well understood. Polar ozone depletion is fundamentally driven by anthropogenic chlorine and bromine, with the severity of the chemical loss each year in both polar regions strongly modulated by meteorological conditions (temperatures and winds) and, to a lesser extent, by the stratospheric aerosol loading and the solar cycle. As noted in previous Assessments, the stratospheric halogen concentration resulting from the emissions of ozone-depleting substances (ODSs) reached its peak in the polar regions around the turn of the century and has been gradually declining since then in response to actions taken under the Montreal Protocol and its Amendments and adjustments. The 2018 Assessment reported for the first time that signs of the onset of ozone recovery from the effects of ODSs had been detected over the Antarctic. More varied and more robust signs of the onset of recovery are now beginning to emerge; as the observational record lengthens, ozone hole recovery trends are expected to continue to become clearer against the background of natural variability. Nevertheless, the Antarctic ozone hole will continue to be a recurring phenomenon until the middle of the century, although with a decreasing average size and some interannual variability. The Arctic is more dynamically variable, precluding identification of a significant increase in Arctic ozone. Cold conditions conducive to substantial stratospheric ozone loss occur in some Arctic winter/spring seasons and are expected to continue to do so, interspersed with warmer years with little or no ozone depletion. Chemistry-climate model (CCM) projections largely confirm previous studies that, in both hemispheres, springtime polar total column ozone (TCO) will return to 1980 historical levels around the middle of this century. For the Antarctic, the timing of this return depends mainly on the declining stratospheric halogen concentrations from decreasing ODS emissions, and the impact of climate change is small. In the Arctic, TCO is expected to return to 1980 levels earlier than in the Antarctic. This is because in the Arctic, springtime stratospheric ozone has a stronger dependence on the future greenhouse gas (GHG) emissions scenarios.*

## Observed changes in polar ozone

- **The Antarctic ozone hole continued to appear each spring during the 2018–2021 period.** The occurrence and character of recent ozone holes are consistent with the current concentrations of ODSs and their small overall downward trend.
- **Recent Antarctic ozone holes exhibited substantial interannual variability in size, strength, and longevity: the 2019 ozone hole was the smallest since 2002, whereas 2020 saw a deep ozone hole of record duration.** In 2019, a strong minor sudden stratospheric warming disrupted the evolution of the ozone hole, leading to the early termination of chemical ozone depletion and relatively high TCO. In contrast, in 2020 and 2021, weak atmospheric wave activity resulted in exceptionally persistent polar vortices. Despite decreasing ODS concentrations, the unusual dynamical state of the stratosphere in 2020 and 2021 induced large and long-lasting late spring ozone holes.
- **Recovery of Antarctic stratospheric ozone continues to progress.** New results since the 2018 Assessment support the findings reported at that time that the Antarctic ozone hole has diminished in size and depth since the year 2000. The remarkable Antarctic ozone holes in 2019, 2020, and 2021 do not challenge the findings of the emergence of recovery.
- **Arctic total ozone reached exceptionally low values in spring 2020.** A very stable, cold, and long-lived stratospheric polar vortex enabled halogen-catalyzed chemical ozone loss exceeding that observed during the previous record-breaking spring of 2011. The strong vortex also inhibited dynamical replenishment of ozone. The evolution of high-latitude ozone in 2020 is successfully reproduced by model simulations, further substantiating our understanding of polar ozone chemistry.
- **No statistically significant signature of recovery in Arctic stratospheric ozone over the 2000–2021 period has yet been detected.** Observed Arctic ozone trends remain small compared to the year-to-year dynamical variability.

## Understanding of factors controlling polar ozone

- **An updated vortex-wide climatology of polar stratospheric cloud (PSC) occurrence and composition based on satellite data enabled advances in the understanding of particle formation mechanisms and trends.** Evidence that heterogeneous nucleation on preexisting ice particles or foreign nuclei, such as meteoritic particles, is the typical formation process for the nitric acid trihydrate (NAT) particles that lead to denitrification has been strengthened. PSC occurrence in the Arctic early winter significantly increased between the 1980s (1978–1989) and the recent past (2006–2018), while in the Antarctic, PSC occurrence was very similar in the two periods.
- **The broad range of polar springtime TCO in recent years in both hemispheres is largely explained by differences in the magnitude of the dynamical forcing.** Both the weak Antarctic ozone hole in 2019 and the record-low Arctic ozone in spring 2020 resulted from atypical dynamical conditions in the respective winters. Although exceptional, the evolution of polar ozone in both years was in line with current understanding of the chemical and dynamical factors controlling its abundance.
- **September, and especially the first half of that month, is the period when the impact of ODSs on stratospheric ozone over Antarctica can be quantified with the greatest certainty, and thus it represents the most suitable time window for monitoring ozone recovery.** Until recently, most studies of Antarctic ozone depletion trends focused on longer time windows or later ones that included

the months of October and November. New analyses indicate that September ozone has the largest sensitivity to decreasing ODSs, and September observations show the strongest and the statistically most significant Antarctic ozone recovery rates.

- **Model simulations with historical emissions scenarios indicate that decreasing atmospheric amounts of ODSs can explain the observed increase in Antarctic springtime ozone over the last two decades.** Model simulations indicate that if ODS concentrations had remained at the peak values attained in the late 1990s, recent polar springtime ozone loss in both hemispheres would have been ~20 DU (~10%) larger than currently observed. Model simulations of unabated ODS emissions (i.e., allowing for a 3–3.5% $yr^{-1}$ increase in emissions since the mid-1980s) indicate that conditions similar to those currently observed over Antarctica would have occurred in the Arctic in years with unusually stable and long-lived stratospheric vortices, such as 2011 and 2020.
- **Future commercial supersonic or hypersonic aircraft fleets would cause stratospheric ozone depletion.** Both types of aircraft would potentially release substantial amounts of water vapor and nitrogen oxides ($NO_x$) into the stratosphere, with concomitant strong effects on stratospheric ozone arising primarily through enhancement of $NO_x$ catalytic ozone destruction at cruise altitudes. This could reduce total column ozone by as much as 10%, depending on aircraft type and injection altitude, and would be most pronounced in the Northern Hemisphere polar region in spring and fall.

## Future evolution of polar ozone

- **The Antarctic ozone hole is expected to gradually close. September multi-model mean (MMM) TCO from updated CCM projections, based on full compliance with the Montreal Protocol and assuming the baseline estimate of the future evolution of GHGs (SSP2-4.5), returns to 1980 values shortly after mid-century (about 2066, with a range between 2049 and 2077 arising from the spread in modeled dynamical variability).** The October TCO MMM returns two years earlier, with a similar uncertainty range.
- **The timing of the recovery of the ozone hole may be affected by anthropogenic climate change, with the MMM from updated CCM projections recovering approximately 15 years earlier for both SSP3-7.0 and SSP5-8.5 GHG scenarios.** This sensitivity of Antarctic return date to different climate change scenarios was not evident in projections presented in previous Assessments. The small set of CMIP6 models included in this Assessment makes interpretation of this scenario sensitivity difficult.
- **Arctic springtime total ozone is expected to return to 1980 values near mid-century (about 2045, with a range between 2029 and 2051), based on full compliance with the Montreal Protocol and assuming the baseline estimate of the future evolution of GHGs (SSP2-4.5).** This return date is around a decade later than projected by simulations in the previous Assessment using a different set of models and scenarios, but with considerable overlap of the large range. The timing of the recovery of Arctic TCO in spring will be affected by anthropogenic climate change. Consistent with previous Assessments, the new model simulations confirm that in the Arctic, dynamical changes induced by enhanced GHG concentrations cause an earlier return of TCO to historical values than do reductions in ODSs alone.
- **Future ozone depletion will be substantial in the Arctic during cold winters/springs as long as ODS concentrations are well above natural levels.** The projected strong increase in GHGs will cause cooling in the stratosphere. This effect, coupled with increases in stratospheric humidity from GHG warming of the tropical tropopause and increases in future tropospheric $CH_4$ emissions, will increase the potential for formation of PSCs in Arctic winter, leading to ozone loss.
- **Noncompliant production (e.g., of CFC-11) could delay the recovery of ozone to 1980 values by several years by slowing the rate of decline of stratospheric chlorine.** The magnitude of the delay depends on the total additional emissions. Additional emissions of 120–440 Gg of CFC-11 over the period 2012–2019 are estimated to delay the return to 1980 levels for Antarctic column ozone by 0.5–3.1 years. Emissions of uncontrolled very short-lived substances (VSLSs; e.g., chloroform [$CHCl_3$], dichloromethane [$CH_2Cl_2$]) could also extend the timeframe for polar ozone recovery by the same mechanism, with the impact dependent on the amount of chlorine delivered to the stratosphere. The future magnitudes of emissions from noncompliant production and anthropogenic VSLSs are highly uncertain.

## 4.1 INTRODUCTION

This chapter presents and assesses our knowledge of the past, present, and future of stratospheric ozone in Earth's polar regions (poleward of 60° latitude) based on the latest results from the peer-reviewed literature. It builds on the long series of similar chapters in previous Assessments. Substantial scientific effort has been dedicated to observing and understanding polar ozone changes, especially in the nearly 40 years since the discovery of the Antarctic ozone hole. Polar ozone remains an issue of great interest to policymakers and the general public alike. The focus of this chapter is to provide a concise update of new observations and understanding, including new results from numerical modeling, since Langematz, Tully et al. (2018), without repeating general background information that can be found in previous Assessments.

### 4.1.1 Summary of Findings from the Previous Ozone Assessment

Equivalent effective stratospheric chlorine (EESC; see *Chapter 1*) peaked around the year 2000 in the polar regions and has been slowly declining since then. At current EESC levels, interannual variability in the size and depth of the Antarctic springtime ozone hole is predominantly driven by meteorological conditions. Langematz, Tully et al. (2018) reported that the characteristics of recent ozone holes had continued to generally fall within the range observed since the early 1990s. However, a warm and unusually disturbed stratospheric polar vortex led to a weak ozone hole in 2017, whereas a cold and undisturbed vortex facilitated a strong and long-lasting hole in 2015. Aerosols from the Calbuco volcanic eruption in April of 2015 may have also contributed to the strong ozone depletion. Despite the severe hole in 2015, by the time of the 2018 Assessment, several lines of evidence had begun to emerge that indicated an increase in observed stratospheric ozone in the Antarctic during September, along with a decrease in the annual maximum ozone hole size and depth. Although the large degree of natural variability makes attribution of these changes challenging, the weight of evidence from statistical analyses and other observational and modeling studies suggested that the decline in EESC in response to controls on ozone-depleting substances (ODSs) under the Montreal Protocol and its Amendments and adjustments played a substantial role in those trends. In the Arctic, large year-to-year dynamical variations precluded robust detection of any recovery trend over the 2000–2016 period. Extreme meteorological conditions early in the 2015/16 winter induced rapid Arctic ozone loss, but a sudden stratospheric warming (SSW) at the beginning of March 2016 curtailed further chemical processing and kept ozone abundances from reaching values as low as those observed in spring 2011. Model simulations demonstrated that in both hemispheres, substantial benefit had already accrued from the controls imposed on ODS production. In the absence of the Montreal Protocol, a deep hole in the ozone layer would have developed during the exceptionally cold 2011 Arctic winter, smaller Arctic ozone holes would have occurred regularly, and the Antarctic ozone hole would have expanded considerably.

Knowledge of the processes controlling polar ozone continued to be refined in the 2018 Assessment (Langematz, Tully et al., 2018). Despite the fact that some detailed aspects of polar stratospheric cloud formation, the heterogeneous reactions that take place on their surfaces, and the cycles of catalytic ozone loss they enable remained unresolved, chemical transport models (CTMs) were generally able to successfully reproduce observed conditions, in particular the amount of ozone loss. Very short-lived substances (VSLSs) were found to make an important contribution to stratospheric halogen loading (e.g., around 25% of total bromine) and thus polar ozone destruction. Understanding of the dynamical control of polar ozone, especially the role of variability in planetary wave driving and the factors giving rise to that variability, had advanced since the 2014 Assessment. The impact of SSWs on Arctic ozone loss was specifically highlighted. The influence of energetic particle precipitation (EPP) related to solar variability, which can lead to substantial (10–15%) ozone loss in the middle and upper stratosphere, was also discussed. Although the resulting variation in total column ozone (TCO) is typically only a few percent, effects can persist for two to three years. Such EPP effects on ozone are not fully accounted for in most current chemistry-climate models (CCMs).

The 2018 Assessment (Langematz, Tully et al., 2018) made use of a new set of CCM simulations to provide updated estimates of the future evolution of polar ozone. These simulations confirmed previous findings on the expected behavior of ozone in both polar regions, with updates in the details of the timing of ozone recovery due to revised ODS scenarios. As in past Assessments, the return of polar ozone to 1980 levels was used as the principal metric for recovery. For the Antarctic, this was projected to occur around 2060. There was little influence from different climate scenarios because of the dominant signal of chemical depletion linked to stratospheric levels of chlorine and bromine and therefore ODSs. In contrast, Arctic springtime ozone showed a much earlier return to 1980 levels (2030s) due to dynamical influences, with a much larger dependence on assumed future climate change due to increasing greenhouse gases (GHGs).

Despite the detection of the onset of recovery in the Antarctic, and the CCM projections of a return to 1980 polar ozone levels by 2030–2060, Langematz, Tully et al. (2018) repeated the point made in earlier Assessments that under meteorological conditions conducive to chemical processing, the potential for large seasonal polar ozone depletion remained high in the near future in both hemispheres. The 2018 Assessment also noted that in the latter half of this century, the evolution of Arctic ozone will become increasingly dominated by GHGs through their climate and, in the case of methane ($CH_4$) and nitrous oxide ($N_2O$), chemical impacts.

### 4.1.2 Scope of Chapter

This chapter provides a concise update of the state of our knowledge of ozone in the polar regions of both hemispheres. The long-term record of meteorological conditions and ozone depletion in the polar vortices of both hemispheres is presented and updated for the years following the 2018 Assessment. The exceptional winter/spring seasons of 2019, 2020, and 2021 in the Antarctic and 2019/20 in the Arctic, characterized by anomalous dynamical states in the atmosphere, are considered in more detail. Progress in the understanding of the many chemical and physical processes underlying and influencing polar ozone depletion is then briefly summarized. Recent studies seeking to identify a statistically significant trend due to declining anthropogenic halogen levels (known as the second stage of Antarctic

ozone recovery, as set out in WMO, 2007) are discussed. Finally, the chapter presents a summary of the latest CCM projections of polar ozone over the 21st century from a combination of simulations performed under the auspices of different programs, including the WCRP Coupled Modelled Intercomparison Project 6 (CMIP6) and the SPARC/IGAC Chemistry-Climate Model Initiative (CCMI).

## 4.2 RECENT POLAR OZONE CHANGES

### 4.2.1 Measurements of Ozone and Related Constituents

Scientific study of polar ozone relies on the long-term record of measurements of ozone and related constituents from ground-based, balloon-borne, airborne, and satellite instruments, in conjunction with meteorological reanalyses. These measurement programs have largely been maintained since the previous Assessment.

Long-standing ground-based and balloon measurements of both total column and vertically resolved ozone have continued under the WMO Global Atmosphere Watch and its contributing network, NDACC (Network for the Detection of Atmospheric Composition Change). Observational data from these networks are freely available from the NDACC database (http://ndacc-demo.org) and the World Ozone and Ultraviolet Radiation Data Centre (www.woudc.org). (See also **Table 3A-2** for a list of ground-based ozone total column and profile measurements considered in *Chapter 3*.)

A summary of available satellite measurements of ozone and related constituents in polar regions was provided in Table 3A-1 of Dameris, Godin-Beekmann et al. (2014), with only a few changes in availability since then. However, as noted in more detail in *Section 3.1.3*, it is expected that a number of currently operational spaceborne instruments whose measurements have been central to the Assessment process will have ceased collecting data by the time of the 2026 Assessment. In particular, the loss of vertically resolved satellite measurements of many trace gases relevant for polar chemistry and dynamics, including ozone itself during polar night, will hinder the ability to monitor and explain changes in polar stratospheric ozone in the future.

### 4.2.2 Evolution of Polar Temperatures and Vortex Characteristics

#### *4.2.2.1 Use of Reanalyses in Polar Process Studies*

Lower-stratospheric polar processes (i.e., polar stratospheric cloud [PSC] formation, denitrification and dehydration, heterogeneous chlorine activation and deactivation) and chemical ozone loss are "threshold" phenomena that depend critically on meteorological conditions. Therefore, polar processing studies often rely heavily on global meteorological datasets, generally using reanalysis datasets as input or as a constraint. Atmospheric reanalysis systems provide gridded datasets representing the best estimates of the past state of the atmosphere (e.g., temperature, wind, humidity, and other meteorological parameters) that are generated by combining information from global forecast models with observations. It is thus essential to understand the accuracy and reliability of reanalysis data for polar processing studies. The WCRP SPARC Reanalysis Intercomparison Project (S-RIP) recently coordinated a comprehensive intercomparison of a broad set of representative diagnostics in major global atmospheric reanalysis datasets (e.g., Fujiwara et al., 2017; SPARC, 2022). One focus of S-RIP was to evaluate diagnostics relevant to polar chemical processing and dynamics, primarily targeting winter conditions in the lower stratosphere, to examine five modern reanalyses: MERRA, MERRA-2, ERA-Interim, JRA-55, and CFSR/CFSv2 (see Fujiwara et al., 2017, for a detailed overview of these reanalysis systems, including key references). The main findings from that evaluation are summarized here. (See also Figure 10.26 of SPARC (2022) for a table encapsulating the overall performance of each reanalysis for many of the polar processing diagnostics considered.)

Any of the recent full-input reanalyses (i.e., systems that assimilate surface and upper-air conventional and satellite data) can be used with confidence in studies of lower-stratospheric polar processing. Temperature biases and other artifacts in older meteorological reanalyses often rendered them unsuitable for investigations of polar stratospheric chemical processing and dynamics; in particular, ERA-40, NCEP-NCAR R1, and NCEP-DOE R2 (e.g., Fujiwara et al., 2017, and references therein) are obsolete and should no longer be used in such studies. However, polar winter temperatures from modern reanalyses agree much more closely with one another than did those from older systems, with a marked convergence to better agreement, especially in the Southern Hemisphere, after 1999, when reanalysis systems switched from assimilating TOVS to ATOVS radiances. Reanalyses generally match well in the Antarctic for many polar temperature and vortex diagnostics. With their extremely cold conditions and relatively small interannual variability, Antarctic winters tend to have similar chemical processing potential and duration every year, keeping sensitivity to differences in meteorological conditions between the reanalyses low. Average absolute differences from the reanalysis ensemble mean in wintertime daily minimum temperatures poleward of 40°S are usually less than 0.5 K in the post-1999 period. Similarly, in recent years, average absolute differences in the area of the Southern Hemisphere with temperatures below PSC thresholds ($A_{PSC}$) are within ±0.5% of the area of the hemisphere, or ~5% of the typical Antarctic $A_{PSC}$ of 10% of the hemisphere, and average relative differences from the reanalysis ensemble mean in the fraction of the vortex volume with temperatures below PSC thresholds are ~10% of typical values (Lawrence et al., 2018). In contrast, wintertime meteorological conditions in the Arctic are frequently marginal for PSC formation, and interannual variability is large, increasing the sensitivity of polar temperature and vortex diagnostics to reanalysis differences. Average relative differences from the reanalysis ensemble mean in the area and volume of the Northern Hemisphere with temperatures below PSC thresholds are ~10% and ~15% of typical values, respectively (Lawrence et al., 2018).

To explore how the spatially and temporally varying differences between reanalyses interact to affect the bottom-line conclusions of typical polar processing studies, SPARC (2022) examined simulations from a single CTM driven by different reanalyses. Although the individual model realizations show largely similar behavior through most of the season in both polar regions for most species, substantial disparities between model runs using different reanalyses develop where composition gradients are largest. For example, comparisons with satellite long-lived

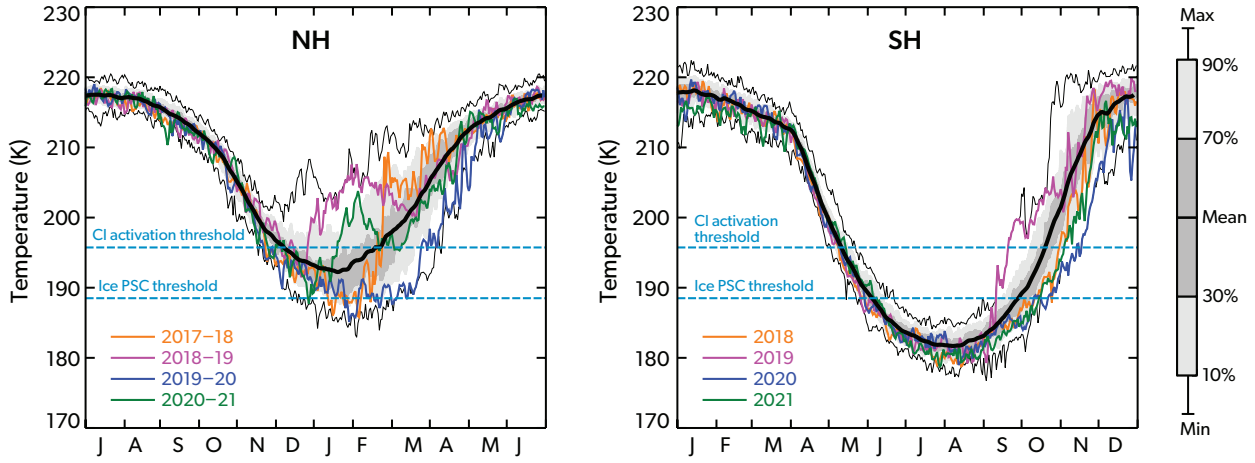


**Figure 4-1.** The annual cycle and variability of 50 hPa minimum temperature for the *(left)* Northern Hemisphere (NH; 50–90°N) and *(right)* Southern Hemisphere (SH; 50–90°S) polar caps, from MERRA-2 reanalysis data (Gelaro et al., 2017). The thick black line indicates the mean of observations since 1979, while light (dark) shading indicates the 10–90% (30–70%) percentiles. Thin black lines show the record maximum and minimum values. Horizontal blue lines indicate the chlorine activation threshold and ice PSC formation threshold. Data are for 1978/79–2020/21 for the Northern Hemisphere and 1979–2021 for the Southern Hemisphere. [Updated from Figure 4-1 in the 2018 Assessment, with data sourced from ozonewatch.gsfc.nasa.gov.]

tracer measurements indicate that the CTM underestimates the strength of confined diabatic descent inside both winter polar vortices for most of the reanalyses, compromising the fidelity of simulated trace gas distributions. Finally, SPARC (2022) reported results from a case study comparing measured and modeled Antarctic ozone loss. Estimates of chemical ozone loss based on satellite measurements were found to be relatively insensitive to the choice of reanalysis used to interpolate the data to isentropic surfaces and to identify the vortex boundary. However, forcing the same model with different reanalyses yields differences in simulated loss in the Antarctic vortex core that can reach as high as ~25 DU (~20–30%), depending on the specific reanalyses being compared.

Although agreement in polar temperatures is generally good, substantial differences between reanalyses are found for some diagnostics. Therefore, whenever feasible it is best to employ multiple reanalyses, even in studies involving recent winters, for which differences between reanalyses are usually small. Use of more than one reanalysis dataset is of particular value for quantities that cannot be directly compared with observations, as it allows estimation of uncertainties and their potential impact on the results. In light of the limitations in earlier reanalyses, some modeling studies have enacted systematic temperature adjustments of 1–2 K or more in an attempt to reproduce observed conditions. Given the accuracy of current polar reanalysis temperatures, strong justification is needed in any studies seeking to ascribe deficiencies in modeled polar processing or ozone loss to reanalysis temperature biases. Finally, reanalysis temperatures are generally unsuitable for quantification of long-term trends in temperature-based diagnostics, especially those encompassing years prior to 1999. Diagnostics that aggregate low temperatures over months and/or vertical levels (e.g., the winter-mean fraction of the vortex volume with air cold enough for PSCs to exist; see *Section 4.2.2.2*) are particularly problematic as they are highly sensitive to the specific temperature thresholds used to define polar processing potential. The differences between the reanalyses in such diagnostics reflect not only any overall temperature biases but also the differing morphology and spatial gradients of the reanalysis fields (as well as the seasonal evolution and interannual variability thereof). Consequently, winter-mean derived diagnostics can vary widely from one reanalysis to another even if differences in the reanalysis temperatures themselves are relatively small (Lawrence et al., 2018).

### *4.2.2.2 Temperatures and PSC Volume*

The annual cycle of polar ozone depletion depends strongly on stratospheric temperature. Low temperatures present in the winter stratosphere permit the formation of PSCs, upon whose surfaces heterogeneous reactions occur. **Figure 4-1** shows the annual temperature cycle over the satellite era (1979–present) of the 50 hPa polar cap temperature. The four recent winters are highlighted in colors for both the Arctic and Antarctic.

The larger interannual variability in polar temperatures in the Arctic than in the Antarctic is well known and understood in terms of planetary-scale atmospheric dynamics. Recent Arctic winter polar temperatures have been outside the 10–90% percentile envelope. The warm and disturbed 2018/19 vortex was followed by a cold and stable 2019/20 vortex (Lawrence et al., 2020), with 50 hPa polar cap temperatures in 2019/20 hovering around the ice PSC formation temperature for extended periods of time. The 2017/18 and 2020/21 vortex temperatures were closer to the mean, although warming during midwinter 2020/21 and a cold midwinter vortex during 2017/18 were observed.

The more stable nature of the Antarctic vortex during midwinter is clearly apparent in the less variable temperatures. An exception to this pattern occurred in 2019, when the Antarctic vortex was unusually warm and disturbed. In that year, a minor sudden stratospheric warming (SSW; Newman et al., 2020; Klekociuk et al., 2021) resulted in polar temperatures setting record warm

levels during September, exceeding those observed during the 2002 major SSW. The 2019 warming was classified as a minor SSW because the 10 hPa zonal-mean zonal winds did not reverse. The following year, 2020, had a very cold, stable, and long-lasting vortex, with record-low temperatures persisting for much of the spring (into December; Klekociuk et al., 2022).

The potential for ozone depletion throughout the season can be quantified by the time-integrated PSC volume, $V_{PSC}$, which is calculated between the 400 K and 700 K isentropic surfaces, where heterogeneous ozone loss typically occurs (e.g., Rex et al., 2006; Strahan et al., 2016). Interannual variability in $V_{PSC}$ is large in the Arctic (**Figure 4-2**), reflecting the interannual variability of Arctic vortex-wide temperatures and, specifically, variability in when those temperatures fall below the PSC formation threshold. It is also evident from **Figure 4-2** that recent cold Arctic winters, with a large $V_{PSC}$ and relatively severe ozone depletion (e.g., 2019/20), are interspersed with warmer winters with much lower $V_{PSC}$ (e.g., 2018/19).

The long-term evolution of PSC volume in the Arctic has been a topic of discussion in the last several Assessments. The 2006 Assessment (Newman, Rex et al., 2007) discussed analyses indicating that cold Arctic winters had become colder over the preceding 40 years, resulting in larger $V_{PSC}$ and more chemical ozone loss. Absent a new maximum in $V_{PSC}$ in the intervening years, it was not possible to confirm the continuation of increasingly severe extreme $V_{PSC}$ values in the 2010 Assessment (Douglass, Fioletov et al., 2011). By the time of the 2014 Assessment (Dameris, Godin-Beekmann et al., 2014), several studies had cast doubt on the statistical robustness of the long-term trend in extreme $V_{PSC}$ values discussed by Newman, Rex et al. (2007). Noting that no in-depth analyses had been undertaken since 2014, the 2018 Assessment stated that large interannual variability precluded detection of a significant trend in $V_{PSC}$ (Langematz, Tully et al., 2018). A recent study revisited the issue of whether the coldest Arctic winters are getting colder by examining trends in PSC formation potential (PFP), which represents the number of days a volume of air equal to the volume of the polar vortex is exposed to conditions cold enough to allow the existence of PSCs in a given Arctic ozone-loss season (von der Gathen et al., 2021). Analyzing data from four meteorological reanalyses (see also **Figure 4-2**), they found statistically significant positive trends in maximum PFP values. Von der Gathen et al. (2021) concluded that the vortex has tended to experience conditions conducive to PSC formation for 3.5 to 4.8 more days per decade during the coldest Arctic winters over the past half-century.

### *4.2.2.3 Polar Vortex Breakup Dates*

The polar vortex decays and breaks up during spring as a result of the return of sunlight warming the stratosphere and by planetary wave forcing. As noted in previous Assessments (e.g., Langematz, Tully et al., 2018), various metrics are used to define when the final warming (or vortex breakup date) occurs (e.g., Nash et al., 1996; Charlton and Polvani, 2007; Haigh and Roscoe, 2009; Hu et al., 2014; Lawrence et al., 2018; Butler et al., 2019; Butler and Domeisen, 2021; Hauchecorne et al., 2022). These metrics include a vortex area threshold, a wind speed along the vortex edge threshold, and the timing of the complete and final wind reversal to easterlies at 10 hPa. Defining the vortex breakup date as the last day on which the vortex area exceeds 1% of the hemispheric area, Lawrence et al. (2018) reported larger differences between reanalyses in breakup date above the Antarctic than above the Arctic, which they attributed to differences in vortex area between the reanalyses. A recent study of the seasonal evolution of the Antarctic vortex edge based on reanalysis data found later breakup dates (and, to a lesser extent, earlier onset dates) during the 1980s and 1990s, at the time the ozone hole was intensifying (Lecouffe et al., 2022).

**Figure 4-3** shows the vortex breakup date for both polar caps. Here the breakup date is calculated using a threshold for the average wind speed along the vortex edge, following Nash et al.

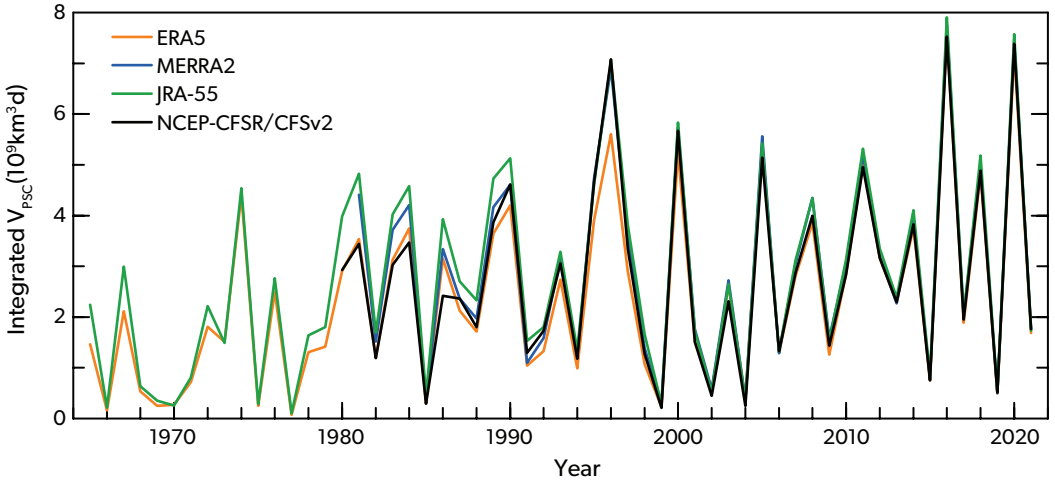


**Figure 4-2.** The Arctic time-integrated PSC volume, $V_{PSC}$, calculated using the method of Rex et al. (2006) for the four indicated reanalysis products. The $V_{PSC}$ values are integrated from 1 November until 30 April for each Arctic PSC season. The ERA5 result is a combination of ERA5-BE (preliminary version, prior to 1979), ERA5, and ERA5.1 (2000–2006). [Updated from Figure 4-2 in Langematz, Tully et al., 2018.]

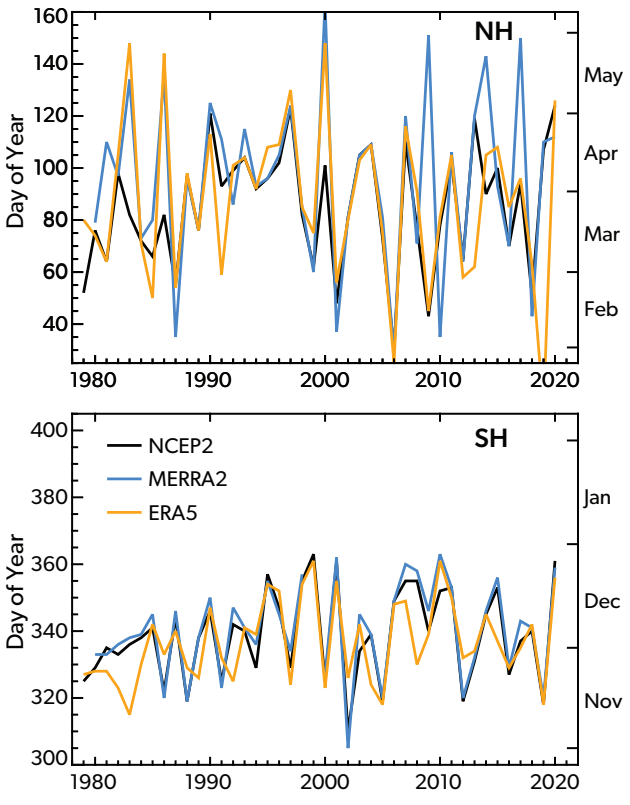


**Figure 4-3.** The Arctic and Antarctic vortex breakup dates, defined as the date on which the wind speed on the 500 K isentropic surface falls below 15.2 m $s^{-1}$, following Nash et al. (1996). Reanalysis data are from ERA5 (Hersbach et al., 2020) except for the period 2000–2006, for which data are from ERA5.1; MERRA-2 (Gelaro et al., 2017); and NCEP/CFSR (Saha et al., 2010). [Updated from Figure 4-3 in Langematz, Tully et al., 2018.]

(1996). The interannual variability of both polar vortices' breakup dates remains similar to that reported in the previous Assessment (Langematz, Tully et al., 2018). For some Arctic winters, the breakup dates are markedly different between the reanalyses, likely because of their differences in stratospheric winds (Butler et al., 2017), resulting in differences in the dates that a specific wind threshold is reached.

## 4.2.3 Ozone Depletion in Recent Antarctic Springs (2018–2021)

**Figures 4-4** to **4-6** show updates for both hemispheres of several diagnostics of the multidecadal evolution of springtime polar ozone that have been discussed in previous Assessments. The agreement among the data from the different satellite sensors used to generate these figures is generally within 2% (McPeters et al., 2008, 2015). This range is much less than the interannual variability of the diagnostics shown. **Figure 4-4** shows the evolution of TCO averaged over the polar cap, poleward of 63°S/N, in October for the Antarctic and in March for the Arctic. The edge of the lower-stratospheric portion of the polar vortex, which encloses the ozone hole, typically lies near 63°S in October, except in years when the vortex is strongly deformed. This is not the case in the Northern Hemisphere, where dynamical variability in the springtime stratosphere is large. Highly variable contributions from mid-latitude air masses affect daily average polar cap ozone and, to some degree, the March averages shown in **Figure 4-4**.

Springtime chemical ozone depletion occurs within the polar vortex. To account for dynamical variations of the vortex edge, Dameris, Godin-Beekmann et al. (2014) introduced a dynamical diagnostic of polar ozone defined as the October/March minimum of the daily total ozone averaged poleward of 63° equivalent latitude (Butchart and Remsberg, 1986), which approximates the edge of the polar vortex in the lower stratosphere. The 63° equivalent latitude contour encloses the same area as the 63° parallel, but its shape and position are dynamical and follow the movements and undulations of the polar vortex. **Figure 4-5** shows an updated version of the time series of this quantity. While each metric is useful for specific applications, the equivalent latitude-based minimum average ozone was found to better correlate, on interannual time scales, with chemical ozone depletion than does the polar cap average (Müller et al., 2008). A more extensive discussion of these diagnostics and their limitations is given in Dameris, Godin-Beekmann et al. (2014).

Three additional diagnostics (**Figure 4-6**) are presented here in order to characterize other aspects of long-term changes and interannual variability in springtime Antarctic ozone in relation to changing ODS concentrations. These are as follows: time-averaged ozone hole area, total ozone minimum, and ozone mass deficit (OMD). The last is the amount of ozone in units of mass needed to bring the total column up to 220 DU and, therefore, combines information about the area and depth of ozone holes. Also shown in **Figure 4-6** are quadratic fits of these quantities to EESC. Several other metrics of the long-term evolution of Antarctic ozone have also been proposed (e.g., Pazmiño et al., 2018; Stone et al., 2021). Starting with the 2014 Assessment, the question of which metrics are the most appropriate for detecting and quantifying Antarctic ozone recovery has been the subject of extensive scientific debate. For example, it is important to consider the calendar periods over which such metrics are calculated, because results based on a single month are not necessarily representative of the entire season, nor are they sufficient for comprehensive analyses of long-term changes. The ongoing scientific debate seeks to reevaluate some of the standard polar ozone diagnostics and identify ones that are best suited for trend studies in the period of ozone recovery. *Section 4.4.2* summarizes the background and the current state of this debate. To provide context for the most recent Antarctic and Arctic springs, the standard metrics shown in **Figures 4-4** to **4-6** are sufficient. They are used in this chapter only as a starting point of a more comprehensive analysis of specific years and provide the added value of connecting the present discussions with previous Assessments.

Evident in **Figures 4-4** to **4-6** is the well-known decline in Antarctic ozone during the 1980s and 1990s, followed by two decades of increased interannual variability and no readily discernible trend in most of the diagnostics. Only OMD exhibits a clear decrease since around 2000 that, together with the initial increase, follows the evolution in EESC (see *Section 4.4.2* for a detailed discussion of Antarctic ozone trends). Compared to **Figure 4-4**, **Figure 4-5** exhibits less variability in the Southern Hemisphere. This is expected because, unlike time-averaged quantities, minima are less sensitive to the dynamically controlled

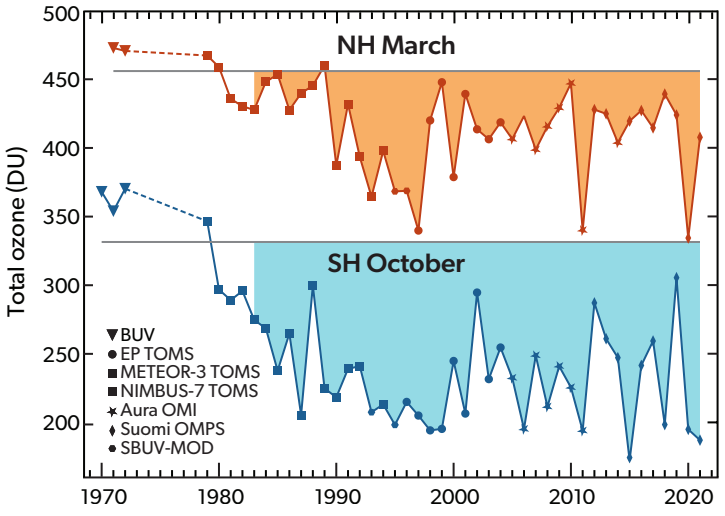


**Figure 4-4.** Total column ozone (Dobson units) averaged over 63–90° latitude in March (Northern Hemisphere [NH]) and October (Southern Hemisphere [SH]). Symbols indicate the satellite data that have been used in different years. The horizontal gray lines represent the average total ozone for the years prior to 1983 in March for the NH and in October for the SH. [Updated from Figure 4-4 in Langematz, Tully et al., 2018.]

and highly variable ozone evolution throughout the month. In addition, the use of equivalent rather than geographic latitude reduces the contributions to the daily averages of air masses outside the polar vortex.

Average October polar cap ozone was particularly high in 1988, 2002, 2012, and 2019 because of anomalously high lower-stratospheric temperatures. In 2002, the warmer temperatures were associated with the only major SSW (defined as a reversal of the 10 hPa zonal-mean zonal wind at 60° latitude) ever observed in the Southern Hemisphere. The minimum of daily ozone (**Figure 4-5**) was anomalously high in 1988, 1993, 2002, and 2019 because of high wave activity in the mid-latitude stratosphere in these years (*Section 4.3.4*). A peak is also present in 2012 but is less pronounced; this is consistent with the observed total ozone values, which were only slightly elevated at the beginning of October 2012 and then increased rapidly shortly thereafter, thus affecting the monthly mean but not the minimum. The lowest October mean polar cap total ozone was observed in 2015 (**Figure 4-4**). This low anomaly is attributed to enhanced heterogeneous chemistry on sulfate aerosols from the Calbuco volcanic eruption in April within the setting of a very cold and stable polar vortex that resulted from weak wave activity between July and October (Langematz, Tully et al., 2018). The most extreme year, when all of these metrics are considered, was 2019, when a minor SSW led to the highest values of Antarctic polar cap ozone (**Figure 4-4**), the highest minimum of the daily average in equivalent latitude (**Figure 4-5**), and the highest time-averaged daily ozone minimum as well as the smallest ozone hole and the lowest OMD in the 21st century (**Figure 4-6**). See *Section 4.2.3.2* for further discussion of the 2019 Antarctic winter.

Since the last Assessment, springtime Antarctic ozone exhibited significant year-to-year dynamically driven variations. The polar cap total ozone ranged from anomalously low in 2018 and 2020 to record high in 2019 (Kramarova et al., 2019, 2020; Wargan et al., 2020; Safieddine et al., 2020). To assist in analyzing the development of the most recent ozone holes in the

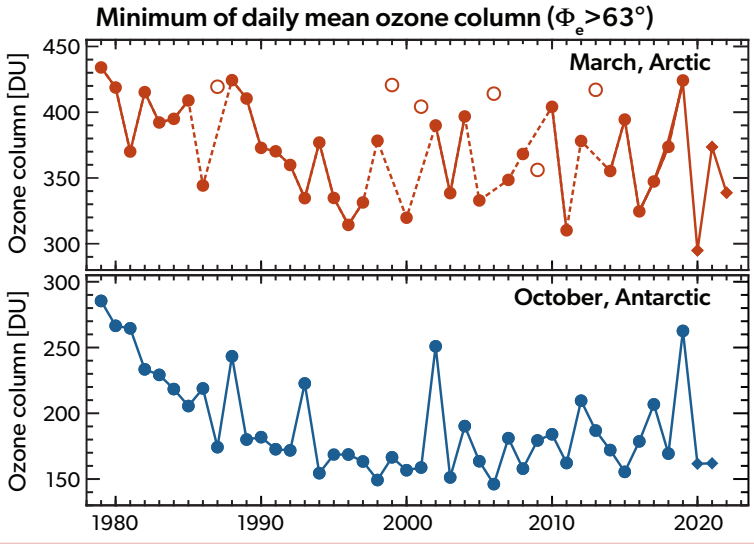


**Figure 4-5.** Minimum of the daily average total column ozone (Dobson units) poleward of the 63° contour of equivalent latitude ($\Phi_e$) in *(top)* March in the Arctic and *(bottom)* October in the Antarctic. Arctic winters in which the polar vortex broke up before March (1987, 1999, 2001, 2006, 2009, and 2013) are shown by open symbols; dotted lines connect surrounding years. [Adapted from Langematz, Tully et al., 2018. Updated using the Bodeker Scientific combined total column ozone database (version 3.5.1, circles; Müller et al., 2008) until 2019 and Aura OMI measurements thereafter (diamonds).]

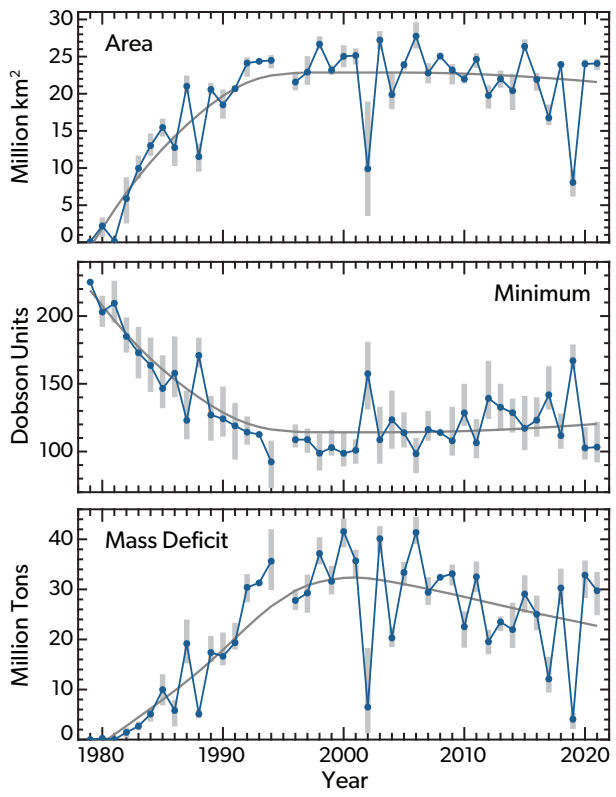


**Figure 4-6.** *(top)* Antarctic ozone hole area for 1979–2021, averaged from daily total ozone area values contained by the 220 DU contour for 21–30 September. *(middle)* An average of daily minimum total column ozone values over Antarctica during the period from 21 September to 16 October. *(bottom)* Ozone mass deficit averaged over the 21–30 September period. For all three panels, the vertical gray bars indicate the range of values over the same periods. The dark gray curves show the quadratic fits of each quantity to EESC as described in Newman et al. (2004). The EESC is derived as in Newman et al. (2007), updated with the current A1 baseline scenario. A mean age of 5.5 years, an age spectrum width of 2.75 years, and a bromine-scaling factor of 65 are assumed. In the polar regions, this EESC estimate is very similar to that derived by Engel et al. (2018) and used in *Chapter 1*. This figure was generated from TOMS (1979–2004), Aura OMI (2005–2015), and Suomi NPP OMPS (2016–2021) data. [Updated from Figure 4-6 in Langematz, Tully et al., 2018.]

following subsections, two additional figures are shown. **Figure 4-7** plots the daily values of OMD (top panel) for the years 2018 to 2021, as well as for the anomalous year 2002, along with their climatological statistics. This figure is a modified and updated version of plots shown in previous Assessments. In addition to the climatological range, the present version of the graph includes selected percentile envelopes, where all statistics are calculated over the 1980–2021 period. This differs from previous Assessments, for which the statistics were calculated starting in 1990 and the three most recent years in each case were excluded.

**Figure 4-8** shows the evolution of several key species involved in chemical processing inside the lower-stratospheric polar vortex and in ozone depletion. In addition to ozone ($O_3$), the figure plots daily vortex-average concentrations of nitric acid ($HNO_3$), water vapor ($H_2O$), hydrogen chloride (HCl), and chlorine monoxide (ClO). Changes in $HNO_3$ and $H_2O$ are sensitive to temperature: At sufficiently low temperatures, gas-phase $HNO_3$ and $H_2O$ undergo condensation, leading to the formation of PSCs (see *Section 4.3.1*), which in turn can lead to denitrification and dehydration of the polar lower stratosphere. Changes in HCl and ClO quantify chlorine activation, with low HCl and high ClO indicating the presence of ozone-destroying active chlorine.

### *4.2.3.1 Antarctic Spring 2018: Moderately Large Ozone Hole*

The 2018 ozone hole area, daily minimum, and OMD, while indicative of below-average ozone, are all within the range of values observed during the other years of last decade (**Figure 4-6**). In September, OMD began to diverge from its climatological mean, reached the 70$^{th}$ percentile by mid-month, and remained relatively high until late October (**Figure 4-7**). The evolution of the ozone hole area followed a similar trajectory, with values consistently higher than the long-term average (Wargan et al., 2020). These relatively high values of OMD and area are consistent with the meteorological conditions in the stratosphere in 2018. Minimum high-latitude temperatures were below average for parts of the austral winter and almost all of October (**Figure 4-1**), leading to high PSC volumes in July and August (Kramarova et al., 2019).

Stratospheric temperatures and the strength of the polar vortex on seasonal time scales are largely controlled by extratropical wave activity (*Section 4.3.4*). The lower panel of **Figure 4-7** shows time series of eddy heat flux between 45 and 75°S. This metric serves as a measure of upward propagation of Rossby waves in the lower stratosphere. The weakly negative values between August and October 2018 indicate low wave activity and are consistent with a strong, large, and cold polar vortex. Despite low temperatures and significant PSC volume, HCl and ClO in the Antarctic in 2018 were well within the 2005–2017 range throughout the winter/spring season, with no evidence of unusually strong chlorine activation (**Figure 4-8**). This suggests that the observed low ozone anomaly was at least in part the result of anomalous transport, likely with weak ozone resupply from higher altitudes, consistent with low wave activity.

Model simulations with the Global Modeling Initiative chemistry model driven by assimilated meteorology realistically reproduce the development of the 2018 ozone hole after accounting for a known constant bias. The same model setup but with the EESC values held constant at their maximum surface levels in 1995 produces an ozone hole more than 4 million km$^2$ (17%) larger than observed, highlighting the role of the Montreal Protocol and its Amendments and adjustments in reducing the severity of the 2018 ozone hole (Kramarova et al., 2019; see also *Section 4.4.4*).

### *4.2.3.2 Antarctic Spring 2019: Impact of the Strong Minor Sudden Stratospheric Warming*

A significant disturbance of the typically quiescent Antarctic stratosphere commenced at the end of August 2019 with a wavenumber-1 displacement of the middle and upper portion of the

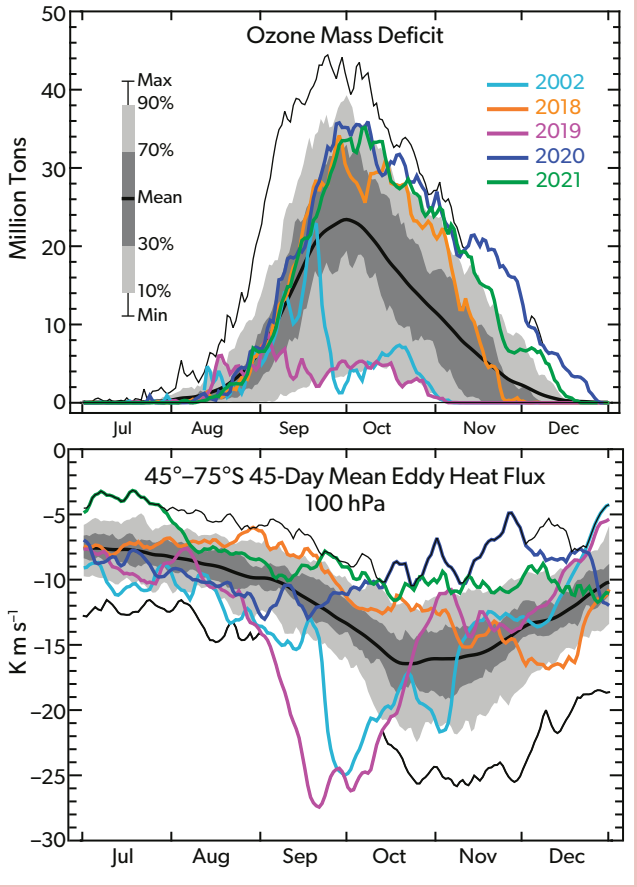


**Figure 4-7.** *(top)* Daily ozone mass deficit (OMD) for various years compared with selected percentiles calculated over the period 1980–2021 (gray shaded areas) and the maximum values for the same period (thin black lines). The thick black line shows the 1980–2021 OMD average. OMD was calculated using data from TOMS, Aura OMI, and Suomi NPP OMPS. [Updated from Figure 4-7 in Langematz, Tully et al. (2018).] *(bottom)* As above but for the 45-day mean eddy heat flux at 100 hPa averaged between 45°S and 75°S. Eddy heat flux at this level is a metric of upward wave propagation in the stratosphere. Highly negative values correspond to strong wave activity. The heat fluxes are derived from MERRA-2. The results from this particular reanalysis serve as an illustrative example.

polar vortex that was accompanied by a significant reduction in vortex size (Hendon et al., 2019; Yamazaki et al., 2020; Liu et al., 2022). This strong, albeit formally minor, SSW resulted in anomalously high polar ozone and a small ozone hole area (**Figures 4-4** to **4-7**; Safieddine et al., 2020; Wargan et al., 2020; Kramarova et al., 2020; Bodeker and Kremser, 2021; Klekociuk et al., 2021). Average ozone hole area, daily ozone minimum, and OMD in 2019 all exhibited larger anomalies than observed following the major (that is, characterized by a reversal of the zonal-mean zonal wind at 60° latitude in the middle stratosphere) SSW of 2002. While declining ODS concentrations contributed to the high Antarctic ozone in 2019, the SSW was the primary cause of the anomaly (Kramarova et al., 2020).

In 2019, the SSW was preceded by a poleward shift of the polar night jet around the stratopause, resulting in a persistent easterly anomaly that started in early winter (Lim et al., 2021). The minor warming in late August was triggered by a strong upward propagating wave flux of tropospheric origin amplified by constructive interference with climatological wave-one pattern (Shen et al., 2020). Energy and momentum were provided by a strong and long-lived mid-latitude circumpolar Rossby wave train in the troposphere in 2019. This wave train is attributed to sustained convection over the subtropics resulting from warm sea surface temperature anomalies associated with a simultaneous occurrence of a positive phase of the Indian Ocean Dipole and El Niño-like conditions in the Pacific (Shen et al., 2020; Rao et al., 2020). It is estimated that the wave driving in 2019 was stronger than that in 2002 (Liu et al., 2022). The SSW was enabled by a favorable phase of the quasi-biennial oscillation and solar minimum conditions (Rao et al., 2020). The existence of these precursor conditions allows long lead-time predictability of the SSW (up to 18 days), underscoring a highly accurate representation of the underlying mechanisms in modern subseasonal-to-seasonal ensemble prediction models (Rao et al., 2020). The unusually high wave activity and its effects on ozone are seen in **Figure 4-7** (bottom and top panel, respectively). The 2019 event was the strongest disturbance of the Antarctic stratospheric polar vortex since 2002, when the only SSW in the Southern Hemisphere classified as major was observed (Newman, Rex et al., 2007). The two events exerted comparable and significant impacts on ozone. This important observation implies that, as has been demonstrated previously for the Northern Hemisphere (Manney et al., 2015), the classification of SSWs as major or minor, while useful, does not automatically characterize the magnitude of their impacts on ozone. The 2019 ozone hole was the smallest in the 21st century and one of the smallest ever observed in October (**Figures 4-4** and **4-6**). The minimum of the daily average total column ozone (TCO; **Figure 4-5**) was also very high, in part because the polar vortex edge was no longer well approximated by the 63°S equivalent latitude contour after the SSW.

**Figure 4-9** (top panel) shows the evolution of the Southern Hemisphere polar (60–90°S) TCO during the 2019 austral winter and spring, along with the 2008–2018 values (Safieddine et al., 2020). Antarctic total ozone sharply increased following the onset of the SSW, reaching 380 DU in mid-September, compared with the multiyear average of less than 250 DU. This anomalous behavior resulted from the reduced size of the polar vortex and its distorted geometry, with ozone-rich air masses transported from the mid-latitudes overlying the lower portion of the vortex, leading to a significant increase of the vertically integrated ozone concentrations (Wargan et al., 2020). These aspects of the 2019 Antarctic winter are similar to the situation in 2002 (Newman, Rex et al., 2007). The wave-induced distortions of the vortex and their effect on the ozone hole are illustrated in the bottom panel of **Figure 4-9**, which shows the evolution of the ozone hole and the polar vortex edge at selected isentropic levels in 2019 and 2018 for comparison.

While the transport-related increase in total ozone was extreme during the first two weeks of September 2019, the rate of chemical ozone depletion was not significantly different from that in 2018. Ozone concentrations at ~18 km were, in fact, lower in 2019 until the end of September (**Figure 4-8**). Lower-stratospheric temperatures began to increase in early September

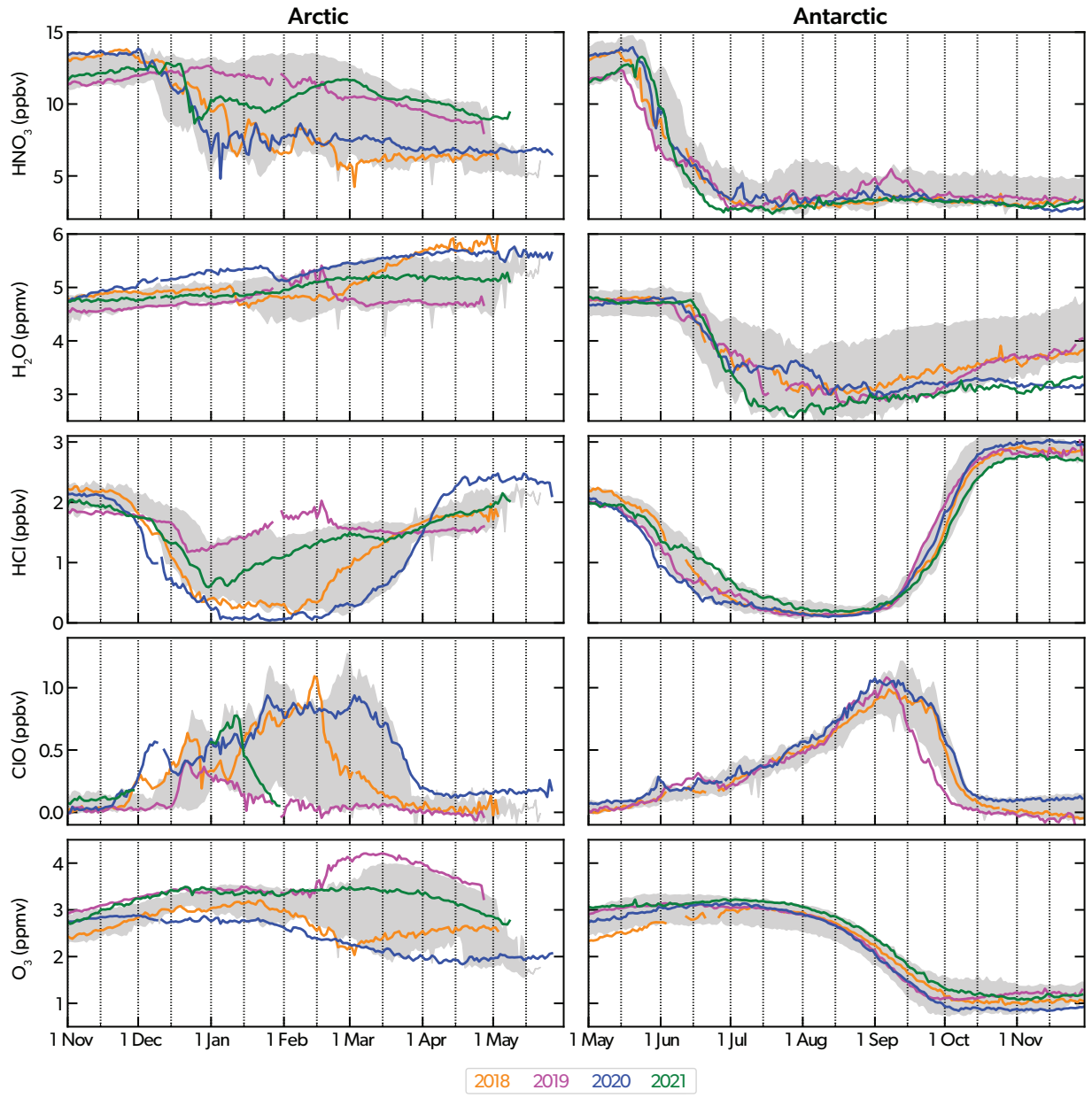


**Figure 4-8.** Evolution of daily $HNO_3$, $H_2O$, HCl, ClO, and $O_3$ from the Aura Microwave Limb Sounder (MLS) averaged within the polar vortex on the 480 K potential temperature surface (approximately 18 km) for the Arctic (November–May; *left*) and the Antarctic (May–November; *right*). Gray shading marks the range of values observed by Aura MLS over the 2005–2017 period. For ClO, only daytime (ascending node) observations are used so that near-zero ClO concentrations during local night do not contribute to the averages. The recent four winter/spring seasons are shown as colored lines as given in the legend; for the Arctic, the year given refers to the spring. [Update of figure first introduced in Dameris, Godin-Beekman et al. (2014) and updated in Langematz, Tully et al. (2018), where only results for the Arctic were shown.]

because of compression warming from the SSW-induced accelerated descent of vortex air, leading to early chlorine deactivation that began to affect ozone chemistry in the second half of September (Wargan et al., 2020; Smale et al., 2021). The daily minimum temperatures at 50 hPa exceeded the nominal threshold for chlorine activation around mid-September (**Figure 4-1**). At that time, ClO decreased to the lowest values ever observed by MLS during the Antarctic late winter. The evolution of lower-stratospheric vortex-averaged ozone shown in **Figure 4-8** indicates a slow increase starting in late September, which was a combined effect of the cessation of chemical depletion and ozone resupply from higher altitudes. The ozone hole closed at the beginning of November, about a month early compared to typical Antarctic springs.

Even though the 2019 SSW did not meet the criteria of a major SSW, it involved a deceleration of the zonal-mean zonal wind at 60°S at 10 hPa of more than 60 m $s^{-1}$, dropping from 80 m $s^{-1}$ to about 15 m $s^{-1}$ over the course of two weeks. A decrease of the same magnitude in the Northern Hemisphere would lead to a zonal wind reversal and thus constitute a major SSW (Wargan et al., 2020; Rao and Garfinkel, 2020). Disruptions of the polar vortex can impact surface weather. While the effects of the 2019 strong minor SSW on Southern Hemisphere weather have yet to be fully evaluated, hot and dry conditions over parts of Australia observed during the austral summer 2019/20 are consistent with the expected response to a weak polar vortex event (Lim et al., 2019; Baldwin et al., 2021; Lim et al., 2021). See *Chapter 5* for a discussion of connections between the Southern Hemisphere stratospheric circulation and conditions at the surface, including the role of ozone feedbacks.

### *4.2.3.3 Antarctic Springs 2020 and 2021: Exceptionally Persistent Ozone Holes*

In contrast to 2019, the 2020 and 2021 Antarctic springs were characterized by strong and long-lasting polar vortices and significant ozone depletion. In both years, the ozone hole area reached a maximum of over 24 million $km^2$, about 5 million $km^2$ above the 1979–2021 average. In late September of 2020 and

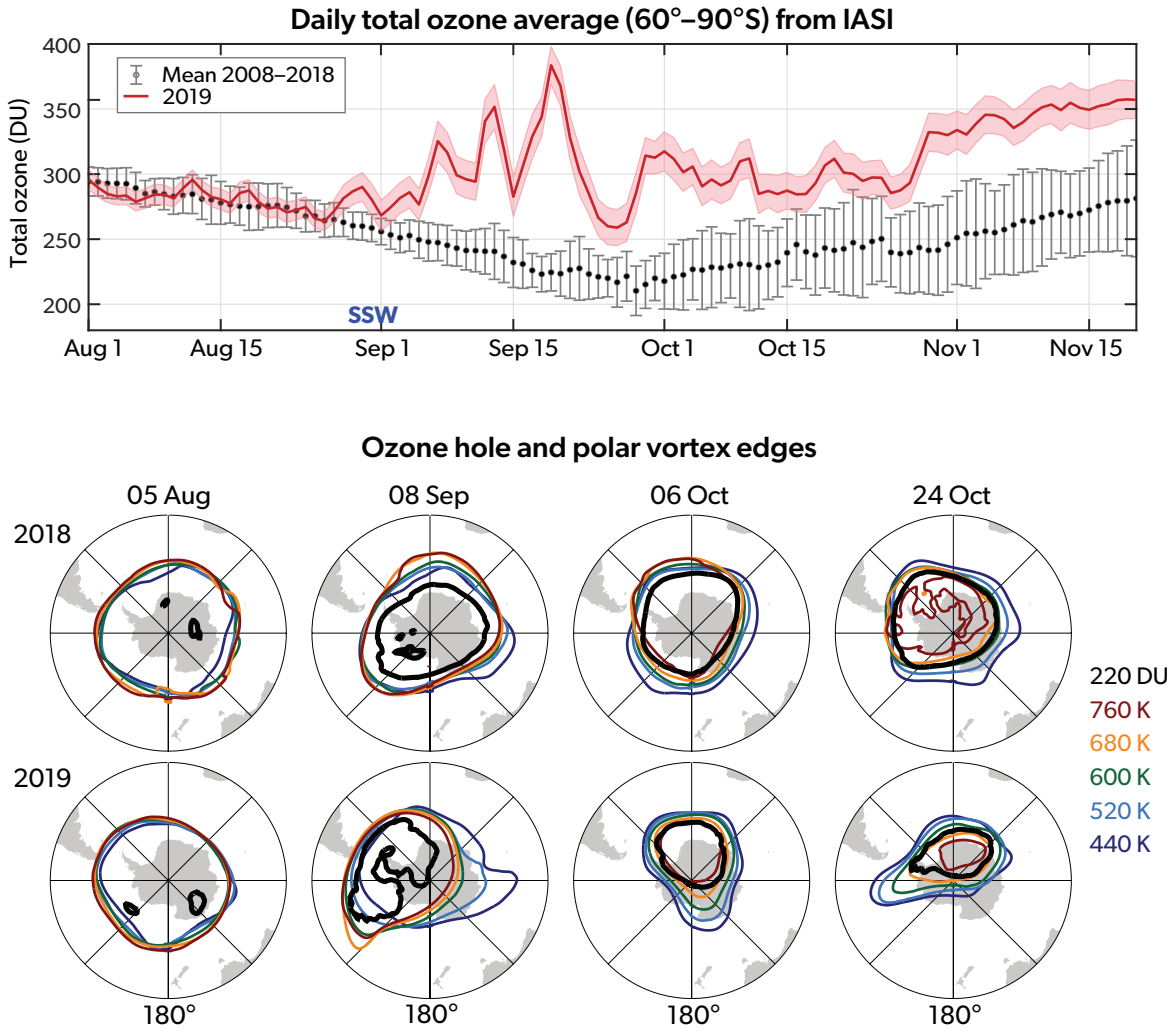


**Figure 4-9.** *(top)* Time series of daily total column ozone from Infrared Atmospheric Sounding Interferometer (IASI) observations, averaged between 60°S and 90°S for 2019 (red). The shading represents the estimated error. Black dots and error bars show the 2008–2018 average of the same quantity and the 11-year standard deviation, respectively. The onset of the SSW is noted as "SSW" in blue text. [Adapted from Safieddine et al., 2020.] *(bottom)* 220 DU contours of total ozone (black lines), defining the edge of the ozone hole, and the edges of the polar vortex (colored lines) on selected surfaces of potential temperature between 440 and 760 K (approximately 17 to 28 km) on four dates between 5 August and 24 October in 2018 and 2019. The vortex edges are defined using threshold values of scaled potential vorticity. The dynamical and ozone fields are from a specified dynamics experiment forced by MERRA-2 meteorology. [Adapted from Wargan et al., 2020.]

2021, both the OMD and the average minimum ozone, while not extreme, exhibited values more in line with those in the first decade of the 21st century than in recent years (**Figure 4-6**). One remarkable feature of the 2020 ozone hole was its record duration (Klekociuk et al., 2022). Areas with ozone below 220 DU persisted until late December 2020, several weeks longer than in a typical austral spring (**Figure 4-7**). The November and December averages of OMD and ozone hole area in 2020 were higher than previously observed. The 2021 ozone hole closed in mid-December, also significantly later than average (**Figure 4-7**).

The relatively large sizes and the extreme longevity of the 2020 and 2021 ozone holes are consistent with the unusual dynamical states of the stratosphere in both years. Wave activity, slightly elevated during the austral winter of 2020, weakened to record-low levels between October and mid-December (**Figure 4-7**). As a result, the springtime increase of vortex temperature, typically driven by a combination of radiative and dynamical warming, was slow relative to other years. Minimum temperatures at 50 hPa remained below the chlorine activation threshold until mid-November, about one month longer than usual (**Figure 4-1**). The vortex breakup occurred almost one month later than average (*Section 4.2.2.3*; Lecouffe et al., 2022). Chlorine deactivation was likely complete by the end of October (as seen at 480 K in **Figure 4-8**), but ozone remained low as OMD decreased at a relatively slow rate (**Figure 4-7**). Debate is ongoing about potential impacts of the Australian New Year's bushfires on the Southern Hemisphere polar ozone in 2020. The current state of this discussion is summarized in *Section 4.3.5.3*.

In 2021, wave activity was also very weak between late September and late November, although not as weak as that in 2020 (**Figure 4-7**). The minimum vortex temperatures, while higher than those in 2020, were well below average in 2021, and active chlorine in the polar vortex at 480 K followed very similar trajectories in 2020 and 2021 (**Figure 4-8**). Correlation analysis of recent measurements suggests that high levels of sulfate aerosols injected into the stratosphere during the eruption of La Soufrière in April 2021 might have contributed to the large size of the ozone hole in that year (Yook et al., 2022). Further research is needed to investigate the dynamical, chemical, and climatic conditions in 2020 and 2021 that led to the prolonged periods of suppressed wave activity and long-lasting ozone holes.

## 4.2.4 Ozone Depletion in Arctic Springs (2018–2021)

The polar vortex in the Northern Hemisphere is more dynamically variable than that in the Southern (*Section 4.3.4.1* and **Figure 4-13**), with major SSWs typically occurring several times per decade (Butler et al., 2017) and minor vortex disruptions being commonplace. The interannual variability of springtime Arctic ozone is driven by dynamical effects on transport and chemistry (Tegtmeier et al., 2008; Manney et al., 2011a; Strahan et al., 2016; de la Cámara et al., 2018; Bahramvash Shams et al., 2022). The main contributions to Northern Hemisphere ozone variability are variations in the dynamical resupply of ozone-rich air through downward transport and year-to-year differences in the amount of mixing across the polar vortex edge. Dynamics also controls variations in chemical ozone depletion on interannual time scales (*Section 4.3.4*). Major SSWs occurred in three of the four most recent Arctic winters: 2018, 2019, and 2021 (Rao et al., 2018, 2019; Butler et al., 2020; Lee, 2021; Pérot and Orsolini, 2021; Wright et al., 2021; Bahramvash Shams et al., 2022). In contrast, the 2020 winter was characterized by an exceptionally strong and stable polar vortex and record-low ozone.

Coupling between the stratospheric polar vortex in the Northern Hemisphere and surface conditions is a subject of ongoing research. For a summary of the current understanding of the stratosphere-troposphere interactions, including Arctic ozone feedbacks, see *Chapter 5*.

### *4.2.4.1 Arctic Springs 2018, 2019, and 2021: Impacts of Disturbed Polar Vortices*

In 2018, wavenumber-2 forcing reversed the 60°N zonal winds on 12 February and split the polar vortex, causing an abrupt deceleration of the zonal-mean winds and rapid temperature increases within a deep layer extending down to at least 70 hPa. Prior to the event, minimum temperatures at 50 hPa (in the lower part of the vortex) were significantly below the average throughout January and the first half of February (**Figure 4-1**). The low temperatures provided conditions for intense PSC formation and chemical processing prior to the SSW. **Figure 4-2** shows that the time-integrated volume of air below the chlorine activation threshold was relatively high in 2018. Concentrations of vortex $HNO_3$ were close to the lower end of the range (**Figure 4-8**), indicative of substantial PSC formation. Observations of HCl and ClO indicate that chlorine activation began in late November, two weeks earlier than usual, and produced high concentrations of active chlorine that would not become fully deactivated until late March (**Figure 4-8**). In early February, prior to the SSW, polar cap total ozone was only about 350 DU, in the low 10th percentile for that time period. As a result of the high concentrations of active chlorine, chemical ozone loss was significant and continued after the vortex split occurred (Bernhard et al., 2019), such that lower-stratospheric vortex ozone in early March 2018 was one of the lowest in the MLS record (**Figure 4-8**). However, because of the SSW and the associated influx of ozone-rich air in the middle and upper stratosphere, the relatively intense chemical destruction did not significantly affect March polar cap total ozone (**Figure 4-4**). Average minimum daily ozone north of 63°N equivalent latitude (**Figure 4-5**) was within the 21st-century range.

The 2019 SSW, which began on 2 January, about 40 days earlier in the season than the 2018 event, had a significant impact on polar chemistry (Bernhard et al., 2020). Unlike the rapid development observed in 2018, the onset of the 2019 SSW was preceded by gradual weakening and displacement of the polar vortex by wavenumber-1 forcing after mid-December (Butler et al., 2020; Lee and Butler, 2020). Minimum vortex temperatures at 50 hPa increased above the threshold for chlorine activation as early as late December (**Figure 4-1**). Vortex $HNO_3$ on 2 January was above its November levels (**Figure 4-8**), indicating very little PSC formation. Following a brief period of chlorine activation in mid-December 2018, average ClO concentrations gradually declined, while HCl increased and reached values above the 2005–2017 maximum in late January. By the end of January, chlorine deactivation was complete, and chemical ozone loss due to chlorine catalytic cycles ceased. Dynamical effects of the slowly downward propagating vortex disturbance led to a further significant increase of ozone concentrations in mid-February. The March polar cap TCO in 2019 was slightly above the typical values seen in the past two decades (**Figure 4-4**), and the average minimum daily ozone north of 63°N equivalent latitude was one of the highest in the

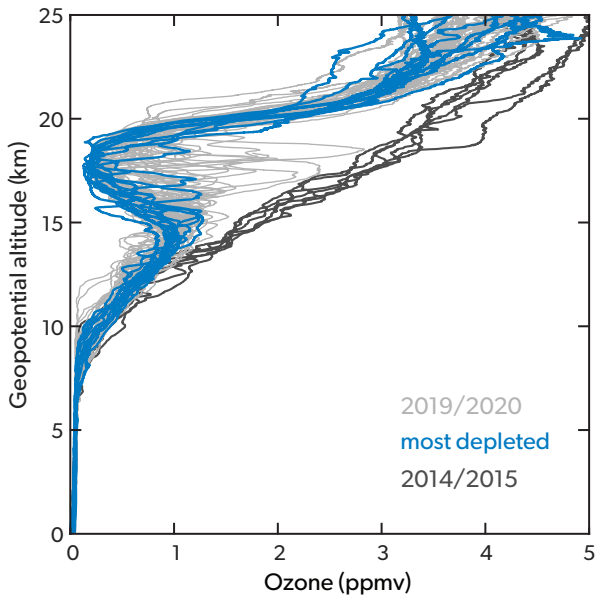


**Figure 4-10.** Ozone profiles inside the polar vortex from 17 March to 17 April 2020 as a function of altitude. A set of 12 sondes was chosen from all measurements to represent the air masses most depleted in ozone (blue lines). All other profiles from 2019/20 are shown in light gray. For comparison, profiles inside the polar vortex from the warm winter 2014/15 (24 March to 9 April) are shown in black. [Adapted from Wohltmann et al., 2020.]

past three decades (**Figure 4-5**), further underscoring the critical role of dynamical effects on ozone variability in the Arctic.

The onset of the 2021 SSW occurred on 5 January (Wright et al., 2021). Unlike in 2019, minimum temperatures at 50 hPa remained below the chlorine activation threshold until mid-January (**Figure 4-1**). A moderate decrease in $HNO_3$ observed by MLS indicates PSC formation in late December (**Figure 4-8**). High ClO concentrations in early January suggest that some chemical ozone depletion occurred initially, but by the end of the month, chlorine was fully deactivated. Vortex-averaged ozone concentrations at 18 km were at the upper end of the 2005–2017 range already in November and remained relatively high throughout the winter and spring (**Figure 4-8**). Nonetheless, likely because of partial compensation from below-average ozone at higher altitudes and outside of the vortex, polar cap total ozone in March was one of the lowest in the last 20 years (**Figure 4-4**), excluding the extreme cases of 2011 and 2020. The minimum of daily averages within the area prescribed by 63°N equivalent latitude (**Figure 4-5**) was typical for recent decades.

While major SSWs occurred in all three years, their effects on ozone varied significantly, as is evident from **Figures 4-4**, **4-5**, and **4-8**. This variability arises from differences in the timing of the SSWs and their dynamical evolution that, in turn, impact the concentrations of active chlorine within the polar vortex and the amount of solar illumination of the chemically processed air within the vortex.

### *4.2.4.2 Arctic Spring 2020: Record-Low Arctic Stratospheric Ozone*

Record-low ozone was observed in the Arctic spring of 2020. The only other two years that saw comparable extremes were 1997 and 2011. As was the case in those years, the exceptionally low ozone anomaly in 2020 was a consequence of a prolonged period of very low temperatures and high stability of the polar vortex, which strongly enhanced chemical depletion while inhibiting ozone resupply through transport (Manney et al., 2020; Lawrence et al., 2020; Inness et al., 2020; Dameris et al., 2021; Feng et al., 2021; Weber et al., 2021; Grooß and Müller, 2021). Pronounced ozone minima occurred within the stratospheric polar vortex at altitudes between 15 and 20 km (**Figure 4-10**). Polar cap ozone during most of the late winter and early spring of 2020 was the lowest on record, with values reaching about 90 DU below the 1979–2021 March average. The February–April mean TCO near the North Pole was about 120 DU below the long-term mean (**Figure 4-11a**). Regions where TCO fell below 220 DU were observed between January and March (Dameris et al., 2021; Kuttippurath et al., 2021), prompting media reports of an "Arctic ozone hole." However, these patches of low ozone lacked almost any defining characteristics of Antarctic ozone depletion (Wohltmann et al., 2020). With areas under 1 million $km^2$, they were small compared to ozone holes, which regularly exceed 20 million $km^2$ in size. Daily total ozone minima in March ranged between 205 and 240 DU, about 50 DU below the average. By comparison, typical minimum TCO over Antarctica in October ranges between 100 and 160 DU (**Figure 4-6**), with ozone concentrations near zero in the most depleted layer in the lower stratosphere (e.g., Solomon et al., 2014; Kuttippurath et al., 2018). Minimum ozone concentrations measured by ozonesondes in March and April 2020 were generally between 0.15 and 0.2 ppmv and occurred at altitudes around 18 km, with the lowest reported value being 0.13 ppmv (Wohltmann et al., 2020; **Figure 4-10**). These values are lower than previously observed in any other Arctic spring, including 2011, but are still an order of magnitude higher than minima observed over Antarctica (Solomon et al., 2014).

The 2019/20 northern winter/spring has been intensely studied. None of the results published to date challenge our now well-established understanding of polar ozone chemistry. Chemistry models constrained by real-world meteorology from reanalyses accurately reproduce the extreme chemical ozone loss of 2020. This has been demonstrated explicitly with the CLaMS (Grooß and Müller, 2021) and the TOMCAT (Feng et al., 2021; Weber et al., 2021) chemistry models.

Similar to the winter/spring seasons of 1996/97, 2010/11, and, to some extent, 2015/16, the prolonged period of very low minimum polar vortex temperatures that lasted from December through April (**Figure 4-1**) and the high vortex strength resulted primarily from exceptionally low wave activity in the stratosphere. **Figure 4-11b** shows an approximately linear relationship between the amount of wave driving, represented by the vertical component of the Eliassen-Palm flux, and the Northern Annular Mode (NAM) index, which quantifies vortex strength. The springs of 1997, 2011, and 2020 are near the lower-right corner of the plot, with the lowest wintertime wave activity and the strongest polar vortex occurring in 2020. Another feature of the 2020 spring was a strong coupling between the polar vortex and tropospheric meteorology, as manifested in a highly zonal circulation

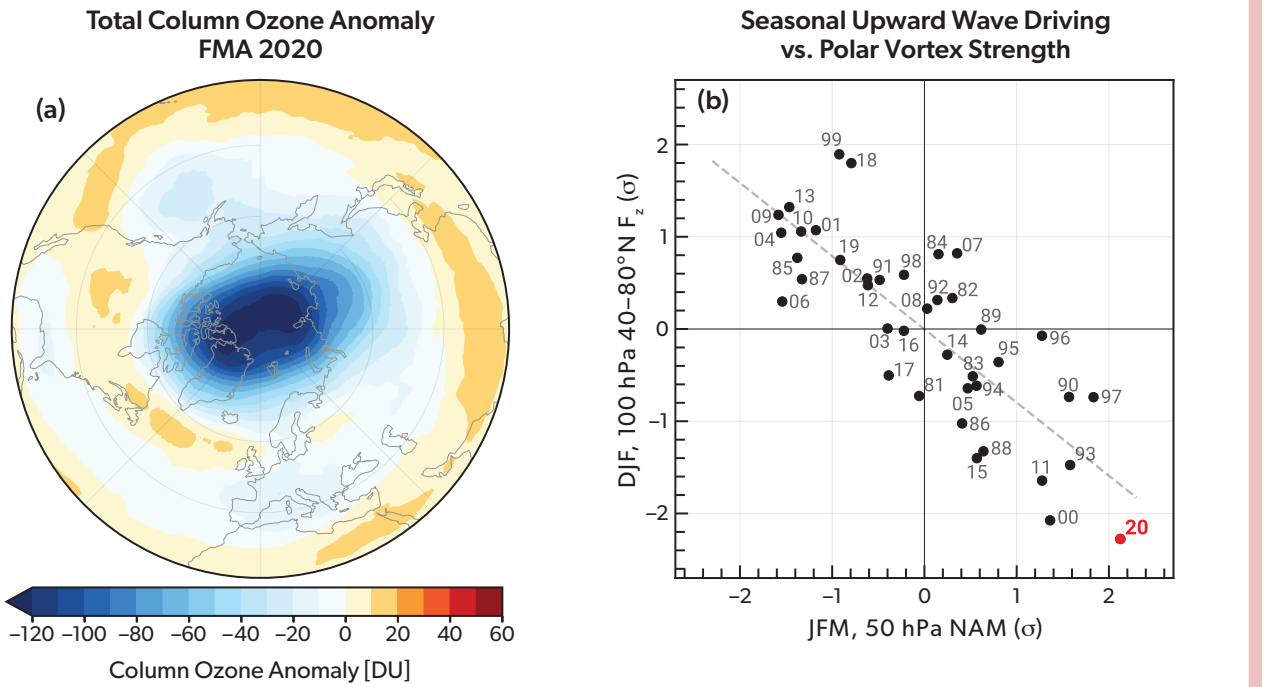


**Figure 4-11.** (a) Northern Hemisphere February–April (FMA) total ozone anomaly with respect to the 1979–2020 average. (b) December–February (DJF) 100 hPa 40–80°N averaged vertical component of the Eliassen-Palm flux ($F_z$) versus the January–March (JFM) 50 hPa Northern Annular Mode (NAM) index. The record year 2020 in (b) is marked in red. The ozone data are from the Ozone Mapping and Profiling Suite Nadir Mapper; the dynamical metrics are derived from the MERRA-2 reanalysis. [Adapted from Lawrence et al., 2020.]

throughout the depth of the stratosphere and troposphere down to the surface (Lawrence et al., 2020).

The extremely low Arctic ozone in the spring of 2020 arose as a combined effect of anomalous transport and exceptionally strong chemical depletion, both caused by the unusual dynamical conditions described above. While chemical destruction in 2020 (discussed below) was significant, weak ozone resupply was the other key factor in the occurrence of the extremely low observed values of TCO in the spring of 2020. When wave activity is less intense, as it was in 2020, the Brewer-Dobson Circulation (BDC) slows down, and ozone replenishment is less effective (*Section 4.3.4*). Furthermore, assimilated meteorological fields from reanalyses provide evidence of downward wave reflection and associated anomalous upwelling between January and March 2020 (Lawrence et al., 2020). The phenomenon of planetary wave reflection was highlighted in Langematz, Tully et al. (2018) as a factor in slowing down the BDC, leading to a colder polar vortex and inhibiting vertical transport. In the winter/spring of 2019/20, the rate of ozone resupply into the lower stratosphere was significantly reduced. Dynamical replenishment over the polar cap in March 2020 was only about 60 DU, compared to the climatological average of 150 DU (Feng et al., 2021).

The extreme stability of the stratospheric polar vortex significantly impacted polar chemistry in 2020. Minimum temperatures remained below the threshold for chlorine activation until mid-March (Lawrence et al., 2020; Wohltmann et al., 2020; Dameris et al., 2021). The time-integrated NAT (nitric acid trihydrate) PSC volume ($V_{PSC}$) reached the second-highest value on record (**Figure 4-2**). Based on satellite measurements, the maximum area covered by PSCs was 8–10 million km$^2$, comparable to typical Southern Hemisphere values (DeLand et al., 2020). These conditions enabled long-lasting chlorine activation and chemical ozone loss. Vortex-averaged chlorine monoxide (ClO) in the lower stratosphere was persistently high, while the chlorine reservoir compound hydrogen chloride (HCl) was the lowest since at least 2005 for most of the season (**Figure 4-8**). Chlorine activation and ozone depletion began earlier than in any previously observed winter, with evidence of some chemical ozone loss as early as November (Manney et al., 2020). High levels of active chlorine and bromine and significant denitrification are also indicated in satellite measurements of chlorine dioxide (OClO) slant columns and of nitrogen dioxide ($NO_2$) total columns (Weber et al., 2021) and in ground-based observations of bromine monoxide (BrO), chlorine nitrate ($ClONO_2$), and nitric acid ($HNO_3$) columns (Bognar et al., 2021). Chlorine deactivation occurred around the March/April boundary, much later than in typical Arctic springs, apart from 2011. The prolonged exposure of chemically processed air to sunlight contributed to the significant chemical ozone depletion in 2020 (Wohltmann et al., 2021). By early April, HCl concentrations increased to record levels, indicating an Antarctic-like deactivation pathway, whereby Cl is incorporated predominantly into this nitrogen-free compound rather than into $ClONO_2$, as typically observed in the Northern Hemisphere (Manney et al., 2020; Grooß and Müller, 2021; Wohltmann et al., 2021).

## *Box 4-1. What is a 'Polar Vortex' and Why Does it Matter?*

As most recently discussed by Manney et al. (2022), there is considerable confusion both within and outside the atmospheric science community about the usage of the term "polar vortex." For instance, in January 2014, a cold air outbreak (CAO) extending through the southern central and eastern United States set new record-low minimum temperatures as far south as Georgia and Texas (e.g., Screen et al., 2015). As discussed by, e.g., Lillo et al. (2021), this CAO was described in the media as "the polar vortex," and this language became commonplace in the popular press. At the time, the term polar vortex in scientific literature most commonly described the stratospheric polar vortex, often without explicit qualification (e.g., Wang et al., 2014); some studies also used "polar" or "circumpolar" vortex to describe a "tropospheric polar vortex" without further qualification (e.g., Wallace et al., 2014; Yu and Zhang, 2015). Waugh et al. (2017) sought to dispel myths about the polar vortex. They described the stratospheric and tropospheric "circumpolar" vortices as the terms had been commonly used in scientific literature, highlighted their differences and relationships to extreme weather events, and provided recommendations for describing them in public forums. Unfortunately, while this work is widely cited, the two concepts are still often conflated or not clearly distinguished, sometimes on educational sites, in studies on climate change communication, or within the atmospheric science community (e.g., Shepherd, 2016; Lyons et al., 2018; UC Davis, 2019; UCAR, 2021; Bushra and Rohli, 2021; Dai et al., 2021; Kömüşcü and Oğuz, 2021).

**Box 4-1 Figure 1** shows examples on two dates (chosen during periods in which CAOs were described in the popular press as polar vortex "outbreaks" or "attacks") depicting the stratospheric polar vortex and the upper-tropospheric jet streams (the dynamical features most closely aligned with common definitions of a "tropospheric polar vortex"). **Box 4-1 Table 1** summarizes key differences between the tropospheric and stratospheric circulations in relation to the "polar vortex."

The stratospheric polar vortex is consistently defined as bounded by the polar night jet, the strong band of eastward winds throughout the stratosphere that forms in the fall and weakens and reverses in spring. Several diagnostics can be used to define the stratospheric polar vortex edge (Lawrence and Manney, 2018, and references therein), any of which pick out approximately the same physically meaningful boundary from the lowermost into the upper stratosphere. ***The stratospheric polar vortex is a single persistent feature that dominates the circulation of and transport throughout the polar stratosphere in fall through spring.***

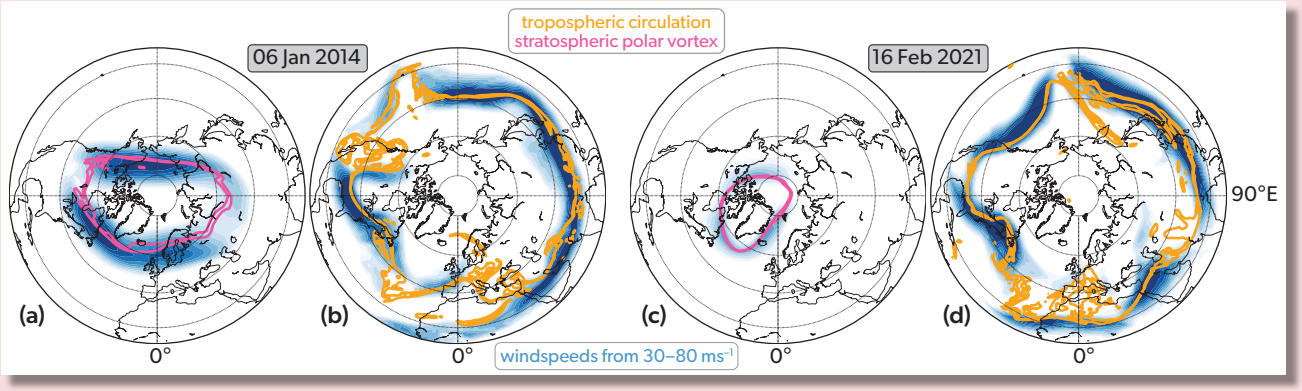


**Box 4-1 Figure 1.** Maps showing the (a, c) stratospheric polar vortex and (b, d) upper-tropospheric jet stream wind speeds (blue color fill) and "vortex edge" contours (magenta for stratosphere, orange for troposphere) on dates during CAOs in two Arctic winters. [Adapted from Manney et al., 2022.]

There is no consensus on the definition of a "tropospheric polar vortex" or on the altitude(s) at which it is defined. Waugh et al. (2017), and articles they cite, used one common method that defined the tropospheric polar vortex such that its edge approximately follows the axis of an upper tropospheric jet stream. These jets have maxima that are very localized in altitude compared to the stratospheric polar night jet, and they vary strongly with longitude (e.g., Manney et al., 2011b, 2014; and references therein; **Box 4-1 Figure 1b, d**). Because smaller-scale motions dominate tropospheric dynamics, ***a "tropospheric polar vortex" by any definition is not a single coherent circumpolar circulation that plays a central role in tropospheric dynamics and transport***.

The stratospheric polar vortices profoundly affect ozone distributions via their role as transport barriers, isolating species involved in ozone depletion from mid-latitude air. This results in strong ozone gradients across those vortex edges, which in turn lead to very different ozone concentrations inside and outside the stratospheric polar vortices. Polar stratospheric chemical processing and ozone destruction are commonly analyzed from a vortex-centered perspective (e.g., *Sections 4.2.3* and *4.2.4*), and the amount of polar ozone loss in a given spring is controlled by the strength and coldness of the winter/springtime stratospheric polar vortex. In contrast, upper troposphere/lower stratosphere (UTLS) ozone variability is dominated by regional variations in stratosphere-troposphere exchange and differences in the amount of ozone in the lower stratosphere that can be transported into the troposphere (e.g., Albers et al., 2018; Olsen et al., 2019; Breeden et al., 2021). The former depends critically on regional variations

in the upper-tropospheric jets and tropopause, and the latter on stratospheric variability (and thus on stratospheric polar vortex conditions). Unlike in the stratosphere, ozone in the troposphere does not show strong gradients on a hemispheric scale, except at the subtropical boundary that separates higher-ozone stratospheric air at mid-latitudes from lower-ozone tropospheric air at low latitudes (e.g., Manney et al., 2022).

CAOs are described as "polar vortex events" in the media and in venues such as peer-reviewed papers on communication of climate change risks (e.g., Lyons et al., 2018), but, based on the dynamical processes involved, they are best described as excursions of the upper-tropospheric jet stream, such as southward advection of cold Arctic air. While they are sometimes described as "local" variations of the tropospheric polar vortex "edge," they are not generally correlated with the strength of the globally defined tropospheric polar vortex (e.g., Celliti et al., 2006; Waugh et al., 2017; Bushra and Rohli, 2021; and references therein), so the usefulness of that description is limited at best. Sudden stratospheric warmings (SSWs, which weaken/disrupt the stratospheric polar vortex) have been linked to some CAOs (e.g., Butler et al., 2017; Domeisen and Butler, 2020; Huang et al., 2021; and references therein), and the media often hails reports of an SSW with warnings that "the polar vortex is coming" and predicts a CAO. That connection is, however, probabilistic, and CAOs may be associated with either strong (**Box 4-1 Figure 1a, b**; January 2014) or weak (**Box 4-1 Figure 1c, d**; February 2021, following an SSW) stratospheric polar vortices. The effects of the stratospheric polar vortex depend on the location of the CAOs and other characteristics of the stratospheric polar vortex in addition to its strength (e.g., Kretschmer et al., 2018; Lee et al., 2019; Cohen et al., 2021).

It is thus clear that, as discussed by Manney et al. (2022), describing the stratospheric polar vortex as the primary factor dominating stratospheric variability and influencing the surface (with probabilistic links to extreme weather events) is accurate and useful. On the other hand, the most relevant features of the tropospheric circulation, particularly those linked to extreme weather events, are best described as local excursions of the tropospheric jet streams. The term "polar vortex" is best used to denote the stratospheric cool-season circulation. However, because that term often is used inappropriately for other atmospheric features, the more precise term "stratospheric polar vortex" should be used for clarity.

**Box 4-1 Table 1.** Key differences between the stratospheric and tropospheric polar vortices.

| Stratospheric Circulation / Stratospheric Polar Vortex | Tropospheric Circulations / Upper-Tropospheric Jet Streams |
|---|---|
| Deep feature extending from the tropopause (about 12–15 km) to the stratopause (about 50–60 km). | Circulation influence of extratropical upper-tropospheric jets is limited by vertically localized wind speed maxima that are strongest in a few-km region centered near 12 km (9 km) altitude at lower (higher) latitudes. No consensus on level at which a "tropospheric polar vortex" is defined. |
| Unique feature whose variations in strength, size, and position dominate the stratospheric circulation in late fall through spring. | No single global feature dominates the circulation; impactful circulation systems / weather (e.g., winter storms) primarily linked to local jet stream excursions rather than to an overall strong or weak circumpolar vortex. |
| Trace gas transport is closely aligned with the vortex; the vortex edge is a global transport barrier whose strength determines the degree of mixing across it. | Transport controlled by upper-tropospheric jet and tropopause variations; jets represent a transport barrier only in regions where they are strong, not around the globe. |
| Provides the "containment vessel" in which lower-stratospheric chemical ozone loss occurs; thus variations in strength/coldness dominate interannual variability in ozone. | Upper-tropospheric ozone variability primarily controlled by ozone abundances in the lowermost stratospheric reservoir and local jet / tropopause variations that lead to stratosphere-troposphere exchange. |

Several methods of estimating chemical ozone loss have been used in polar ozone studies (for a concise summary, see Newman, Rex et al., 2007), all of which are subject to considerable uncertainties (Livesey et al., 2015; Griffin et al., 2019). Estimates of chemical ozone loss in the Arctic in 2020 are nonetheless in broad agreement in that they all indicate exceptional depletion. The peak chemical loss occurred around the 450 K potential temperature surface, which corresponds to about 16–18 km above the surface. Estimates of the cumulative chemical ozone destruction at that level range between 2.2 and 3.4 ppmv (Wohltmann et al., 2020; Manney et al., 2020; Kuttippurath et al., 2021), at least 75% of the initial ozone abundance. The maximum loss within the vortex core was higher and is estimated to be as large as 93% (Wohltmann et al., 2020). These values are similar to those for 2011, although the maximum depletion in 2020 occurred at a lower altitude, amounting to a larger ozone mass loss in 2020. These maximum values significantly exceed ozone destruction during a typical Arctic spring and approach the range characteristic for the Antarctic, although in the Antarctic, such severe depletion affects a broader range of altitudes and a larger portion of the polar vortex (Wohltmann et al., 2020; Solomon et al., 2014; Livesey et al., 2015). Observation and model-based estimates of the vortex-averaged and vertically integrated loss in the lower stratosphere range between 105 and 131 DU (Weber et al., 2021; Wohltmann et al., 2020; Grooß and Müller, 2021), where the latter value is limited to the vortex core and includes a small amount of chemical loss that occurred in November. Estimates of the total column net ozone loss (implicitly including middle- and upper-stratospheric photochemical ozone production) are 88 and 106 DU, depending on the method used (Weber et al., 2021). These estimates of column ozone loss are quantitatively similar to those for 2011. However, because the March polar vortex area in 2020 was about 25% larger than that in 2011, ozone loss integrated over the vortex was more extensive in 2020 (Weber et al., 2021).

## 4.3 UNDERSTANDING OF POLAR OZONE PROCESSES

The chemical and dynamical processes controlling polar stratospheric ozone are generally well understood and have been discussed in detail in previous Assessments (e.g., Dameris, Godin-Beekmann et al., 2014; Langematz, Tully et al., 2018). Since the last Assessment, research has focused on refining our understanding of both chemical and dynamical influences on polar ozone, thus reducing uncertainties in model projections of future polar ozone in a changing climate. For example, the fundamental understanding of polar stratospheric cloud (PSC) formation pathways and particle characteristics has progressed, and multi-decadal trends in PSC occurrence could be analyzed for the first time (*Section 4.3.1*). High-resolution measurements obtained from research aircraft campaigns in the UTLS provided new insight into chlorine chemistry (*Section 4.3.2*). *Section 4.3.3* raises the potential but still rather uncertain role of iodine as a halogenated very short-lived substance (VSLS) contributing to chemical ozone depletion. New pathways of dynamical forcing of Arctic ozone associated with future Arctic sea ice decline and North Pacific sea surface temperature anomalies (SSTAs) are addressed in *Section 4.3.4*. Other factors influencing polar stratospheric ozone (*Section 4.3.5*) include, in particular, the role

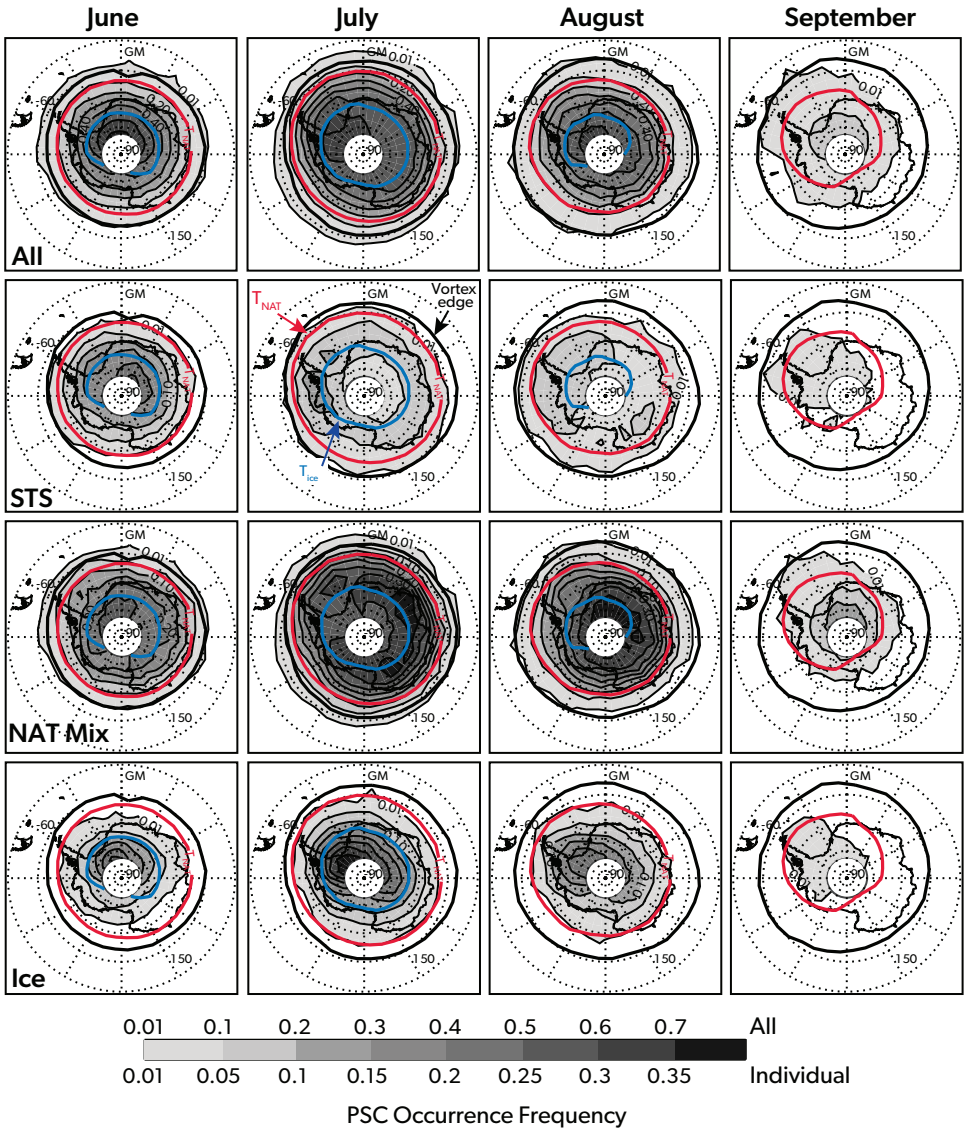


**Figure 4-12.** Monthly mean polar maps of CALIOP Antarctic PSC occurrence frequency at 500 K (~20 km), averaged over 2006–2018. *(row 1)* All PSCs. *(row 2)* Supercooled ternary solution (STS). *(row 3)* NAT mixtures, including enhanced NAT due to mountain waves. *(row 4)* Ice, including wave ice. Black contours show the mean vortex edge. Solid red and blue contours, respectively, enclose regions where mean $T < T_{NAT}$ and $T < T_{ice}$. The white region over the pole is not sampled by CALIOP. Note that different grayscale ranges are used for "all" PSCs and "individual" compositions. [Adapted from Tritscher et al., 2021, updated from Pitts et al., 2018.]

of wildfire emissions, such as those from the severe bushfires in southeastern Australia in late December 2019 and early January 2020, and the possible ozone depletion by the emissions of a fleet of supersonic and hypersonic aircraft, currently under consideration for future civil transportation.

### 4.3.1 Polar Stratospheric Clouds: Observations and Modeling of PSC Occurrence, Extent, and Composition

The critical role of PSCs in affecting polar ozone and chlorine chemistry is considered to be well understood (see Dameris, Godin-Beekmann et al., 2014, and Langematz, Tully et al., 2018, for a more detailed description). Nevertheless, as discussed in Dameris, Godin-Beekmann et al. (2014), uncertainties still exist in various aspects, for example the nucleation mechanism for nitric acid trihydrate (NAT) particles, including large "NAT-rocks," or the origin and effects of refractory particles (low-volatility particles of terrestrial or extraterrestrial origin that can promote heterogeneous nucleation). This section reviews the progress made in closing the gaps on the extent, composition, and formation mechanisms of PSCs since the last Assessment. A more comprehensive review is provided by Tritscher et al. (2021).

Following Tritscher et al. (2021), the term "composition" as it relates to PSCs includes their chemical components (e.g., stratospheric sulfuric acid aerosols [SSA, $H_2SO_4$-$H_2O$], supercooled ternary solution [STS, $H_2SO_4$-$HNO_3$-$H_2O$] droplets, nitric acid trihydrate [NAT, $HNO_3 \bullet 3H_2O$] or other hydrates of $HNO_3$ or $H_2SO_4$, or $H_2O$ ice), particle phase states (e.g., droplets or crystals), and states of mixing. Contemporary observations by three spaceborne instruments—MIPAS, MLS, and CALIOP—provide an unprecedented seasonal polar vortex-wide data record of PSC occurrence and composition in both hemispheres from 2002 to present (2021; Pitts et al., 2018; Höpfner et al., 2018; Spang et al., 2018; Tritscher et al., 2021). A detailed comparison of these datasets revealed consistency in the PSC coverage between CALIOP and MIPAS, and in PSC composition for homogeneous cloud scenes between CALIOP, MIPAS, and MLS. Agreement between PSCs observed by the spaceborne instruments and ground-based lidars in Antarctica is also good regarding the general features of the PSC season, such as the occurrence in the different composition classes and its altitude dependence during the season. However, differences were detected on the basis of daily observations, mainly owing to the high geographic variability of PSCs (Snels et al., 2019, 2021). The new PSC climatology allows further analyses of PSC characteristics, such as the seasonal, geographical, and height coverage of the different PSC composition classes and their interannual variability. **Figure 4-12** shows the 2006–2018 average of monthly mean polar maps of CALIOP Antarctic PSC occurrence frequency at about 20 km altitude for different PSC composition classes. PSC occurrence is roughly bounded by the $T < T_{NAT}$ contour and increases poleward, with the highest occurrence frequencies (>60%) generally located within the region of $T < T_{ice}$. The contours of the frequency of PSC occurrence and of the cold pool are pushed slightly off the pole toward the Antarctic Peninsula, in association with frequent mountain wave activity (i.e., wave ice in **Figure 4-12**) in this region, as also found by Spang et al. (2018) in PSC observations from MIPAS.

With the new CALIOP PSC climatology, it became possible to investigate multi-decadal trends in PSC occurrence by comparing the CALIOP dataset from 2006–2017 with the Stratospheric Aerosol Measurement (SAM) solar occultation PSC occurrence record from 1978–1989 (Poole and Pitts, 1994). It was found that in the Antarctic, PSC occurrence is very similar between the two periods, whereas in the Arctic PSC occurrence has significantly increased in early winter (December and January; Pitts et al., 2018). This different development of Arctic versus Antarctic PSC occurrence is consistent with lower-stratospheric temperature trends derived from MSU4 satellite observations, which show a significant Arctic cooling in December and January for the period 1998–2016, while Antarctic temperature changes in this period are small relative to the period 1979–1997 (Figure 5-6a, c in Karpechko, Maycock et al., 2018). The Arctic PSC increase may have had implications for Arctic lower-stratospheric ozone, which decreased between 1998 and 2018 (Hu et al., 2022; see also *Section 4.3.4.3*). Any future cooling of the Arctic lower stratosphere (either by reduced dynamical forcing from the troposphere or induced by climate change) is expected to enhance PSC occurrence and—provided ozone-depleting substances (ODSs) are still present—reduce lower-stratospheric ozone abundances.

In the previous Assessment, two major NAT particle formation mechanisms were discussed: homogeneous nucleation from STS droplets, producing large NAT particles relevant for explaining the observed denitrification, and heterogeneous nucleation of NAT on ice, producing small particles. It was also proposed that refractory particles of meteoritic origin might serve as condensation nuclei of large NAT particles, so-called NAT-rocks (Langematz, Tully et al., 2018, and references therein). As reviewed by Tritscher et al. (2021), the fundamental understanding of PSC formation pathways and particle characteristics has advanced since then. While there are strong indications that homogeneous nucleation of NAT particles from STS droplets seems to be largely suppressed under stratospheric conditions, two heterogeneous NAT nucleation processes exist: NAT nucleation on ice, which has been shown to be efficient in mountain wave ice clouds; and NAT nucleation on foreign nuclei, observed at $T > T_{ice}$. The heterogeneous nuclei may be of meteoritic origin, although other refractory materials or organics have also been identified in stratospheric aerosol particles (James et al., 2018; Schneider et al., 2021).

As reported in Dameris, Godin-Beekmann et al. (2014) and Langematz, Tully et al. (2018), unusually large PSC particles, also called NAT-rocks, had been detected in earlier Arctic aircraft campaigns. They are of interest as sequestering of nitric acid in these particles might lead to efficient denitrification (Tritscher et al., 2021, and references therein). By applying a new method to detect such populations of $HNO_3$-containing particles using infrared limb observations, populations of aspherical NAT particles with median radii ≥3 μm were detected vortex-wide during Arctic winter 2011/12 (Woiwode et al., 2019). The study emphasizes the key role of the detected particles for the denitrification of the Arctic winter stratosphere. However, the measured extensive gas-phase $HNO_3$ sequestration and condensed gas-phase equivalent $HNO_3$ of 10 ppbv or more exceed model simulations for different Arctic winters by up to one order of magnitude. Likewise, models fail to reproduce the long persistence and slow sedimentation of the detected populations, which might be due to the highly aspherical shape of the detected particles and their lower fall speeds (Westbrook, 2008; Woiwode et al., 2019).

## 4.3.2 Polar Chemistry: Observations and Modeling

### *4.3.2.1 Observations*

Since the last Assessment, various studies have focused on the chlorine and bromine chemistry in the polar lowermost stratosphere during the exceptionally cold Arctic winter of 2015/16. Extreme meteorological conditions early in the 2015/16 winter induced rapid ozone loss, until a sudden stratospheric warming at the beginning of March 2016 curtailed further chemical processing. High-resolution and high-accuracy datasets obtained from instruments onboard the High Altitude and LOng Range Research Aircraft (HALO) allowed the variations in trace gas distributions in the UTLS over the course of this exceptional Arctic winter to be probed in fine detail.

A consistent series of in situ high-resolution mass spectrometric observations of HCl and $ClONO_2$ from the AIMS instrument onboard HALO was analyzed to study the chemistry of the lower-stratospheric outflow region of the 2015/16 Arctic polar vortex, together with total inorganic chlorine ($Cl_y$) and active chlorine ($ClO_x$) derived from simultaneous measurements of CFC-12. The new data highlight the altitude dependence of the pathway for chlorine deactivation in the lowermost vortex, with HCl dominating below the 380 K isentropic surface and $ClONO_2$ prevailing above (Marsing et al., 2019).

Chlorine activation and deactivation in the lowermost stratosphere during the 2015/16 Arctic winter were further analyzed utilizing time series of satellite measurements, remote-sensing measurements from the airborne limb imager GLORIA, and simulations with atmospheric models (Johansson et al., 2019). Time series of the satellite measurements reveal unusually low HCl and $ClONO_2$ at 380 K from the beginning of January to the end of February 2016, while ClO was strongly enhanced. In March 2016, unusually rapid chlorine deactivation into HCl was observed instead of deactivation into $ClONO_2$, the more typical pathway for deactivation in the Arctic. This is explained by very low ozone abundances together with low temperatures, conditions that favor HCl reformation. During this exceptional Arctic winter, the high-resolution GLORIA instrument observed strongly enhanced $ClONO_2$ values of up to 1100 pptv in the tropopause region, showing mesoscale structures in the two-dimensional vertical cross sections of $ClONO_2$ that result in part from local chlorine deactivation and in part from transport of previously deactivated air. In addition, GLORIA measurements of $ClONO_2$ and $O_3$ were used to evaluate simulations from a chemistry transport model and a chemistry climate model; the comparisons showed agreement within the expected performance of both models (Johansson et al., 2019).

GLORIA observations along the flight track of HALO together with tracer-tracer correlations also enabled the quantification of $HNO_3$ distributions in the lowermost stratosphere with high spatial resolution throughout the Arctic winter 2015/16. Large-scale as well as local fine structures with enhanced absolute $HNO_3$ volume mixing ratios as high as 11 ppbv were found at altitudes of 13 km in January, with nitrified filaments persisting until the middle of March (Braun et al., 2019). Narrow coherent structures tilted with altitude of enhanced $HNO_3$, observed in mid-January, were interpreted as regions recently nitrified by sublimating $HNO_3$-containing particles.

Calculations of $Cl_y$ in the lower stratosphere derived from chlorinated source gas measurements onboard the HALO aircraft during the campaign in the Arctic in 2015/16 were compared with those from a campaign in the Antarctic in austral winter/spring 2019 (Jesswein et al., 2021). A new air mass classification system was used, based on high-resolution in situ measurements during the campaigns, to map measurements to the vortex, vortex boundary region, and mid-latitudes. Although the Antarctic vortex was unusually weak in 2019 in the wake of a minor sudden warming, up to 50% of the total chlorine could be found in inorganic form inside the vortex at about 5 km above the tropopause. In the mid-latitudes, only about 15% of the total chlorine was found in inorganic form. In contrast to the Antarctic polar vortex in 2019, the Arctic polar vortex in 2015/16 was one of the strongest compared to previous years (Matthias et al., 2016). At a comparable altitude inside the vortex, only around 40% of total chlorine was found in inorganic form, whereas roughly 20% was found at mid-latitudes. Inside the respective vortices, the amount of $Cl_y$ was higher during the Southern Hemisphere campaign than during the Northern Hemisphere campaign by up to 540 ppt (at the same altitude).

### *4.3.2.2 Theoretical Basis and Modeling*

In Langematz, Tully et al. (2018), the chemical reactions involved in polar ozone depletion were discussed for specific winters, including the relevant reaction pathways and cycles. Since then, this work has been continued (Zafar et al., 2018), and the known stratospheric chemistry has been evaluated for the Arctic winter and spring 2020/21 (Feng et al., 2021; Grooß and Müller, 2021).

The record ozone depletion in the Arctic spring 2020 is well reproduced by chemical transport models (CTMs) that include state-of-the-art chemistry schemes and that obtain meteorological information from reanalyses, such as the CLaMS and TOMCAT chemistry models. As discussed in detail in *Section 4.2.4.2*, the simulated stratospheric ozone loss in Arctic spring 2020 in both CTMs agrees well with satellite observations and balloon-borne ozone sondes (Grooß and Müller, 2021; Feng et al., 2021; Weber et al., 2021), demonstrating that known stratospheric chemistry in combination with transport can explain the observed severe Arctic ozone depletion for the specific meteorological conditions in winter/spring 2019/20 (i.e., a stable stratospheric polar vortex and low temperatures).

Despite the capability of state-of-the-art CTMs to reproduce the observed polar ozone depletion, one open issue, already noted in the previous Assessment (Langematz, Tully et al., 2018), remains unresolved. Analysis of chlorine chemistry in current CTMs and CCMs (chemistry-climate models) revealed that the simulated HCl depletion in the cold and dark early-winter polar vortex is too weak and occurs too late compared to that observed (Wohltmann et al., 2017; Grooß et al., 2018). This discrepancy, which is more prominent in the Antarctic but has also been seen in cold Arctic winters (Grooß et al., 2018; Grooß and Müller, 2021), seems to be due to some unknown process. As the HCl discrepancy occurs in early winter, when ozone loss rates are slow, its effect on the ozone column loss throughout the Antarctic winter and spring is minor (~2%; Grooß et al., 2018).

As discussed in Langematz, Tully et al. (2018), high levels of active chlorine are maintained in the core of the Antarctic lower-stratospheric polar vortex during spring, despite rapid

gas-phase production of HCl. Maintenance of active chlorine is achieved through HCl null cycles in which HCl production is balanced by immediate reactivation (Müller et al., 2018). Using box-model simulations representative of vortex core conditions, Zafar et al. (2018) showed that the chemistry of the methyl peroxy radical ($CH_3O_2$) is essential for these HCl null cycles and thus for Antarctic lower-stratospheric chlorine and ozone loss chemistry.

### 4.3.3 Very Short-Lived Halogenated Substances

Chemical destruction of ozone in the polar spring occurs through catalytic cycles involving ClO and BrO radicals. These species are part of the inorganic chlorine and bromine families, which are produced in the stratosphere following the degradation of natural and anthropogenic source gases. Because air in the polar lower stratosphere is aged, even ODSs with relatively long lifetimes (decades or more) are largely decomposed to the inorganic families. Therefore, the contribution of different chlorine- and bromine-containing source gases to polar ozone depends on the additional amount of Cl or Br delivered to the stratosphere, which provides a way of comparing the impact of chlorine and bromine VSLSs on polar ozone with longer-lived species.

Natural brominated VSLSs (e.g., $CHBr_3$ [bromoform] and $CH_2Br_2$ [dibromomethane]) transport around 5 ppt bromine to the stratosphere (see discussion in *Chapter 1*) out of the current total bromine loading of around 20 ppt. This bromine will have a proportionate effect on polar ozone loss that occurs via the BrO + ClO catalytic cycles. Although there are few direct recent observations in the polar region, the contribution of VSLSs to polar bromine is expected to be similar to the mean contributions (sum of product gas and source gas injection) at lower latitudes (Wang et al., 2019; Barrera et al., 2020; Fiehn et al., 2018; Filus et al., 2020; Adcock et al., 2021), for which there is no observational evidence of a long-term trend. In situ aircraft observations of total and speciated bromine from aircraft flights in the late summer and fall UTLS at northern middle and high latitudes confirmed estimates of the current mean bromine loading of 19.2 ± 1.2 ppt and also found evidence for a somewhat variable stratospheric input of short-lived bromine species such that there are regions of higher bromine of 20.9 ± 0.8 ppt (Rotermund et al., 2021). Understanding this variability is important for understanding extra-polar transport pathways, but the impact on polar ozone loss will depend largely on the mean abundance of bromine. As the levels of brominated ODSs decrease, natural bromine, including VSLSs, will make a relatively larger contribution to polar ozone loss.

Chlorinated VSLSs are mainly anthropogenic in origin (e.g., dichloromethane [$CH_2Cl_2$]) and currently contribute around 130 (100–160) ppt (**Table 1-6**) to the current total chlorine loading of around 3500 ppt. The chlorine from VSLSs is thus expected to make a proportional contribution to polar ozone loss through the main ClO + ClO and ClO + BrO catalytic cycles. An increase in chlorinated VSLSs (Hossaini et al., 2019; Harrison et al., 2019; Claxton et al., 2020) is estimated to have slowed the decline of long-lived HCl in the upper stratosphere in the period 2004–2017 by about 15% (Hossaini et al., 2019).

There is renewed interest but significant uncertainty in the possible role of iodine in stratospheric chemistry. Iodine is present in very small abundances and is largely natural in origin (*Chapter 1*). Previous estimates of the upper limits on the amount of iodine reaching the stratosphere have recently been revised upward, to up to 1 ppt (Koenig et al., 2020). CCM simulations show that stratospheric iodine abundances consistent with those from low-latitude observations (0.77 ppt; Koenig et al., 2020) could contribute 4% of the observed Antarctic springtime column ozone loss, equivalent to the loss induced by 3.1 pptv bromine (Cuevas et al., 2022). Further work is needed to assess the uncertainties in iodine chemistry and elucidate the possible role that iodine trends may play in polar ozone trends.

### 4.3.4 Dynamical Impacts on Polar Ozone

#### *4.3.4.1 Synthesis of the Role of Dynamics in the Last Four Arctic and Antarctic Springs*

As discussed in *Sections 4.2.3* and *4.2.4*, the evolution of total column ozone (TCO) in the four Arctic and Antarctic springs since the last Assessment was characterized by large interannual variability. In the Northern Hemisphere, a series of three springs with weak ozone loss (2018, 2019, 2021) was interrupted in spring 2020, when record-low TCO was measured over the Arctic. In the Antarctic, ozone holes consistent in size and depth with what is expected from the slow decline in ODSs appeared in three of the four spring seasons (2018, 2020, 2021), while in the Southern Hemisphere spring of 2019, an unusually weak ozone hole developed. Also noteworthy was the record persistence of the 2020 and 2021 Antarctic ozone holes well into December. Although the weak Antarctic ozone loss in 2019, the strong Arctic ozone loss in 2020, and the duration of the 2020 and 2021 Antarctic ozone holes were exceptional, they are in line with the current understanding of the chemical and dynamical factors that determine polar ozone loss.

As explained in more detail in previous Assessments (e.g., Dameris, Godin-Beekmann et al., 2014; Langematz, Tully et al., 2018), polar ozone loss is controlled by both chemical and dynamical processes. In most Northern Hemisphere winters, tropospheric planetary waves propagate upward into the stratosphere, where they weaken the stratospheric polar vortex and warm the Arctic stratosphere. These effects lead to reduced chemical ozone depletion and enhanced descent of ozone-rich air into the lower stratosphere by the Brewer-Dobson circulation (BDC) and thus to higher ozone abundances throughout winter and spring. During sudden stratospheric warmings (SSWs), for example, Arctic TCO may increase rapidly by up to about 50 DU due to eddy transport linked to enhanced wave drag (de la Cámara, 2018; Hong and Reichler, 2021). After SSW events, the eddy transport of ozone is reduced in the upper stratosphere, leading to a more rapid decay in ozone toward climatological values than in the lower stratosphere, where isentropic irreversible mixing delays the return to pre-SSW values (de la Cámara, 2018; Hong and Reichler, 2021). In contrast, in winters with weak planetary wave activity, as is common in the Southern Hemisphere, stable and large polar vortices enclosing cold air develop, providing conditions for efficient chemical ozone depletion. In combination with suppressed dynamical replenishment of ozone, strong and occasionally long-lasting ozone loss occurs, as was the case in the austral springs of 2020 and 2021.

Both the weak Antarctic ozone hole in 2019 and the strong Arctic ozone loss in March 2020 resulted from atypical dynamical conditions in the respective winters. In September 2019,

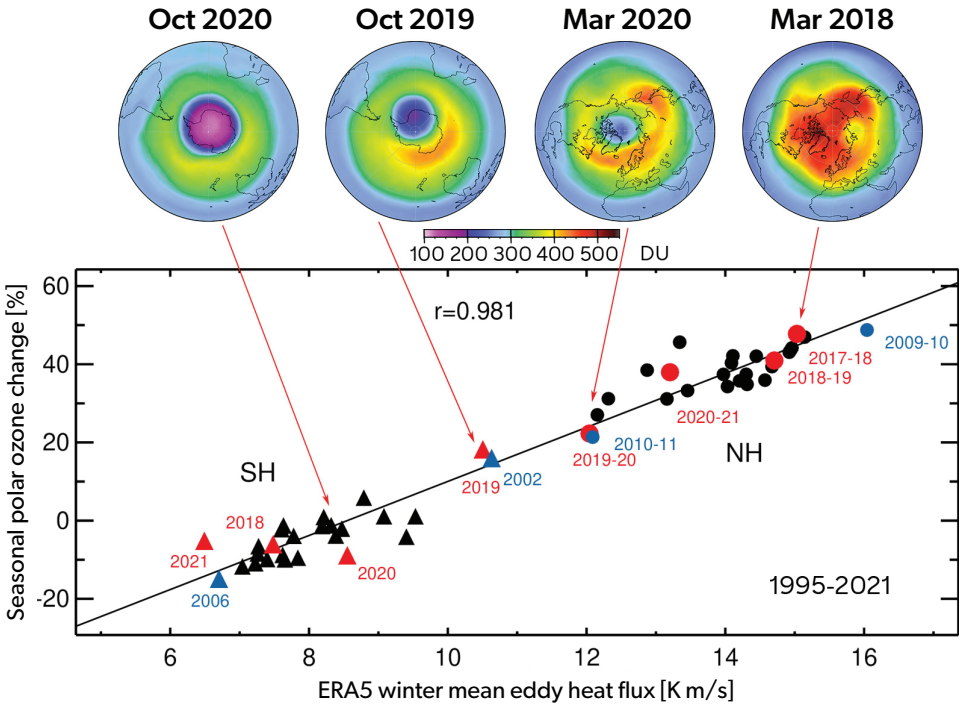


**Figure 4-13.** Observed polar cap (>50° latitude) total column ozone (TCO) change between spring and the preceding autumn (%) as a function of the extratropical winter-mean eddy heat flux (September to March in the Northern Hemisphere [NH, dots] and March to September in the Southern Hemisphere [SH, triangles]) derived from GOME-SCIAMACHY-GOME-2 ozone (1995–2021) and ECMWF ERA5 meteorological data (1995–2021) separately in each hemisphere. The four recent SH and NH winters are labeled in red. Years with extreme low and high TCO in either hemisphere are labeled in blue. Polar TCO distributions from GOME-2B for two selected recent years in the Antarctic *(left pair)* and Arctic *(right pair)* are shown at the top. [Updated from Weber et al., 2011, and Langematz, Tully et al., 2018.]

chemical ozone depletion was halted by a strong minor SSW that weakened the polar vortex and warmed stratospheric air above PSC formation temperatures (see *Section 4.2.3.2*). In the Arctic winter 2019/20, the stratospheric polar vortex was the strongest and most persistently cold in over 40 years, leading to enhanced chemical ozone depletion and reduced dynamical replenishment of ozone (see *Section 4.2.4.2*). While anomalous, both cases are fully in line with the established linear relationship between the seasonal high-latitude TCO change between autumn and the following spring and the mid-latitude winter-mean eddy heat flux, used as a metric for dynamical activity (Weber et al., 2011; **Figure 4-13**). These two winters are very close to the previous extreme cases in austral spring 2002 and boreal spring 2011 and bridge the two separated Northern and Southern Hemisphere value clusters.

### *4.3.4.2 Predictability of Arctic Spring Ozone*

The dominant role of dynamical variability for Arctic spring ozone gives rise to the question of whether polar spring ozone is predictable based on meteorological forecast systems. The evolution of Arctic ozone in spring is strongly coupled to the evolution of the stratospheric polar vortex throughout the previous winter (e.g., Weber et al., 2011). To predict the stratospheric state in winter, meteorological forecast systems need to capture both stratospheric extremes, i.e., strong polar vortex events, which may last for several weeks, sometimes enhanced by wave reflection, and SSWs, which evolve more rapidly and are driven by tropospheric planetary wave forcing. Both states are additionally affected by the phases of the 11-year solar cycle, the Quasi-Biennial Oscillation (QBO), and the El Niño-Southern Oscillation (ENSO). Forecasts from six seasonal prediction systems consistently predicted the extreme Northern Hemisphere stratospheric polar vortex in winter 2019/20, with the ensemble mean forecasts for January/February/March 2020 from two models exceeding any equivalent in their hindcast periods (Lee et al., 2020). This study showed that seasonal prediction systems are able to produce exceptional signals for a strong stratospheric polar vortex. The prediction skill of Arctic ozone in the three Arctic springs with strongest ozone loss (1997, 2011, 2020) was assessed by Rao and Garfinkel (2020, 2021). They found predictive skill for low March 2011 Arctic ozone when initializing the seasonal forecast systems in early March and then applying empirical models using different forecasted metrics of the stratospheric polar vortex as predictors. The predictive skill from these empirical models, however, was lower than the ozone prediction from the chemical scheme of the forecast system that provided the meteorological input fields to the empirical models. March ozone loss in 2011 was more predictable than the 1997 and 2020 ozone losses, possibly due to more favorable meteorological background conditions (Rao and Garfinkel, 2020).

### 4.3.4.3 Arctic Winter Variability Under Climate Change

As discussed in recent Assessments (e.g., Langematz, Tully et al., 2018, and references therein), year-to-year variability and trends in Arctic ozone in winter and spring are strongly influenced by dynamical processes. Upward propagating and dissipating planetary waves, often associated with SSWs, lead to weaker stratospheric polar vortices with higher temperatures, thus reducing the number of days cold enough for heterogeneous chemical ozone depletion. In addition, the BDC is enhanced in years with high planetary wave activity, which leads to a stronger poleward-downward transport and increased meridional mixing of ozone-rich air into the Arctic stratosphere. Simulations with climate and chemistry-climate models consistently project an increase of the BDC in a future climate with enhanced greenhouse gas (GHG) abundances (Karpechko, Maycock et al., 2018; see also *Section 5.2.4*). Hence, more ozone would be transported to Northern Hemisphere high latitudes in winter and spring, and Arctic ozone recovery would be accelerated. On the other hand, no robust evidence of future changes in major SSWs was found in a multi-model assessment of CCMI projections of the 21st century (Ayarzagüena et al., 2018). An analysis of CMIP6 climate model projections for quadrupled carbon dioxide ($CO_2$) concentrations revealed that the SSW frequency is sensitive to an increase in $CO_2$ forcing; however, there was no consensus among the models on the sign of these changes in SSW frequency (Ayarzagüena et al., 2020).

Changes in SSW occurrence in a future climate—in either direction—will likely be driven by changes in the dynamical forcing from tropospheric planetary waves in combination with a changed stratospheric background climatology. For example, Langematz, Tully et al. (2018) discussed in detail the impact of the dynamical forcing of the polar stratosphere by sea surface temperature anomalies (SSTAs) in the tropical Pacific Ocean during ENSO. Likewise, SSTAs over the North Pacific were suggested to have significant effects on the stratospheric Arctic vortex via dynamical processes (e.g., Hurwitz et al., 2012; Hu et al., 2018; Li et al., 2018). A link between North Pacific SSTAs and ozone was suggested by Hu et al. (2022), who show that about 30% of the observed negative ozone trend in the Arctic lower stratosphere in March, derived from MERRA-2 reanalyses for the period 1998–2018, can be explained by North Pacific SSTAs in February, associated with the second leading mode (PC2), the so-called Victoria mode, of North Pacific SST variability (Bond et al., 2003). Arctic ozone concentrations decrease with the warm phases of Victoria mode–related North Pacific SSTAs and increase with its cold phases. The decrease in Arctic lower-stratospheric ozone during 1998–2018 is consistent with an increase in the PC2 of the North Pacific SSTAs. The Victoria mode–related SSTAs tend to weaken the Aleutian low, thus impeding the upward propagation of wavenumber-1 waves into the subpolar lower stratosphere. As a result, the BDC is weakened and less ozone is transported from the ozone-rich middle stratosphere to the ozone-poor lower stratosphere. The derived Arctic lower-stratospheric ozone decrease in 1998–2018 was thus to a large degree the result of natural decadal SST variability rather than evidence for continuous chemical ozone depletion by ODSs.

In recent years, a further potential source of dynamical forcing of the stratosphere has attracted increasing attention. This forcing is driven by the observed seasonal decline in Arctic sea ice concentration over the last decades, particularly in the Barents and Kara (BK) Seas. A stratospheric pathway has been proposed that links Arctic sea ice decline and mid-latitude weather anomalies. The hypothesis is that decreased sea ice cover during early winter, especially over the BK Seas, enhances the upward propagation of planetary waves with wavenumbers 1 and 2, subsequently weakening the stratospheric polar vortex in mid-winter (Kim et al., 2014; Nakamura et al., 2016). So far, no consensus has been reached on the influence of the Arctic sea ice decline and the associated Arctic warming (Arctic amplification) on European mid-latitude winter weather (see Cohen et al., 2020, for a review). However, modeling studies with regional sea ice melt confined to the BK Seas and a well-resolved stratosphere do simulate a weakened stratospheric polar vortex and a cooling of the mid-latitudes in winter, consistent with the observations (Screen, 2017; Zhang et al., 2018; Mori et al., 2019; Hoshi et al., 2019). In an analysis of CMIP5 simulations forced with the high RCP8.5 GHG emissions scenario, Kretschmer et al. (2020) found a nonlinear response of the stratospheric polar vortex to a future global mean warming that includes a weakening of the vortex caused by sea ice loss in the BK Seas and an opposite vortex response once the BK Seas are ice free. The identified polar vortex weakening is accompanied by an increase of the eddy heat flux at 100 hPa, indicating enhanced dynamical forcing from the troposphere. The results of Kretschmer et al. (2020) are consistent with those of Manzini et al. (2018), who analyzed the stratospheric winter response in two consecutive global warming periods of 2 K each in a large ensemble of experiments from a single climate model. They found a shift from an easterly wind change (i.e., a vortex weakening) in the first warming period to a westerly wind change (i.e., a vortex strengthening) in the second warming period and concluded that Arctic sea ice changes can act to trigger a nonlinear atmospheric response. Studies thus suggest an increase in stratospheric dynamical activity in the Northern Hemisphere late winter throughout the remainder of the 21st century, i.e., the period of Arctic sea ice decline. However, the role of the stratospheric pathway for the Arctic/mid-latitude linkage, and in particular the dynamical forcing of the Northern Hemisphere winter stratosphere by Arctic sea ice loss, remains an open question (Kretschmer et al., 2020) and is intensely debated.

A recent analysis of simulations from CMIP5 and CMIP6 models highlights that in an extreme GHG scenario, the potential for the formation of PSCs in individual cold winters that experience little or no dynamical forcing from the troposphere will rise toward the end of the 21st century, providing favorable conditions for episodic large seasonal loss of Arctic TCO (von der Gathen et al., 2021; see discussion in *Section 4.5.3.3*). Similar episodes with future high PSC formation potential are found in models with interactive ozone chemistry. However, in these models, the impact of increasing dynamical forcing becomes the dominant factor for Arctic ozone in the second half of the 21st century (Langematz et al., 2014; Bednarz et al., 2016). This is consistent with projections from CCMI models (Dhomse et al., 2018) and four CMIP6 models with interactive ozone (Keeble et al., 2021; see *Section 4.5.3.4* and **Figure 4-24**) of an accelerated Arctic ozone recovery and a super-recovery (higher TCO than in 1980) by the end of the 21st century for the more severe GHG scenarios.

In general, the quantification of Arctic polar ozone is complicated by uncertainties in the applied methods and models. These uncertainties include limitations in the ability of models to

reproduce observed polar temperatures, as well as the fact that most CMIP6 models lack the chemical modules necessary to properly account for ozone feedbacks.

## 4.3.5 Other Factors Affecting Polar Ozone

### *4.3.5.1 Solar Variability*

Langematz, Tully et al. (2018) reported in detail on the impact of energetic particle precipitation (EPP) on polar ozone and on the progress in deriving EPP effects on atmospheric composition and ozone from satellite data and chemistry-climate models (CCMs). Since then, a number of studies have contributed to better quantification and understanding of the solar forcing amplitude in both solar electromagnetic radiation and EPP.

Motivated by the construction of new solar input datasets for the CMIP6 model intercomparison study, Kunze et al. (2020) compared the implications of the prescribed spectral and total solar irradiance (SSI/TSI) dataset for the simulated 11-year solar ozone response in simulations with two CCMs. Both sets of CCM simulations used five different solar forcing datasets, including the most recent CMIP6 dataset (Matthes et al., 2017). They found that at polar latitudes, the magnitude of the solar TCO signal is only marginally affected by the solar irradiance dataset used (Kunze et al., 2020).

Polar ozone can be destroyed by EPP either through sporadic large fluxes of solar protons (solar proton events [SPEs]) after solar coronal mass ejections (CMEs) or by the continuous impact of the solar wind on Earth's magnetosphere, leading to energetic electron precipitation (EEP) associated with geomagnetic storms. Both types of EPP induce enhanced ionization levels in the middle and upper polar atmosphere, leading to the production of $NO_x$. The $NO_x$ is long lived during winter and destroys ozone either locally in the upper stratosphere and mesosphere (EPP direct effect) or in the lower stratosphere after being transported downward by the BDC in the winter polar vortex (EPP indirect effect; see, e.g., the reviews of Sinnhuber et al., 2012, and Mironova et al., 2015).

EPP is closely linked to the phase of the 11-year solar cycle and is thus characterized by quasi-regular oscillations with sporadic enhancements after SPEs. It mainly affects polar ozone in the upper stratosphere and mesosphere. Nevertheless, EPP effects on polar ozone are non-negligible. Sinnhuber et al. (2018) find an average EPP-induced decrease in Antarctic TCO of about 4% in each winter/spring. The timing of the strongest ozone response to SPEs in the winter/spring season coincides with the maximum signal of upper-stratospheric polar ozone recovery from ODSs, with trends maximizing in the autumn/winter seasons in both hemispheres (Stone et al., 2018). Thus, accounting for SPEs is important for the detection of ozone recovery in the upper stratosphere. Moreover, EPP has the potential to affect lower-stratospheric polar ozone by interfering with catalytic ozone depletion in Antarctic spring, as originally suggested by Jackman et al. (2000) and Funke et al. (2014). Observational evidence from different satellite datasets suggests that Antarctic springtime ozone increases in the lower stratosphere are associated with higher-than-average EPP during the preceding winter (Gordon et al., 2020, 2021). Due to the EPP indirect effect, $NO_x$ is transported from the upper mesosphere into the lower stratosphere, where it remains at least until late spring (Gordon et al., 2020). Through reaction with chlorine monoxide (ClO), chlorine nitrate ($ClONO_2$) is formed, preventing some of the $NO_x$- and $Cl_x$-driven catalytic ozone destruction. This buffering mechanism will be less effective when the atmospheric chlorine loading decreases in the future.

Toward the second half of the 21st century, polar EPP-$NO_x$ is expected to increase in the stratosphere due to circulation changes associated with rising GHG concentrations. The projected increase in downward transport from the mesosphere in a stronger BDC leads to an enhanced EPP indirect effect. With declining ODSs, $NO_x$ catalytic ozone destruction, and thus the contribution of EPP-$NO_x$, will become more prominent (Maliniemi et al., 2020; see also *Section 4.5.3.4*).

To investigate the impacts of EPP on polar ozone, models including either high-top ionization/chemistry schemes or employing parameterizations of EPP effects are applied. Simulations with CCMs forced with EPP-induced $NO_y$ anomalies from satellite data or including simple parameterizations of $NO_x$ and $HO_x$ production by SPEs qualitatively reproduce the observed decrease of polar ozone following SPEs in the upper stratosphere (see also Langematz, Tully et al., 2018). However, recent studies suggest that the impact of both SPEs and EEP might be underestimated in current models. Kalakoski et al. (2020) show that the polar ozone response to SPEs in the upper stratosphere is enhanced when detailed ion chemistry reactions in the lower ionosphere are included, as they lead to increased conversion of HCl to reactive $Cl_x$ species. New observational evidence has also emerged that the current CMIP6 parameterizations of EEP from Earth's radiation belt (van de Kamp et al., 2016) underestimate the effects of EEP on polar ozone. Nesse Tyssøy et al. (2019) found that the CMIP6 model fails to reproduce the electron flux level and variability associated with the strongest CMEs as well as the duration of EEP events during solar maximum. As a result, the modeled $NO_x$ enhancements by EEP in the mesosphere and upper stratosphere are too low, and the associated ozone loss is too weak (Nesse Tyssøy et al., 2019). This result is consistent with CCM simulations that showed better agreement with observations of the descent of $NO_x$ when—in contrast to the CMIP6 parameterization—improved electron flux information was used (Pettit et al., 2019). Similar conclusions were also drawn based on calculated ionization rates from balloon observations of 500 EEP events (Mironova et al., 2019). The authors found differences from the CMIP6 recommended ionization rates that lead to an underestimation of the $NO_x$ enhancement by more than 100% and of the associated ozone loss by up to 25% in the mesosphere. However, with an average EPP-induced decrease in Antarctic TCO of about 4% in each winter/spring (Sinnhuber et al., 2018), the effect of such an underestimation of mesospheric ozone loss by EPP on TCO is likely to be small.

The above findings are supported by Duderstadt et al. (2021), who estimated electron precipitation by scaling observations from the Van Allen Probes instruments, which measure trapped electrons directly in the radiation belts, to observations from the FIREBIRD II CubeSats, which measure precipitating electrons from polar low-Earth orbit. The derived flux ratios from 35 conjunctions of the satellites between 2015 and 2017 were statistically analyzed in terms of 50th, 75th, and 100th percentiles, indicating the $NO_x$ and ozone changes from the median (50% percentile) to the highest (100% percentile) values of the distribution. **Figure 4-14** shows the modeled enhancement of $NO_x$ and reduction of $O_3$ averaged over the stratospheric polar vortex during the weeks following the March 2013 electron precipitation event. Enhancements of $NO_x$ descending into the upper

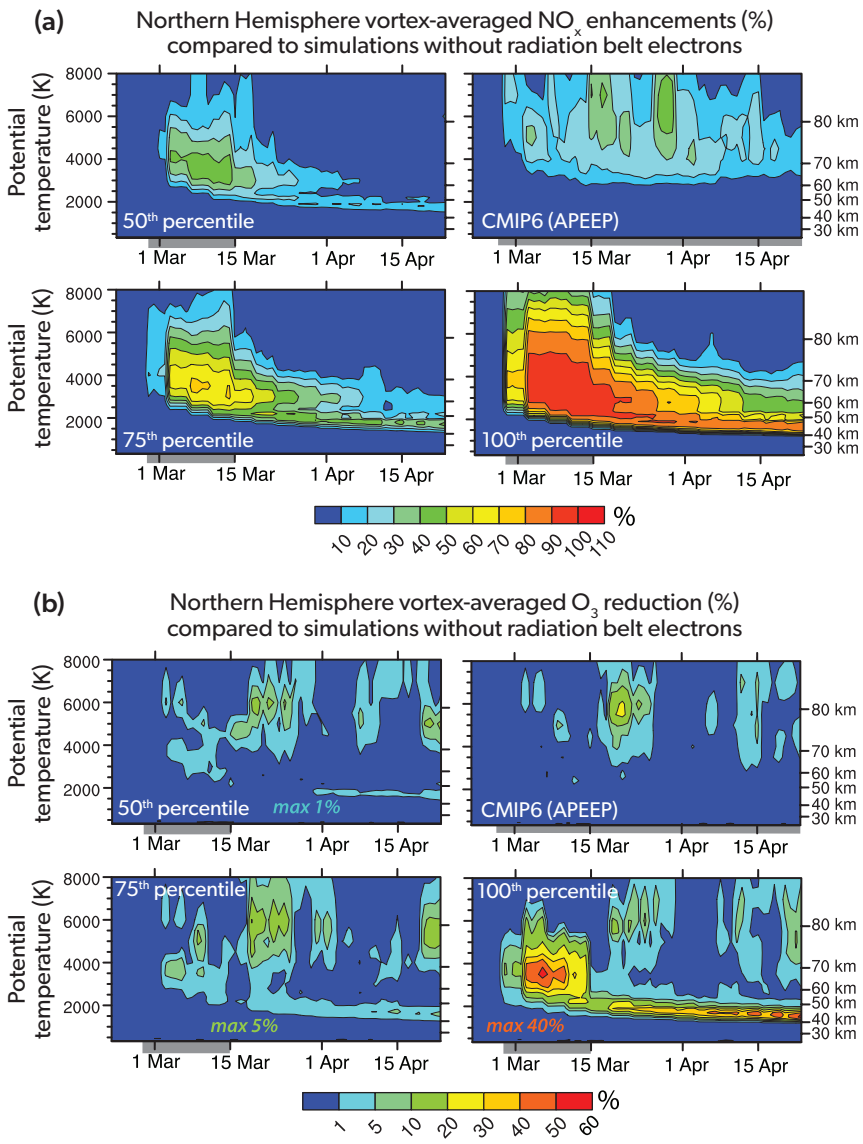


**Figure 4-14.** WACCM simulations for the March 2013 electron precipitation event showing longer-term (a) enhancements of $NO_x$ and (b) reductions of $O_3$ averaged over the Northern Hemisphere polar vortex from radiation belt electrons. Gray bars along the x-axis represent times when medium energy electron ionization is included in the simulations. Percentiles refer to the flux ratios of the two instruments. [From Duderstadt et al., 2021.]

stratosphere (40–50 km) reach 20–30% for the 50th percentile flux ratios and 80–90% for the 100th percentile case, and the enhancements persist through April. In situ reductions of ozone at 40–50 km altitude are only 1% for the 50th percentile case but up to 40% for the 100th percentile case (Duderstadt et al., 2021).

### *4.3.5.2 Volcanic Eruptions*

In Langematz, Tully et al. (2018), the impact of large volcanic eruptions, which increase the amount of sulfate aerosols in the stratosphere, was highlighted. Observations from ozonesondes and Aura MLS, as well as CCM simulations, suggested that the eruption of the Chilean volcano Calbuco contributed to the record-large Antarctic ozone hole in spring 2015.

Comparisons of coupled chemistry-climate-aerosol model simulations with satellite and balloon observations (Stone et al., 2017; Zhu et al., 2018) show that volcanic sulfate aerosols from the Calbuco eruption were transported from mid-latitudes toward the Antarctic and slowly descended during transport. The modeled aerosol number density indicates that Calbuco sulfate aerosols penetrated into the Antarctic polar vortex starting in May and led to ozone depletion in September 2015, particularly at around 100 hPa and 70°S, up to 35% higher than if there had been no eruption. The simulated aerosol surface area density, earlier ozone loss, and larger area of the ozone hole are consistent with the presence of volcanic sulfate layers observed at 16 km, as well as with previous model studies (e.g., Solomon et al., 2016).

As discussed in the previous Assessment (Langematz, Tully et al., 2018), the injection of halogens from large volcanic eruptions into the stratosphere is expected to become more relevant in a future atmosphere with declining anthropogenic halogens. Simulations with 2-D CTMs have suggested substantial ozone reductions in the polar regions from the injection of volcanic halogens, and they also highlighted the increasing role of short-lived brominated substances in determining whether future volcanic eruptions will cause ozone depletion (Klobas et al., 2017). Combining for the first time a complex 3-D CCM with

a measurement-based dataset of sulfur, chlorine, and bromine releases from tropical volcanic eruptions, Brenna et al. (2019) investigated the effects of halogen emissions by large, explosive volcanic eruptions under preindustrial atmospheric conditions. A volatile mass representative of large sulfur- and halogen-rich eruptions was deduced from an average of 28 eruptions of variable composition along the Central American Volcanic Arc (CAVA) over a time interval of 200 ka. Assuming an injection of 10% of the erupted halogen mass into the stratosphere, their simulations reveal a decade-long depletion of the ozone layer by about 20% globally. In the Arctic, a maximum TCO decline of more than 200 DU (45%) takes place in the first spring after the eruption, followed by ozone decreases of more than 120 DU (20%) in the post-eruption years 2 and 3. In the Antarctic, ozone depletions comparable to present-day ozone holes occur in springs 3–6 after the eruption, with minimum TCO below 100 DU and maximum ozone hole area extent in October of year 4. These results are, however, sensitive to the halogen injection efficiency, with a reduced ozone response for a halogen injection efficiency smaller than 10%.

### *4.3.5.3 Wildfire Emissions*

Severe bushfires in southeastern Australia in late December 2019 and early January 2020 (the Australian New Year's event [ANY]) injected large amounts of smoke and tropospheric air into the Southern Hemisphere stratosphere (Kablick et al., 2020; Khaykin et al., 2020; Allen et al., 2020; Schwartz et al., 2020). Satellite observations show that heterogeneous chlorine activation occurred on the smoke particles at Southern Hemisphere mid-latitudes, leading to strong and persistent depletion in stratospheric HCl and enhancement of ClO that peaked in mid-2020 (Santee et al., 2022; Bernath et al., 2022). However, although such strong and sustained mid-latitude chlorine activation was unprecedented, it was still an order of magnitude or more weaker than that in a typical winter polar vortex (Santee et al., 2022). Southern Hemisphere mid-latitude ozone was anomalously low during that period, but there is currently no consensus about the relative roles of transport and chemistry in inducing the mid-latitude ozone anomaly (see related discussion in *Section 3.2.1.3*) or the potential contribution of ANY to polar ozone depletion in 2020. Some studies suggest non-negligible chemical depletion of polar ozone caused by the ANY smoke, with the contribution to ozone loss comparable to that of the sulfate aerosols from the Calbuco eruption in 2015 (Yu et al., 2021; Rieger et al., 2021). One model simulation yielded 10–20 DU of additional ozone loss due to heterogeneous reactions on sulfuric acid–coated smoke particles between August and September, resulting in a 12% increase in the ozone hole area compared to a control simulation with no smoke (Yu et al., 2021). However, an analysis of the ANY plumes using satellite observations and meteorological fields from a reanalysis that succeeded in tracking several of the largest plumes found no evidence that any of them penetrated or altered the chemistry of the then-developing Antarctic vortex (Schwartz et al., 2020). Thus, the impact of the ANY smoke on Antarctic ozone remains highly uncertain.

### *4.3.5.4 Supersonic and Hypersonic Aircraft Emissions*

Different organizations and companies are once again reconsidering the development of a supersonic transport (SST) aircraft fleet designed for the commercial and business jet airline markets. SST aircraft would fly at supersonic speeds (Mach 2–2.5) at cruise altitudes between 13 and 23 km in the lower stratosphere. In parallel, new technologies are being explored with the aim of developing a hypersonic transport (HST) aircraft fleet flying at a speed of Mach 5–8 and cruise altitudes between 30 and 40 km (Yanes, 2020). Both types of aircraft will potentially release substantial amounts of water vapor ($H_2O$) and nitrogen oxides ($NO_x$) into the stratosphere, with concomitant strong effects on stratospheric ozone. Updated estimates of the expected ozone change were recently presented for a range of $H_2O$ and $NO_x$ emissions scenarios based on WACCM simulations.

Zhang et al. (2021) investigated the potential effects on stratospheric ozone of a hypothetical fleet of 500 or 1000 High Speed Civil Transport (HSCT) aircraft, based on projections made in NASA's 1999 Atmospheric Effects of Aviation Project (AEAP) Report (Kawa et al., 1999). The HSCT aircraft had been designed for long-range flights at Mach 2.4. Different levels of $NO_x$ emissions with either constant or zero $H_2O$ emissions from the AEAP report were prescribed, with atmospheric background conditions of the year 2015 assumed. Due to interactions between different ozone loss cycles, ozone responses of different signs were found in different regions of the atmosphere. For the basic $NO_x$ scenario, the model simulates maximum ozone production of +1.4% in the UTLS at 11 km and ozone reduction above that level, reaching a maximum of −1.2% at 22 km at high latitudes in June. The same ozone change pattern appears for all scenarios with enhanced $NO_x$. Ozone depletion maximizes in the Northern Hemisphere, where most of the flights take place, at cruise altitudes (between 21 and 25 km), with peak ozone loss at high latitudes. TCO loss is found over most of the globe for the entire year, but maximum TCO loss occurs in the polar regions in springtime (–0.4% in March in the Northern Hemisphere and –1.2% in October in the Southern Hemisphere). While $H_2O$ emissions generally have a much smaller effect on ozone depletion than $NO_x$ emissions, they become more important in the Southern Hemisphere polar winter because they increase the surface area density of ice and thus promote heterogeneous ozone depletion.

In addition to the ongoing development of SSTs, the concept of a civil HST fleet is under consideration for future intercontinental travel. Estimates of the emissions of hypersonic aircraft are much more uncertain than those for SSTs, due to the present-day lack of concrete information on the type of engines to be used, the combustion systems and their emissions, and the size of the future fleet and flight conditions, such as the optimal flight altitudes. To assess the impact on the stratospheric ozone layer of such a hypothetical future HST aircraft fleet, Kinnison et al. (2020) conducted sensitivity studies, using estimated $H_2O$ and $NO_x$ concentrations emitted by aircraft flying at either 30 or 40 km altitude. The emissions and flight routes used to establish these concentrations were identical to the 1999 AEAP scenario, also adopted by Zhang et al. (2021). In summary, the study shows that $NO_x$ emissions of an HST fleet of the assumed size would have the potential to substantially reduce the atmospheric ozone column. At high northern latitudes, the reduction in the ozone column is of the order of 8–10% (25 DU) for a 30 km injection, near the ozone maximum, and close to 5–8% (20 DU) for a 40 km injection (**Figure 4-15**). The emissions prescribed in the simulations of the HSCT (Zhang et al., 2021) and HST (Kinnison et al., 2020) aircraft fleets are the same. However, as they are emitted at different

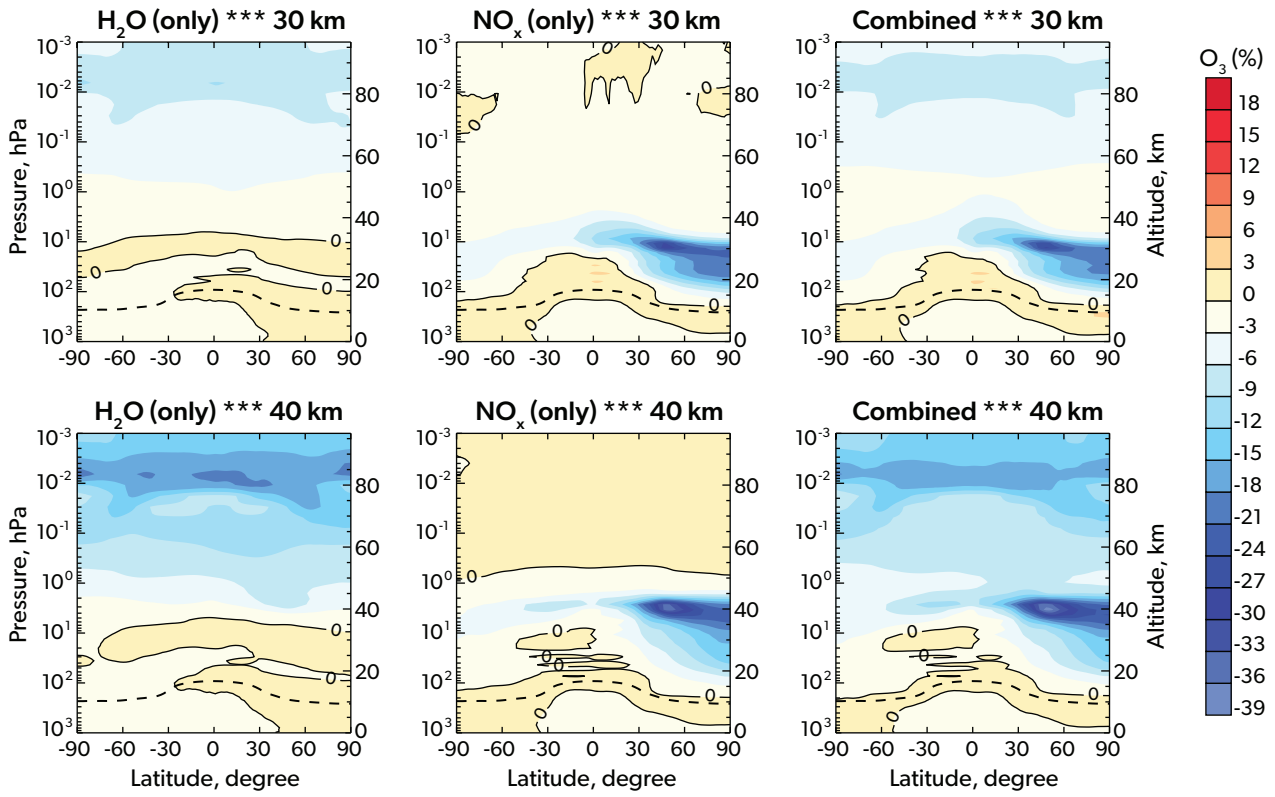


**Figure 4-15.** Percent change in the atmospheric concentration of ozone for an injection of $H_2O$ *(left panels)*, $NO_x$ *(middle panels)*, and combined $NO_x$ + $H_2O$ *(right panels)* by a fleet of HST operating at 30 km *(upper panels)* and 40 km *(lower panels)*. The black dashed lines denote the tropopause. [From Kinnison et al., 2020.]

heights in the stratosphere, their impact on ozone is larger for the HST fleet. Most of the ozone reduction is due to the release in the atmosphere of $NO_x$, while $H_2O$ emissions primarily reduce ozone in the upper atmosphere (**Figure 4-15**) and, therefore, have a minor effect on the TCO response. The ozone depletion is largest in the Northern Hemisphere polar region (**Figure 4-15**) and most pronounced in spring and fall. The maximum reduction at high latitudes in the Southern Hemisphere is of the order of 2%.

In contrast, the $NO_x$ emitted by a hypothetical scenario of hydrogen-fueled hypersonic airplanes has been estimated to have a negligible effect on global stratospheric ozone, but with enhanced impact over the poles (Ingenito, 2018).

While Zhang et al. (2021) and Kinnison et al. (2020) should be regarded as sensitivity studies using a specified dynamics setup for the simulations and estimated aircraft emissions, they both show an enhanced risk of a reduction in the stratospheric ozone layer by potential future fleets of SST or HST aircraft, consistent with previous assessments (e.g., Dameris et al., 1998; Kawa et al., 1999).

#### *4.3.5.5 Rocket Emissions*

With improving availability of commercial space launches and a growing interest in human settlements in space, the impact of rocket emissions on stratospheric polar ozone is expected to increase substantially in the coming decades. The composition of the rocket emissions products and their potential to deplete ozone strongly depend on the type of propellant used (solid, liquid, or hydrogen). A review of the ongoing research is presented in *Section 7.2.8.1*.

## 4.4 RECOVERY OF POLAR OZONE

### 4.4.1 Polar Ozone Recovery in Previous Assessments

The 2006 Ozone Assessment (Bodeker, Waugh et al., 2007) defined three stages of stratospheric ozone recovery: 1) a statistically significant slowing of the rate of ozone decline, 2) the onset of ozone increases above the previous minimum values (so-called turnaround) due to declining equivalent effective stratospheric chlorine (EESC), and 3) full recovery, which, in the absence of factors that alter the sensitivity of ozone to ozone-depleting substances (ODSs; e.g., volcanic eruptions), is likely to occur when EESC returns to 1980 levels. It should be noted, however, that even 1980 EESC levels are well above natural ODS abundances.

The 2014 Ozone Assessment (Dameris, Godin-Beekmann et al., 2014) noted that although Antarctic total column ozone (TCO) appeared to have begun increasing since reaching a minimum at the turn of the 21st century, and that the rate of that increase appeared to be consistent with the decline in ODSs, uncertainties

in measurements and statistical analyses precluded definitive attribution of the increasing Antarctic stratospheric ozone to decreasing ODSs. The most recent Assessment (Langematz, Tully et al., 2018) concluded that evidence had emerged after the 2014 Assessment that the second stage of ozone recovery had started. Trends in ozone over Antarctica during the month of September since the year 2000 were shown to be statistically significant, with an increase in observed total ozone and a decrease in ozone hole size and depth. Furthermore, these changes could be attributed at least partly to decreasing ODSs, particularly to declining stratospheric chlorine. For Arctic springtime stratospheric ozone, in contrast, recovery trends had not yet been reported. This is not unexpected, as Arctic springtime stratospheric ozone is dominated by large year-to-year dynamically induced variability of the polar vortex. The third stage of recovery, with springtime polar TCO returning to 1980 historical levels (see *Section 4.5*), is not expected until around mid-century.

The 2018 Assessment (Langematz, Tully et al., 2018) also reported that many studies since the 2014 Assessment had explored recovery detection. They noted that because of differences in datasets used, time periods over which trends were calculated, and analysis methods, direct comparison between published results was difficult and not very meaningful. However, all reported studies found clear signs of recovery despite these differing approaches, and this was considered to be a sign of the robustness of the finding of detectable ozone recovery. Updating trend values from those particular studies in this Assessment by extending the length of their analysis periods—even if practicable—would not resolve the complexities of their intercomparison. Hence, we focus on new publications since the previous Assessment, as well as recent Antarctic ozone holes and whether they have challenged the 2018 Assessment findings.

## 4.4.2 Long-Term Antarctic Ozone Trend and Onset of Antarctic Ozone Recovery

### *4.4.2.1 New Research into Antarctic Ozone Recovery*

Since the last Assessment (Langematz, Tully et al., 2018), several studies have been published on trend detection in Antarctic stratospheric ozone and attribution of trends to ODSs.

One metric that has been explored is the frequency of occurrence of (extremely) low ozone concentrations and episodes of near-complete Antarctic stratospheric ozone destruction at selected altitudes due to ozone loss saturation. Ozone loss saturation refers to the concept that once near-complete ozone loss occurs, adding more ODSs will not result in more ozone depletion. As a consequence, with currently decreasing ODSs, expectations are that at some point in the future ozone loss saturation will no longer occur. Thus, the occurrence of loss saturation and/or extremely low ozone concentrations provides an alternative metric for monitoring ozone layer recovery. Although Antarctic ozone loss saturation is predicted to occur until at least mid-century, its frequency is expected to decline. Detection of such a decline would be an important milestone in stratospheric ozone layer recovery. A wide range of ozone data for the period 1979–2017, including profile measurements from balloon soundings and satellites, as well as TCO observations from Antarctic ground-based stations and satellites, show that extremely small ozone concentrations and ozone loss saturation started to occur after 1987 and peaked near the year 2000, after which a marked decrease was observed (Kuttippurath et al., 2018). The reduction in the frequency of occurrence of ozone loss saturation over the period 2001–2017 is consistent throughout the datasets.

Langematz, Tully et al. (2018) reported the first detection of post-year-2000 statistically significant trends in Antarctic stratospheric ozone based on different methods specifically for the month of September (Solomon et al., 2016; de Laat et al., 2017; Pazmiño et al., 2018; Weber et al., 2018). Building on those findings, Strahan et al. (2019) analyzed chemical transport model (CTM) simulations of past, present, and future Antarctic stratospheric ozone to identify which commonly used Antarctic ozone hole metrics best track declining ODS levels. The largest sensitivity of vortex-average column ozone was found for the period 1–20 September. Stronger dynamical variability during Antarctic spring increasingly obscures the ODS signal in post-September long-term ozone trends. In addition, the ozone mass deficit (OMD) best tracks trends in ODSs. The OMD relative to the 250 DU level was found to be a slightly better metric compared to the commonly used OMD relative to the 220 DU level. The former better samples the vortex edge region, which is where model simulations show that the largest decreases in ozone loss occur. In addition, approximately 25% of the increase in Antarctic springtime ozone levels can be attributed to seasonal pre-ozone hole Antarctic stratospheric ozone conditions (e.g., in the month of June).

Changes in the strength of the Brewer-Dobson circulation (BDC) have also been analyzed recently for their links to polar ozone trends (Fu et al., 2019). Satellite observations of stratospheric temperatures and meteorological reanalysis data show that the global annual mean BDC accelerated over the period 1980–1999 compared to 2000–2018. These decadal differences are attributed almost exclusively to the Southern Hemisphere BDC cell and stratospheric ozone depletion and healing in the ozone hole (see also Polvani et al., 2017). They are accompanied by a trend in post-year-2000 Antarctic stratospheric radiative warming during the month of September. An analysis of regional patterns of past Antarctic stratospheric warming in September and October similarly attributed at least part of an observed 2007–2017 warming to ozone recovery (Xia et al., 2020). Prior warming trends, between 1979 and 2006, in the Southern Hemisphere high-latitude stratosphere were mainly attributed to changes in the BDC and phase shifts of the stratospheric stationary waves.

Linear trends in a number of standard Antarctic ozone hole metrics for the period 1979–2017 have also been analyzed (Tully et al., 2019). These metrics include the minimum in 15-day average total ozone, maximum in 15-day average 220 DU ozone hole area, minimum in 15-day average OMD, and the duration of the ozone hole. Trends for the periods before and after the year 2000 are calculated for both unadjusted raw data and data that have been adjusted to account for the impact of stratospheric dynamics. The analysis uses TOMS, OMI, and OMPS TCO data, as well as temperature data from MERRA-2 for the adjustment. Trends towards reduced ozone depletion since 2001 are found to be statistically insignificant in the unadjusted data; statistically significant trends of a similar magnitude are found in the adjusted data (Tully et al., 2019).

Significant trends in September-average Antarctic ozone hole area (defined by the 220 DU contour) were found if only years characterized by similarly cold meteorological conditions

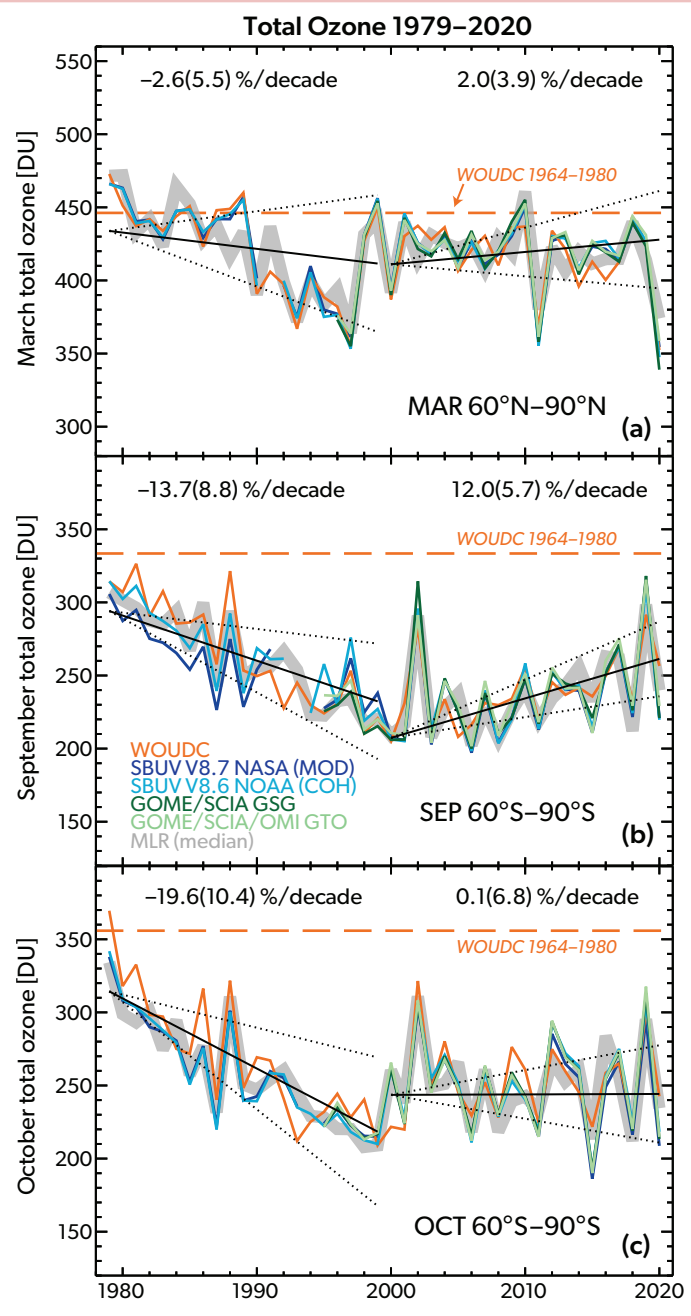


**Figure 4-16.** Total ozone time series for (a) the Arctic (60–90°N) in the month of March and (b, c) the Antarctic (60–90°S) in the months of September and October, derived from five long-term observational datasets: WOUDC (based on the GAW network of ground-based Dobson and Brewer instruments; orange line), SBUV 8.7 processed by NASA (blue line), SBUV 8.6 processed by NOAA (cyan line), GOME-SCIAMACHY-GOME-2 (GSG; dark green line), and GOME-type Total Ozone (GTO; light green line). The dashed orange lines show the 1964–1980 mean ozone levels from the WOUDC data. In each panel, the median of the datasets has been used to show the results of applying a multiple linear regression (MLR) with independent linear trends analysis (thick gray line). Regressor terms include the solar cycle, QBO, ENSO, volcanic aerosol, and the strength of the Brewer-Dobson circulation. The black solid lines indicate the linear trends before and after the year 2000, the ODS peak in the polar regions. The black dotted lines indicate the 2σ uncertainty of the MLR trend estimates. Trend numbers are indicated for the pre- and post-ODS peak period in the top part of the plots. Numbers in parentheses are the 2σ trend uncertainty. [Adapted from Weber et al., 2022, updated from Langematz, Tully et al., 2018.]

were considered (Kramarova et al., 2021). Using years identified (based on MERRA-2) as having 50 hPa September 60–90°S mean temperature at least one standard deviation below the 1980–2020 mean (33rd percentile), a significant downward trend in post-year-2000 September-average ozone hole area was calculated, in good agreement with expectations based on trends in ODSs.

Bodeker and Kremser (2021) reported a trend reversal in Antarctic ozone hole metrics around the turn of the century using the National Institute of Water and Atmospheric Research/Bodeker Scientific (NIWA-BS) TCO database covering the period 1979–2019. The trend reversal was attributed to the turn-of-the-century peak in stratospheric chlorine and bromine concentrations. Note that a robust attribution analysis of the drivers of long-term variability in Antarctic ozone hole metrics has not been conducted using the NIWA-BS record.

A recent study explored changes in the onset of early spring ozone depletion by comparing an ensemble of chemistry-climate model multi-member simulations for 1980–2024 with observed September Antarctic ozone hole area through 2021 (Stone et al., 2021). Agreement between the model simulations and observations was generally good. Significantly later start dates for the onset of rapid ozone depletion were found after the year 2000. In addition, a substantial reduction over the past decade was found in both measured and modeled ozone hole depth during September but not October. The significant September

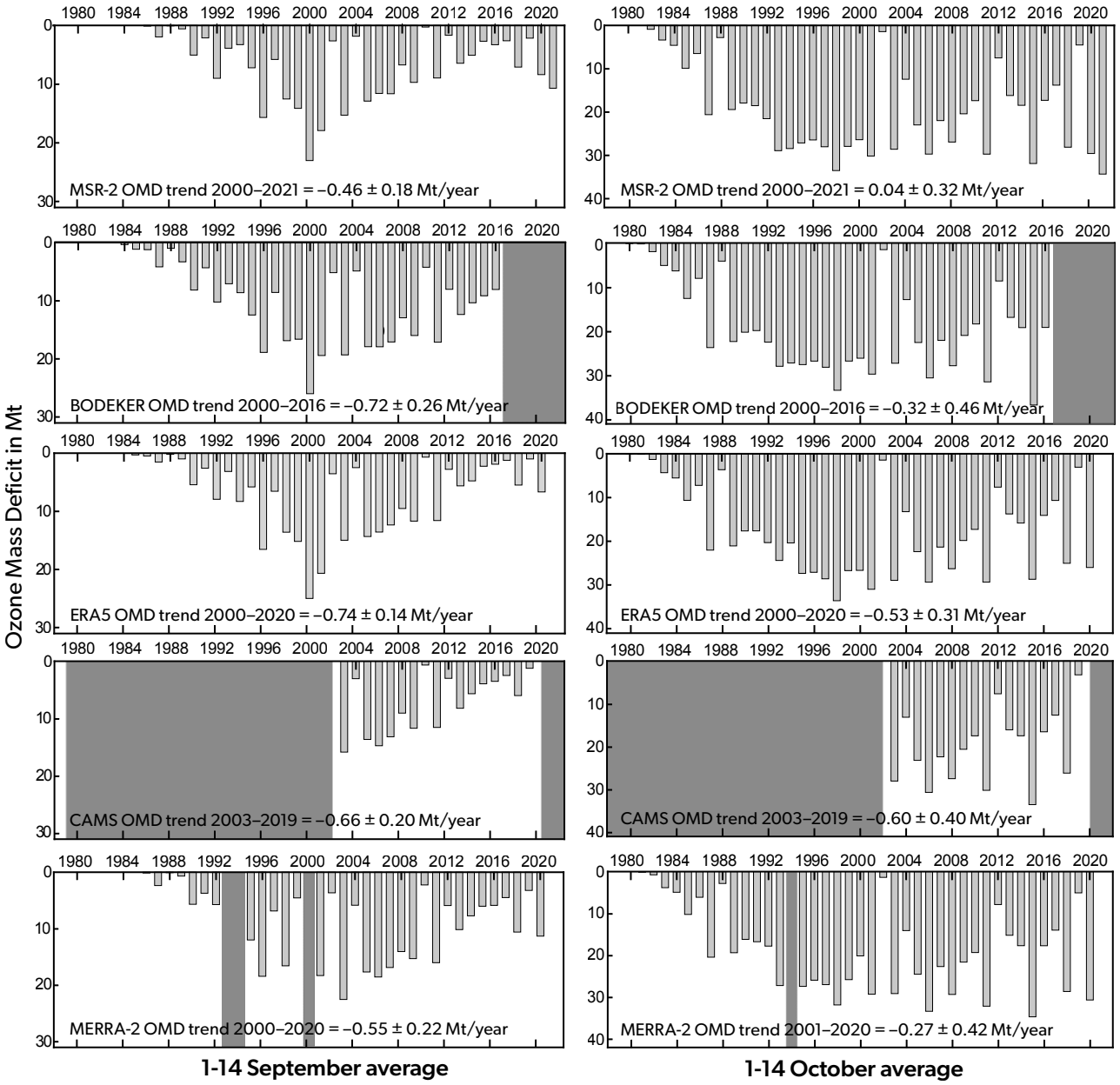


**Figure 4-17.** Antarctic 220 DU ozone mass deficit (in megatons) averages for 1–14 September *(left column)* and 1–14 October *(right column)* for different daily total column ozone reanalysis datasets. Dark grey bars indicate unavailable or unreliable years in the datasets. For MERRA-2, unreliable years (September 1993, 1994, 2000; October 2000) are related to orbital drifts in various SBUV-carrying satellites (Davis et al., 2017; Wargan et al., 2017). Linear trends are based on a standard ordinary linear regression. MERRA-2: Gelaro et al. (2017); MSR-2: van der A et al. (2015); ECMWF/ERA5: Hersbach et al. (2020); ECMWF/CAMS: Inness et al. (2019); BODEKER v3.51: Bodeker et al. (2021). MSR-2 and BODEKER datasets accessed December 2021; all other datasets accessed December 2020.

results were derived even without accounting for dynamical variability via, for example, a multivariate regression. For the years 2015, 2018, 2020, and 2021, dynamical processes were found to be the main cause of large (late) spring Antarctic ozone holes, possibly exacerbated by volcanic eruptions (2015) and bushfire smoke (2020). The differences in results between September and October point to chemical processes dominating the early part of the ozone hole season from August through September, while dynamical processes play a leading role in determining ozone hole size and depth from October through December. As a consequence, it is more complicated to derive recovery information from October–December data than from September data. The later start date for the onset of rapid ozone depletion is considered a robust sign of ozone recovery post-2000, despite the occurrence of large Antarctic ozone holes later during austral spring.

### *4.4.2.2 Recent Antarctic Winters in the Context of Stratospheric Ozone Recovery*

As noted in *Section 4.2.3*, since the last Assessment three remarkable Antarctic springtime stratospheric ozone seasons have been observed. The evolution of the Antarctic ozone hole in these three years—2019, 2020, and 2021—was discussed in detail in *Sections 4.2.3.2* and *4.2.3.3*. In short, in 2019, strong wave driving resulted in enhanced early springtime stratospheric warming and a strong September minor sudden warming. Hence, springtime Antarctic ozone depletion was substantially reduced in 2019. In contrast, a lack of strong tropospheric wave driving in 2020 and 2021—especially from October onwards—resulted in an anomalously cold Antarctic stratosphere in both years. In 2020, the time period with temperatures below the chlorine activation threshold was prolonged by approximately one month, with chlorine remaining activated through October; depletion also persisted for several weeks longer than typical in 2021. The unusually quiescent dynamical state resulted in ozone holes persisting into late December in 2020 and mid-December in 2021. Overall, the average TCO south of 60°S since 2018 continued to follow the pattern of past years in September and October, with statistically significant post-year-2000 trends in September but not in October (**Figure 4-16**).

In 2019, the ozone destruction rate in September prior to the occurrence of the strong minor sudden stratospheric warming was similar to rates observed during previous years (Wargan et al., 2020; Kramarova et al., 2020; Saffiedine et al., 2020). In 2020 and 2021, the early September OMDs were larger than those during the decade 2010–2019 but still significantly smaller than those during the decade 2000–2010, while the OMDs reached during the first half of October were comparable to those in the 1990s and 2000s (**Figure 4-17**). It is not unexpected that, under favorable atmospheric conditions, very large ozone depletion can be reached despite decreased levels of ODSs. Müller et al. (2018), for example, noted that even with the expected continued decline in ODSs, years with extremely low Antarctic stratospheric ozone concentrations may continue to occur until the middle of the 21st century. Model simulations also show that large and long-lasting ozone holes are likely to occur occasionally during the period of ozone recovery (Stone et al., 2021).

Post-year-2000 trends for the average 1–14 September Antarctic 220 DU OMD for a range of TCO reanalysis datasets are indistinguishable in magnitude within statistical uncertainties (**Figure 4-17**). This agreement indicates that trends in Antarctic early to mid-September total ozone are robust with regard to the choice of total ozone reanalysis dataset. The average 1–14 October 220 DU OMD trend values do not show signs of the start of recovery, consistent with the emerging consensus that the month of September—especially the first half of that month—is more appropriate for recovery detection (Solomon et al., 2016; de Laat et al., 2017; Strahan et al., 2019; Stone et al., 2021).

In summary, recently published studies provide additional support for the conclusion of the previous Assessment (Langematz, Tully et al., 2018) that evidence has emerged for statistically significant trends in stratospheric ozone since the year 2000 over Antarctica, particularly in the month of September. Results from alternative trend analysis approaches and metrics such as ozone loss saturation and ozone hole start dates are also consistent with recovery detection. Indications are also emerging of recent Antarctic stratospheric warming consistent with increasing ozone. Of the plethora of Antarctic ozone recovery metrics and approaches, early September OMD appears to best track trends in ODSs (with the 250 DU OMD providing slightly better results than the 220 DU OMD). However, while decreasing post-year-2000 early springtime Antarctic stratospheric ozone depletion can be largely explained by declining ODSs, whether other processes have contributed—and by how much—remains an outstanding question. Finally, reported detection of recovery is not challenged by the remarkable recent Antarctic ozone holes in 2019, 2020, and 2021, including the record-breaking duration of the 2020 and 2021 ozone holes and their near-record ozone depletion in the month of October.

## 4.4.3 Long-Term Arctic Ozone Trend

As stated in previous Assessments, detection of stratospheric ozone recovery in the Arctic is much more difficult than in the Antarctic. Persistence of the springtime vortex facilitates strong ozone destruction; however, in a typical year, stratospheric dynamical activity leads to vortex breakup before the end of March (see **Figure 4-3**). In rare instances when the Arctic vortex has remained intact well into April, substantial stratospheric ozone depletion has been observed, most recently in 2020 (see *Section 4.2.4* and references therein; other years were 1997 and 2011). Increasing greenhouse gas concentrations will affect stratospheric ozone loss during future cold Arctic winters by lowering stratospheric temperatures (see *Section 4.5.3.3* for further discussion). Some recent Arctic winters have been characterized by particularly low stratospheric temperatures (**Figure 4-2**). However, the low frequency of occurrence of cold Arctic winters with large ozone loss precludes definitive assessment of decadal Arctic stratospheric ozone trends, which remain statistically not significant (see **Figure 4-16a**). The lack of robust decadal ozone trends, in turn, precludes attribution to decadal changes in ODSs, temperature, water vapor, and possibly even Arctic stratospheric vortex stability. Thus, confident conclusions cannot be drawn about Arctic stratospheric ozone recovery at this time.

## 4.4.4 Benefits Achieved by the Montreal Protocol and Its Amendments and Adjustments

Langematz, Tully et al. (2018) reported that model simulations assuming continuous growth of ODSs indicated that in the absence of Montreal Protocol controls, by 2013 the Antarctic ozone hole would have been significantly larger and longer-lived than observed, and ozone loss at subpolar southern latitudes would also have been larger. For example, a continuous 3% $yr^{-1}$ increase in ODSs after 1987 would have yielded a 40% deeper Antarctic ozone hole in 2011 (Chipperfield et al., 2015). In addition, in Arctic winters favoring catalytic ozone loss, much more extensive ozone loss would have occurred, resulting in conditions previously only observed over Antarctica.

Feng et al. (2021) and Wilka et al. (2021) further explored what Arctic polar stratospheric ozone conditions would have been in 2020 under unabated emissions of ODSs, assuming a 3–3.5% $yr^{-1}$ increase since 1985. This represents another decade of emissions compared to the case discussed in Langematz, Tully et al. (2018) and results in ODS levels approximately 2.5 times the actual 2020 levels and approximately twice the peak late-20th-century levels. Under such a scenario, minimum Antarctic TCO values

of 50 DU would have occurred by 2020. This is approximately half the minimum TCO values of about 100 DU that occasionally have been observed for the past three decades over Antarctica. It represents approximately a 75% reduction in minimum TCO values compared to those in 1980, and an 85–90% reduction in minimum TCO values compared to the level of 1960 (1960 and 1980 estimates from Dhomse et al., 2018). In addition, springtime Arctic ozone depletion would have begun earlier and lasted longer. In the Arctic for the unusually cold spring of 2020, minimum column values of about 100 DU were modeled. However, given the large interannual variability in the stability of the Arctic polar stratospheric vortex, the occurrence of large Arctic stratospheric ozone depletion would have remained rare. Nevertheless, under such a scenario, Arctic conditions similar to those currently occurring over Antarctica would have become reality for years with an unusually stable and long-lived stratospheric vortex, such as those in 2011 or 2020. Furthermore, for typical Arctic springtime conditions, TCO would also have been significantly smaller by up to several tens of percent, and even in summertime, TCO would have been smaller due to gas-phase depletion.

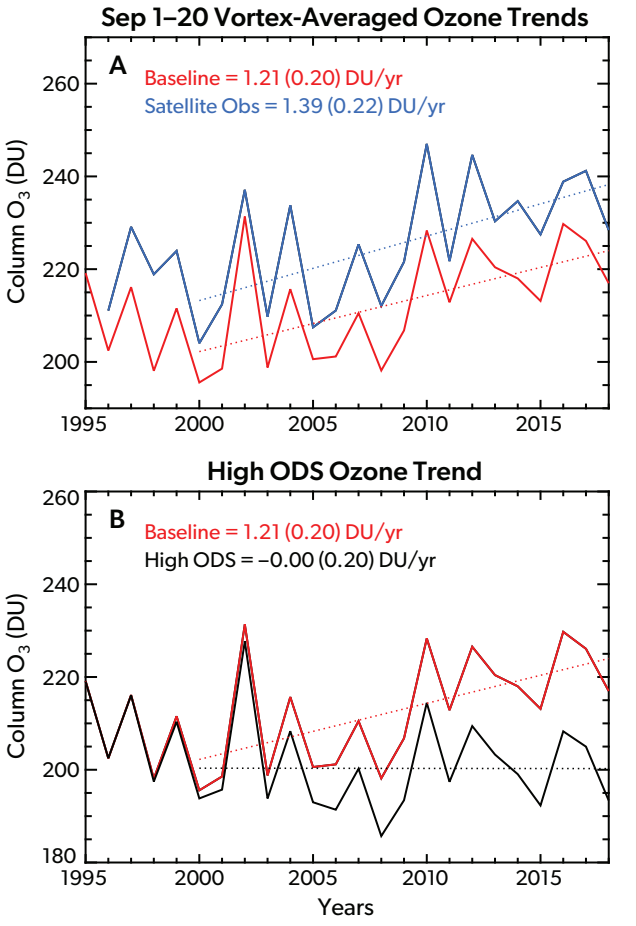


**Figure 4-18.** The 1–20 September Antarctic vortex-mean column ozone and 2000–2018 trends (with 95% confidence intervals in parentheses) for (a) TOMS/OMI/OMPS (blue) and model simulations using realistically varying ODS levels (baseline; red), and (b) simulations using baseline (red) and high (black) ODSs. [From Strahan et al., 2019.]

The benefits of the Montreal Protocol can also be assessed by estimating the recovery signal in ozone, i.e., how much more severe ozone depletion would have been under certain conditions with the "peak halogen" loadings observed in the late 1990s. A simulation using the TOMCAT CTM with halogenated ODSs fixed at 1995 levels produced Arctic polar cap-averaged TCO 20 DU lower than that observed in the cold winter of 2019/20 (Feng et al., 2021). Strahan et al. (2019) also explored scenarios in which ODS levels remained similar to the maximum observed levels of the late 1990s. They used CTM simulations (GMI integrated with MERRA-2 meteorology) with ODSs resembling observed ODS trends, resulting in Antarctic vortex-average post-peak-ODS ozone trends consistent with observations, apart from a small offset (CTM simulations were biased low compared to observations). The "fixed 1995 ODS" simulation showed no post-peak positive trend in TCO (**Figure 4-18**). Furthermore, with maximum halogen loading, recent Antarctic ozone holes would have been deeper by approximately 20 DU. This indicates that the observed positive trend in 1–20 September Antarctic vortex average total ozone can be attributed to decreasing ODSs rather than to interannual variability in Antarctic vortex dynamics. Given a post-1960 decline of approximately 100 DU (models) or 150 DU (observations) of Antarctic springtime ozone (Langematz et al., 2016; Amos et al., 2020), an increase of 20 DU corresponds approximately to a 15–20% recovery.

Overall, these findings reinforce that the Montreal Protocol and its Amendments and adjustments averted more extreme polar stratospheric ozone depletion and the development of an Arctic ozone hole. Furthermore, these findings bolster the conclusion that the occurrence of record-breaking (or nearly so) ozone depletion in 2020 over both the Arctic and the Antarctic was caused by rare but not unexpected atmospheric conditions and is not cause for concern about the effectiveness of the implementation of the Montreal Protocol.

## 4.5 FUTURE CHANGES IN POLAR OZONE

This section examines the projected future changes in polar ozone from chemistry-climate model (CCM) simulations from three model intercomparison exercises:

- **CCMVal-2**: Based on the second phase of the SPARC Chemistry-Climate Model Validation (CCMVal; Morgenstern et al., 2010; WMO, 2010; WMO, 2014). The ODS mixing ratios that drive EESC projections originate from WMO (2007).
- **CCMI-1**: Based on phase one of the SPARC Chemistry-Climate Model Initiative (CCMI; Eyring et al., 2013; Morgenstern et al., 2017; WMO, 2018). The ODS mixing ratios that drive EESC projections originate from WMO (2010).
- **CMIP6**: Based on the Coupled Model Intercomparison Project Phase 6 (O'Neill et al., 2014; Meinshausen et al., 2017). The ODS mixing ratios that drive EESC projections originate from Meinshausen et al. (2020).

The recent CMIP6 results have not been part of any previous WMO Scientific Assessment of Ozone Depletion. The CCMVal-2 and CCMI-1 results are shown in this Assessment for continuity with the two previous Assessments (WMO, 2014, 2018). Results from the currently ongoing CCMI-2022 intercomparison (Plummer et al., 2021; ODS projections from WMO, 2018) are not included in this Assessment. At present, only a few models have

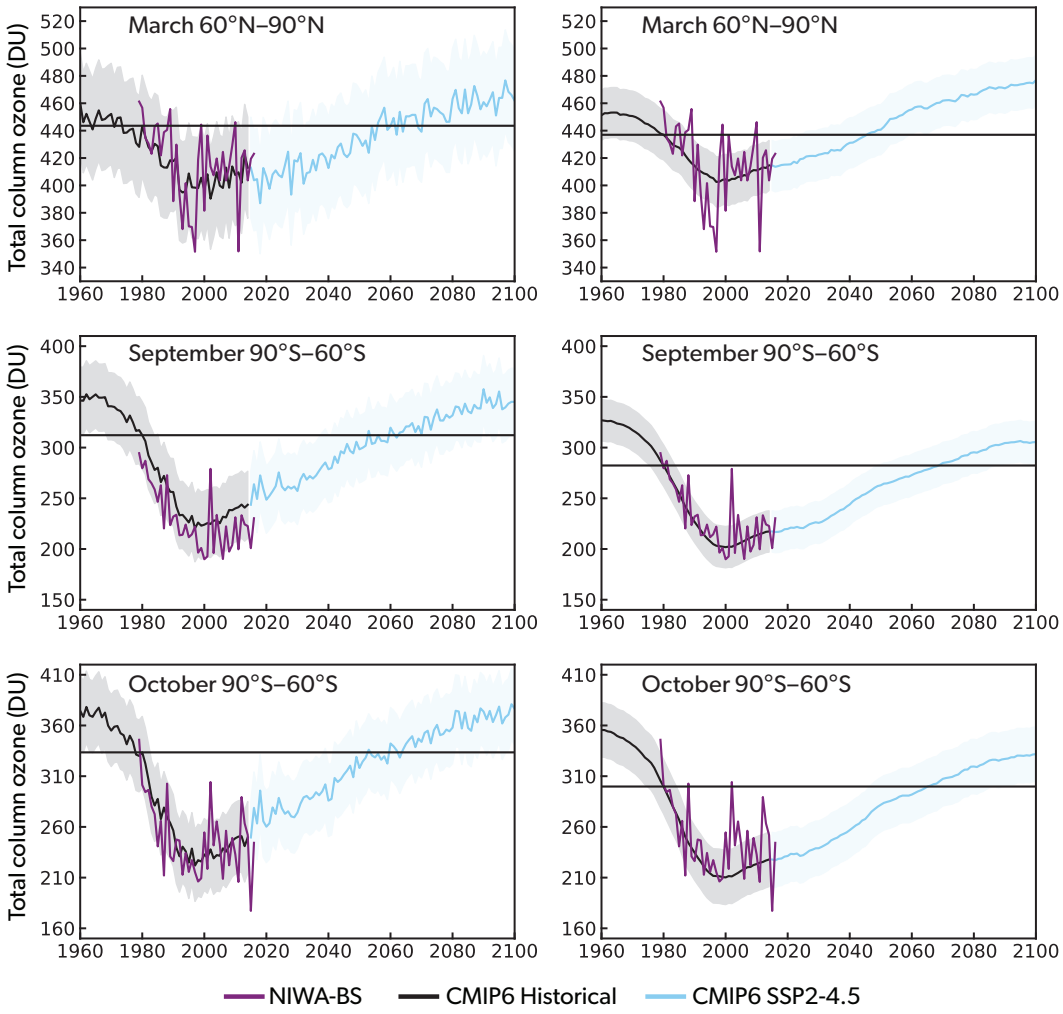


**Figure 4-19.** Time series of the multi-model mean (MMM) polar total column ozone (TCO, in Dobson units) from CMIP6 simulations for the Northern Hemisphere in March *(top row)*, Southern Hemisphere in September *(middle row)*, and Southern Hemisphere in October *(bottom row)*. In all cases, mean TCO is calculated as an average across 60–90° latitude. The CMIP6 results (Keeble et al., 2021) are for SSP2-4.5 (see **Figure 4-21** for other emissions scenarios) and include data from five participating CCMs for the Antarctic (CESM2-WACCM, CNRM-ESM2-1, GFDL-ESM4, MRI-ESM2-0, and UKESM1-0-LL); for the Arctic, MRI-ESM2-0 was excluded from the MMM (see text). The solid black horizontal lines show the 1980 reference values for each latitude band. The left column shows the unadjusted model values. The right column follows the approach discussed in Dhomse et al. (2018), where the mean biases between the observational data (the NIWA-BS dataset) and the reference simulation are derived for the 1980–1984 period and subtracted from all years over the 1960–2100 period. The right column also has an 11-year boxcar filter applied. Also shown are the observations based on NIWA-BS data (purple lines; Bodeker et al., 2021). The shaded region is the 1σ deviation.

completed the future simulations, and no analysis has been performed. This paucity of information precludes robust conclusions and the inclusion of CCMI-2022 results here.

### 4.5.1 New Ozone Projections from Chemistry-Climate Models

The CCMs that participated in CCMVal-2 (WMO, 2010, 2014) and CCMI-1 (WMO, 2018) were developed circa 2013 or before. The CCMI-1 projections are discussed in detail in Dhomse et al. (2018) and Langematz, Tully et al. (2018). Many CCMs that performed simulations used in prior WMO Assessments have been updated for participation in the CMIP6 (Keeble et al., 2021) activities. This includes updates to chemistry schemes (updated rate constant representation and enhanced tropospheric chemistry in all models) and interactive coupling of atmosphere-only CCMs to deep-ocean models. Many of the CCMs have also increased horizontal resolution. The scenarios for CMIP6 include a hindcast period (1960–2014) and a forecast period (2015–2100) that follows the CMIP6 shared socioeconomic pathway (SSP) scenarios. In this Assessment, we show forecast scenarios based on the SSP1-2.6, SSP2-4.5, SSP3-7.0, and SSP5-8.5 scenarios (O'Neill et al., 2014). (The number after the hyphen in the SSP name defines the Representative Concentration Pathway [RCP] used. For example,

for SSP2-4.5, the mean global radiative forcing will be 4.5 W $m^{-2}$ by the year 2100.) The relevant simulations and forcing for this Assessment are summarized in Braesicke, Neu et al. (2018, Box 3-2; CCMVal-2, CCMI-1) and **Box 3-4** (CMIP6).

## 4.5.2 Projections of Polar Ozone: Long and Near Term

This section focuses on the future evolution of Antarctic and Arctic polar ozone by CCMs that have participated in the CCMI-1 and CMIP6 assessments. Comparison of the results from these two sets of simulations builds on the discussion in *Section 3.4* and the associated discussion regarding ozone return dates; refer to that section for a discussion of uncertainties in model internal variability, structural uncertainty, and scenario uncertainty (see also Box 3-3 in Braesicke, Neu et al., 2018).

The baseline GHG scenario for CCMI-1 is based on the RCP6.0 scenario (Dhomse et al., 2018), while for CMIP6 it is based on the SSP2-4.5 (i.e., RCP4.5) scenario. More information on how uncertainties affect return dates is given in *Section 4.5.4.2*. The ozone recovery metric in the following two sections is the commonly used date of return of the ozone layer to values in 1980, the year when the ozone hole started appearing and polar observations became routinely available.

### *4.5.2.1 Future Antarctic Spring Total Column Ozone*

**Figure 4-19** shows the modeled evolution of total column ozone (TCO) in the Antarctic (60–90°S) in September and October (middle and bottom rows, respectively) for the multi-model mean (MMM) from the CMIP6 simulations of all five models, along with past observations. The shaded regions around the MMM TCO represent the 1σ standard deviation across the models. September is shown since many recent studies focusing on the detectability of Antarctic ozone recovery (Solomon et al., 2016; Pazmiño et al., 2018; Strahan et al., 2019; see related discussion in *Section 4.4.2.1*) have shown that this is a key month with a relatively dynamically stable vortex and that this month includes the initial onset and growth of the chemical ozone loss. October is also shown for continuity with previous Assessments. The CMIP6 MMM is divided into two periods: 1) the hindcast period (1950–2014, black lines) and 2) the forecast period (2015–2100, light blue lines). The CMIP6 ensemble has only five CCMs with interactive chemistry, whereas CCMI-1, used in the WMO (2018) projections, has 19 models with interactive chemistry.

The left column in **Figure 4-19** shows unadjusted results. In order to make a robust estimate of ozone return dates, biases between each model's simulation and the observations need to be accounted for. The right column follows the approach discussed in Dhomse et al. (2018), where the mean biases between the observational data (the NIWA-BS dataset) and the reference simulation are derived for the 1980–1984 period. Here an adjusted time series (in DU) for each model is then calculated by subtracting the respective observational bias. An 11-year boxcar filter is also applied to the adjusted model results to remove the effects of natural cycles in the data, particularly the 11-year solar cycle in TCO. This smoothing is applied to the bias-adjusted model results because these are used to determine return dates and the interannual and decadal variability seen in model projections can mask the long-term recovery trends. In contrast, the observed data reflect real-world variability in TCO resulting from dynamical variability and therefore are expected to be more variable. Despite these differences in variability represented by the modeled and observed time series shown in **Figure 4-19**, over the full hindcast period the bias-adjusted MMM TCO shows good agreement with observations, including during the strong decrease of Antarctic ozone in the 1980s and early 1990s. In both, a broad TCO minimum occurs around the year 2000.

A large spread in potential return dates in the model simulations arises partly because the bias-corrected model time series start to diverge as they proceed through the 21st century (**Figure 4-19**), but principally because the model time series approach the return threshold at very shallow angles, so even a few-DU difference between simulations translates into many years for the return dates. Smaller variability in return dates from previous Assessments was possibly due to the larger number of models available from the CCMI-1 and CCMVal-2 intercomparison projects (see discussion of the variance in the TCO projections in **Figure 3-24a**).

Simulated Antarctic September TCO is projected in the CMIP6 MMM (using SSP2-4.5) to return to the 1980 abundance shortly after mid-century (year 2066). The shaded region in **Figure 4-19** shows the 1σ uncertainty error bars about the MMM.

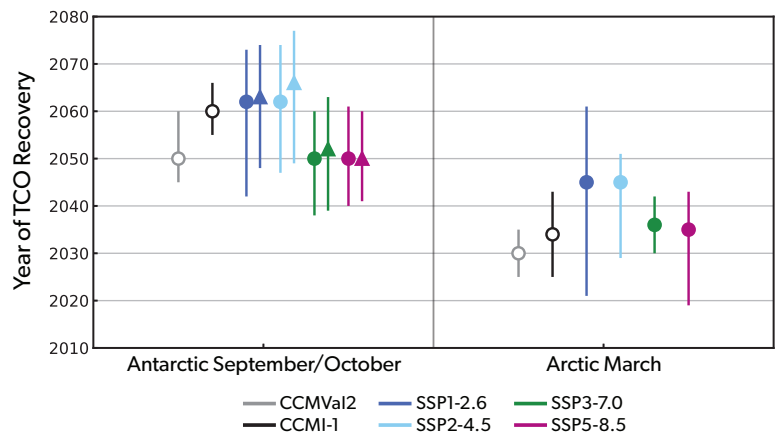


**Figure 4-20.** Total column ozone 1980 return dates for different CCM experiments. The left panel shows the Antarctic (90–60°S) mean for September (triangles) and October (circles), along with the estimated 1σ uncertainties (whiskers). The error bars are calculated as the first and last time the 1σ envelope around the projection in **Figure 4-19** crosses the return threshold. The right panel shows the Arctic (60–90°N) mean for March (circles) with estimated 1σ uncertainties (whiskers). [Update of Figure 4-22 from Langematz, Tully et al. (2018) now including CMIP6 projections using various SSPs (filled symbols), in addition to CCMVal2 and CCMI-1 projections (open circles).]

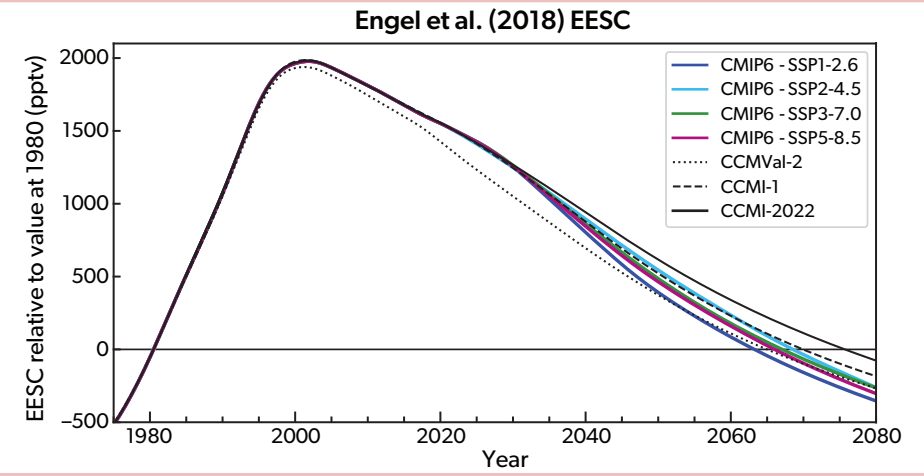


**Figure 4-21.** Equivalent effective stratospheric chlorine (EESC; pptv) for a mean age-of-air of 5.5 years (representative of the polar lower stratosphere) with an alpha factor for bromine reactivity equal to 60 (Engel et al., 2018). Seven different halogen recovery scenarios used as input to CCM experiments are shown.

The first and last time the 1σ envelope around the projection crosses the return threshold is shown as whisker lines in **Figure 4-20**. The October TCO MMM returns 4 years earlier (year 2062) with a similar range. Compared to results in Langematz, Tully et al. (2018), the current October TCO CMIP6 MMM estimate is later by ~2 years. The equivalent effective stratospheric chlorine (EESC) evolution is similar between the two intercomparisons (see **Figure 4-21**); however, CCMI-1 (used in the WMO, 2018, projection) was based on the RCP6.0 GHG scenario, which differs from the CMIP6 SSP2-4.5 (i.e., RCP4.5) such that the MMM in the CCMI-1 assessment would tend to recover earlier (see *Section 4.5.3.4*). The return date and its uncertainty are discussed in more detail in *Section 4.5.4*.

### *4.5.2.2 Future Arctic Spring Total Column Ozone*

The temporal evolution of the Arctic March TCO MMM (60–90°N) derived from the CMIP6 SSP2-4.5 simulations is presented in **Figure 4-19** (top row). The Arctic MMM includes all participating CCMs except MRI-ESM2-0, which was removed from the MMM because of its lack of hindcast TCO depletion. As in the Antarctic, the bias-adjusted MMM TCO shows good agreement with observations (purple lines). In the forecast period, a TCO return date to 1980 conditions is expected near mid-century for CMIP6 SSP2-4.5 (year 2045), with a range between 2029 and 2051 (**Figure 4-20**). These new CMIP6 TCO projections suggest an MMM return date for Arctic spring that is later by ~11 years compared to the CCMI-1 estimate (Langematz, Tully et al., 2018). In the Arctic, the influence from the differences in the GHG scenario will play more of a role; all things being equal, the CCMI-1 MMM would be expected to recover earlier than the CMIP6 MMM (see *Section 4.5.3.1*). The return date and its uncertainty are discussed in more detail in *Section 4.5.4*.

## 4.5.3 Factors Controlling Future Polar Ozone

### *4.5.3.1 Changing Role of ODSs and GHGs*

Ozone-depleting substances (ODSs) are expected to decrease in the future, and greenhouse gases (GHGs) are on a trajectory to increase (**Box 3-4**). Therefore, the relative radiative and chemical effects of ODSs and GHGs on polar ozone will change with time. CCMI-1 simulations using separate forcing assumptions addressed the sensitivity of TCO to ODSs and GHGs. The CCMI-1 reference simulation (i.e., REF-C2; RCP6.0) and two separate forcing simulations (i.e., SEN-C2-fODS and SEN-C2-fGHG; Morgenstern et al., 2017) are shown in Langematz, Tully et al. (2018, Figure 4-19). The REF-C2 included the RCP6.0 GHG forcing scenario, while the SEN-C2-fODS (also using the RCP6.0 GHG scenario) and SEN-C2-fGHG scenarios set the abundance of ODSs and GHGs, respectively, to a constant 1960 value between 1960 and 2100. In the Antarctic (October mean), the SEN-C2-fODS shows no ozone depletion from 1960 through 2100, with only a slight ozone increase (<5 DU) by the end of the 21st century. The same region and period for the SEN-C2-fGHG simulation has a temporal evolution in TCO similar to that of the REF-C2 reference simulation, which includes a hindcast period of large ozone depletion consistent with observations. However, after the middle of the century, the GHG forcing contained within the REF-C2 shows an increase in the TCO recovery (~10 DU) relative to the SEN-C2-fODS. In the Arctic (March mean), the ODS and GHG sensitivity is different. Here, the SEN-C2-fODS shows a stronger influence of GHGs from 1960 to 2100, and the SEN-C2-fGHG deviates more from the REF-C2 than modeled in the Antarctic (October mean). This ozone increase is caused by increasing GHG abundances, which both cool the stratosphere, thereby reducing gas-phase chemical ozone loss, and strengthen the Brewer-Dobson circulation (BDC), leading to increased poleward and downward transport of ozone in Arctic spring (e.g., Oman et al., 2010; Oberländer et al., 2013). Note that the multi-model study of Polvani et al. (2019) showed that ODSs are responsible for more than half of the modeled increasing BDC trend in the 1980–2000 period. In the future, decreasing ODSs as a consequence of the Montreal Protocol and its Amendments and adjustments are projected to strongly decelerate the BDC until year 2080, reducing the mean age-of-air trends by more than one half and thus substantially mitigating the impact of carbon dioxide ($CO_2$) strengthening the BDC. Polvani et al. (2019) also found that the depletion/recovery of stratospheric ozone over Antarctica contributes to seasonal and hemispheric asymmetries in the BDC trends, and they suggest that this impact could be a method for detection of a BDC trend in the coming decades. However, it should be noted that there is still a discrepancy between age-of-air trends derived from models and those derived from observations (Strahan et al., 2020; Prignon et al., 2021).

### 4.5.3.2 Impact of Noncompliant CFC-11 Production

The global emissions of CFC-11 were expected to decrease after 2010 based on full phaseout of production and consumption. However, Montzka et al. (2018) showed that emissions started to increase in 2013 and remained elevated through 2018 (*Chapter 1*), in violation of the Montreal Protocol. The mean emissions enhancement during the period 2014–2017 relative to 2008–2012 is estimated to be 13.7 Gg $yr^{-1}$ (Montzka et al., 2021), and the cumulative unexpected emissions of CFC-11 during 2012–2019 are estimated to be 120–440 Gg (WMO, 2021). See *Chapter 1* for more discussion on the observed changes in chlorofluorocarbons (CFCs).

Subsequent modeling studies have examined the effects of these and hypothetical other additional CFC-11 emissions on TCO recovery (Dhomse et al., 2019; Dameris et al., 2019; Fleming et al., 2020; Keeble et al., 2020; Lickley et al., 2020; WMO, 2021). Due to the large fractional release of CFC-11 abundance in the polar region (Newman et al., 2007), the delay in TCO recovery is linearly dependent on the resultant inorganic chlorine increase. Simulations using the GSFC2D model show, for example, that sustained emissions at the large level of 72 Gg $yr^{-1}$ would shift the 1980 return date for Antarctic ozone by 25 years (Fleming et al., 2020). This example of sustained CFC-11 emissions is probably not realistic but was included as a sensitivity study by Carpenter, Daniel et al. (2018). Using the UKCA CCM, Keeble et al. (2020) also note that the largest delay in ozone recovery due to enhanced CFC-11 concentrations occurs in the Antarctic spring.

**Figure 4-22** shows the Antarctic TCO return date to 1980 levels for various cumulative additional CFC-11 emissions compared to baseline halogen simulations (Carpenter, Daniel et al., 2018, A1 scenario) for two CCMs (UKCA and GEOSCCM), one two-dimensional model (GSFC2D), and one three-dimensional CTM (TOMCAT). Atmospheric CFC-11 abundances in the baseline halogen scenario are based on compliance with the Montreal Protocol over the full timeline. Three models (UKCA, GSFC2D, and TOMCAT) performed perturbation simulations with different assumptions of additional CFC-11 (and in some cases CFC-12 converted to equivalent CFC-11) emissions based on noncompliant production. Model sensitivities in return date to additional noncompliant CFC-11 emissions are shown (i.e., return date versus cumulative additional CFC-11 emissions in Gg). This was done for September mean ozone in the Antarctic, since that is the month with the largest ozone loss rates. The linear fits to the model scenarios in **Figure 4-22** suggest that they can be scaled to other emissions scenarios. The TOMCAT CTM, which does not include climate feedbacks, gives the largest slope of 7.1 years per 1000 Gg. The GSFC2D gives the smallest slope of 4.0 years per 1000 Gg, but, as a 2-D model, it cannot capture the full 3-D behavior of the Antarctic polar vortex. The UKCA results are in between, with a slope of 6.4 years per 1000 Gg. The suggested range is most likely 4–7 years per 1000 Gg of cumulative noncompliant CFC-11 emissions. Therefore, the observed cumulative additional emissions of 120–440 Gg in the 2012–2019 period would add an additional 0.5–3.1 years to the September date of return to 1980 conditions (WMO, 2021).

### 4.5.3.3 Dynamical Variability in Arctic Spring

There is uncertainty about the role of dynamical variability in modulating future stratospheric Arctic ozone. Observations and model studies have shown that chemical loss of Arctic ozone from halogens is strongly controlled by low temperatures that promote the formation of polar stratospheric clouds (PSCs). In the future, as ODSs decrease and GHGs increase, large Arctic ozone depletion events may still occur. That is, with the persistence into springtime of a cold and dynamically isolated Arctic vortex, ozone loss could be comparable to that in the cold Northern Hemisphere springs of 2011, 2016, and 2020 (see discussion in *Section 4.3.4*). CCM studies have shown that enhanced GHG abundances will cause cooling in the Arctic winter upper and middle stratosphere (Langematz, Tully et al., 2018, and references therein). This cooling will accelerate ozone recovery from ODSs in the upper stratosphere by slowing down the rates of gas-phase ozone loss

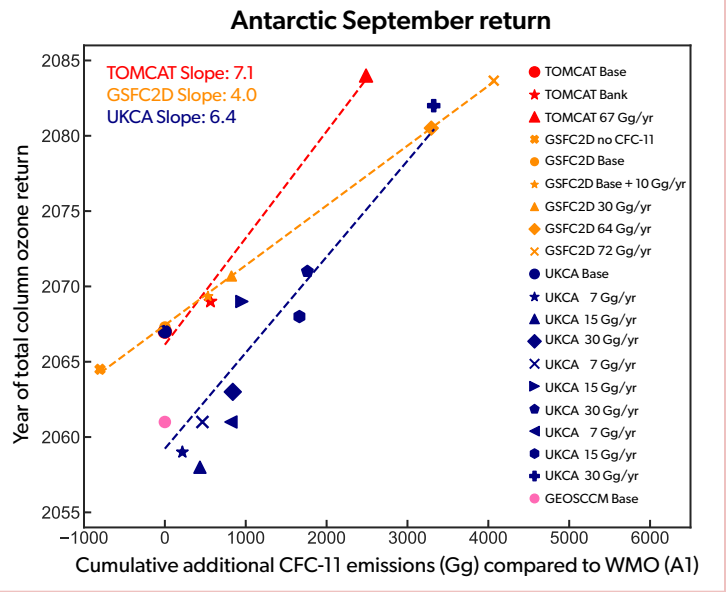


**Figure 4-22.** Dependence of September mean Antarctic (90–65°S) column ozone 1980 return dates on cumulative additional (compared to WMO, 2018, A1 baseline scenario) equivalent CFC-11 emissions (Gg), as in **Figure 3-28** for global ozone. The colors indicate the model, and the symbols correspond to different simulations with that model. Each model performed a base simulation using the WMO (2018) A1 baseline scenario. The models also performed perturbation simulations with different assumptions of additional CFC-11 emissions (and in some cases CFC-12 emissions converted to equivalent CFC-11 emissions), quantified as Gg equivalent CFC-11 emissions along the x-axis. The dashed lines (with numerical values giving the slope in years per 1000 Gg) show the best linear fits to the simulations for each model.

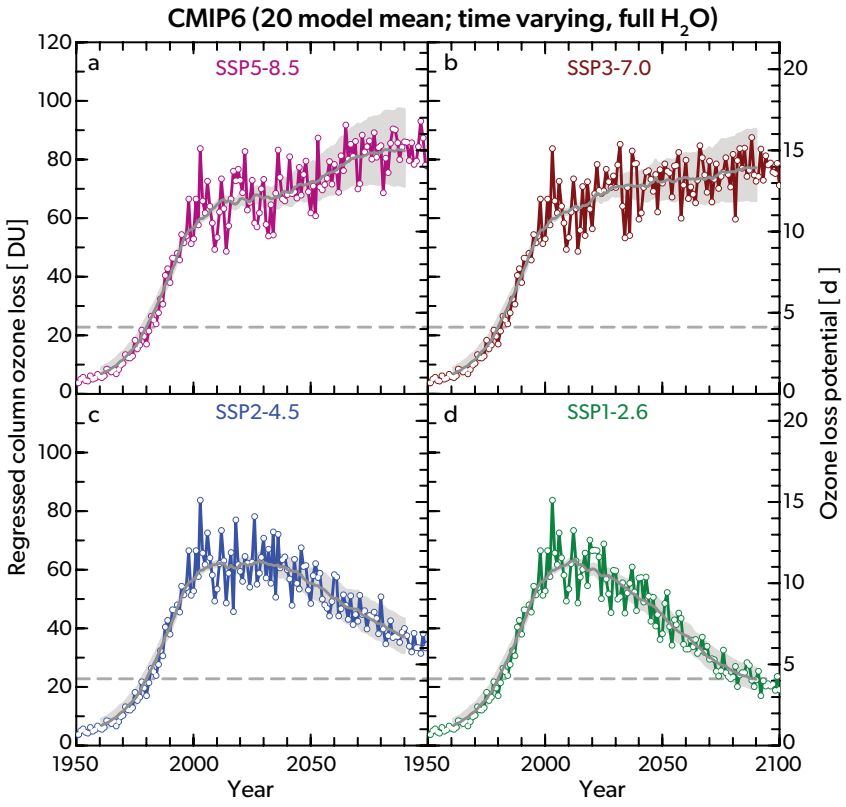


**Figure 4-23.** Ensemble-mean regressed Arctic column ozone loss ($\Delta O_3^{REG}$, DU; left ordinate) and Ozone Loss Potential (OLP, days; right ordinate) as a function of year. $\Delta O_3^{REG}$ represents the chemical ozone loss in the lower-stratospheric portion of the Arctic vortex, and OLP represents the number of days a volume of air equal to that of the Arctic vortex is exposed to PSC conditions over the course of an ozone loss season. The OLP derivation uses the model polar stratospheric $H_2O$, which accounts for increasing stratospheric humidity due to both increasing $CH_4$ oxidation and warming of the tropical tropopause; the $HNO_3$ abundance is taken from present-day observations. The regressed column ozone loss is computed from each of the model OLPs. The gray solid line shows a 21-year running mean (±10 years) of the ensemble mean of the regressed column ozone loss ($\Delta O_3^{REG}$) for each SSP, the gray shaded area represents a 21-year running mean of the range in $\Delta O_3^{REG}$ for exponents of 1 (upper boundary) and 1.4 (lower boundary) of the expression for OLP, and the gray dashed horizontal lines denote the 1980 value of $\Delta O_3^{REG}$. (a) SSP5-8.5, (b) SSP3-7.0, (c) SSP2-4.5, and (d) SSP1-2.6 scenarios. [From von der Gathen et al., 2021.]

reactions. A recent study examining PSC formation potential (PFP, the seasonal integral of the ratio of the volume of the region containing PSCs [$V_{PSC}$] to the volume of the Arctic vortex) from four reanalysis datasets suggests that cold Arctic stratospheric winters have become colder over the past 40 years (von der Gathen et al., 2021; see also Vargin et al., 2022, and related discussion in *Section 4.2.2.2*). For future projections, von der Gathen et al. (2021) used a simple relationship between PFP and EESC to derive an ozone loss potential (OLP). The derived OLP and regressed column loss (from the OLP based on present-day observations of ozone loss) from 16 general circulation models (GCMs) and four CCMs (with interactive chemistry) for four different GHG scenarios (SSP5-8.5, SSP3-7.0, SSP2-4.5, and SSP1-2.6) are shown in **Figure 4-23**. The seasonal chemical ozone loss diagnostic shown here represents the amount of ozone chemically removed in the lower-stratospheric portion of the Arctic vortex, rather than the resulting TCO depletion over the polar cap. This figure uses the GCM- and CCM-derived time series of polar stratospheric water vapor ($H_2O$), which reflect increases in stratospheric humidity arising from both increasing methane ($CH_4$) oxidation and warming of the tropical tropopause. Moister conditions in the lower stratosphere are more conducive to PSC formation. Therefore, the net effect of strong GHG increases on polar chemical loss in the future is the combination of stratospheric cooling and enhanced supply of $H_2O$ and $CH_4$ from the troposphere.

Von der Gathen et al. (2021) concluded that if stratospheric humidity rises as projected and GHGs follow either the SSP5-8.5 or the SSP3-7.0 trajectories, then there is an increased potential for Arctic column ozone depletion to occur until the end of the century, despite the expected decline in halogen loading. That is, cooling and moistening of the Arctic stratosphere could act in concert to prolong the period over which significant seasonal chemical ozone losses are expected to occur in the future and could even lead to losses larger than those currently seen in severe Arctic winters (von der Gathen et al., 2021). However, it should be noted that the four CCMs, which have a better representation of stratospheric dynamics (e.g., planetary wave activity influence on the BDC, etc.), showed 20–25% lower OLP at the end of the century than that found for the 16 GCMs. The potential for increased chemical ozone depletion later in the century will be affected by many dynamical processes that may not be adequately represented in current models, especially those lacking interactive ozone chemistry. See further discussion of dynamical control of polar ozone under climate change in *Section 4.3.4.3*.

### *4.5.3.4 The Role of GHG Scenarios*

Future ozone recovery is influenced by carbon dioxide ($CO_2$), methane ($CH_4$), and nitrous oxide ($N_2O$) through radiative processes that cool the stratosphere (*Chapter 5*). $CH_4$ and $N_2O$ also have chemical effects that can impact future ozone abundances. Many studies have investigated the impact of the assumed $CH_4$ and $N_2O$ future scenarios on ozone abundance and recovery (see

Section 4.5.3.3 of Langematz, Tully et al., 2018, and references therein). It is well known that increases in $CH_4$ and $N_2O$ will generate larger amounts of hydrogen oxides ($HO_x$) and nitrogen oxides ($NO_x$), respectively, and also that increased $NO_x$ will enhance catalytic middle-stratospheric ozone loss. Therefore, in general, the ozone return date is expected to be later if there are increases in $N_2O$ or earlier if there are decreases in $N_2O$. However, the effect of future increases in $N_2O$ varies with altitude and also depends on the temporal evolution of other GHGs.

For changes in $CH_4$, the situation is more complicated. In a similar manner to $NO_x$, increased $HO_x$ from $CH_4$ oxidation will decrease upper-stratospheric ozone. However, $CH_4$ can also affect the partitioning of reactive chlorine through the reaction of $CH_4 + Cl \rightarrow HCl + CH_3$, with more $CH_4$ generally leading to an increase in stratospheric ozone via a decrease in the abundance of reactive chlorine. Thus, future increases in $CH_4$ are expected to lead to increases in stratospheric column ozone, notwithstanding the impact on Arctic $H_2O$ discussed in *Section 4.5.3.3*. Recently, experiments with $2\times CH_4$ and $5\times CH_4$ present-day mixing ratios were conducted using a CCM (Winterstein et al., 2019). Twenty-year time-slice simulations were conducted consistent with year-2010 halogen conditions. These very large quasi-instantaneous increases in $CH_4$ strongly affected tropospheric chemistry by reducing the hydroxyl radical (OH) abundance, which resulted in extending the lifetime of $CH_4$ and many other chemical substances. In the stratosphere, there were substantial increases in stratospheric water vapor (SWV) of 50% and 250% for the $2\times CH_4$ and $5\times CH_4$ simulations, respectively, which cooled the stratosphere by several degrees. This cooling caused an increase in the TCO globally, except in the Antarctic spring due to enhanced PSC chemistry. Ozone in the tropical lowermost stratosphere decreased due to enhanced upwelling. This work did not specifically examine Arctic PSC chemistry, although both the $2\times CH_4$ and the $5\times CH_4$ simulations did show lower-stratospheric ozone decreases of a few percent in the wintertime Arctic. Prescribed sea surface temperatures were used, so tropospheric warming feedbacks were not included. A follow-up study (Stecher et al., 2020) incorporated a mixed-layer ocean model into the CCM to account for additional tropospheric warming. As in the previous study, they found that strong increases in $CH_4$ reduced OH in the troposphere and extended the $CH_4$ lifetime. However, a slow climate feedback also arose and counteracted this reduction in OH through increases in tropospheric water vapor and ozone, thereby damping the quasi-instantaneous response found by Winterstein et al. (2019).

Future scenarios with larger GHG abundances lead to an overall higher level of simulated stratospheric ozone (Langematz, Tully et al., 2018). Increased GHG levels result in lower temperatures in the middle atmosphere. These cooler conditions will decrease ozone loss reactions and result in an ozone increase in the upper stratosphere. The choice of GHG scenario can also affect the modeled amount of polar $NO_x$ that is transported from the upper mesosphere and thermosphere into the upper stratosphere. Using a CCM, Maliniemi et al. (2021) showed that $NO_x$ produced by energetic electron precipitation (EEP) and partly by solar ultraviolet above the stratopause is transported down into the polar upper stratosphere. This study used four different GHG scenarios. They showed that the larger the GHG forcing scenario, the greater the amount of $NO_x$ transported into the upper stratosphere (see *Section 4.5.3.1*). This additional $NO_x$ depletes more

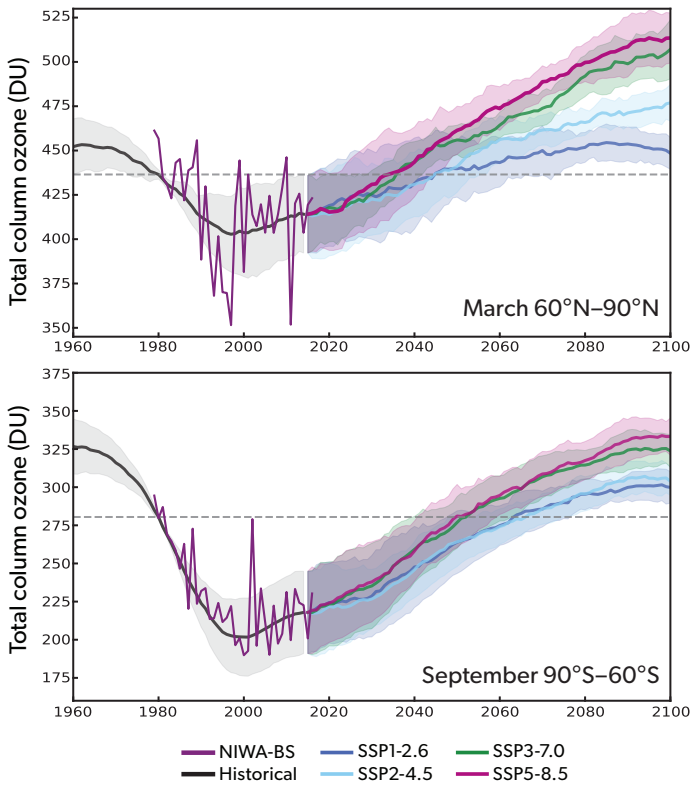


**Figure 4-24.** Impact of GHG scenarios (SSP1-2.6, SSP2-4.5, SSP3-7.0, SSP5-8.6) on polar total column ozone in the CMIP6 model ensemble; for the list of models included in each hemisphere, see the caption of **Figure 4-19**. Historical and projected polar cap average TCO is shown for March in the Arctic *(top)* and September in the Antarctic *(bottom)*. Observations (purple lines) are from the NIWA-BS dataset. The dashed gray lines show the 1980 reference values for each latitude band.

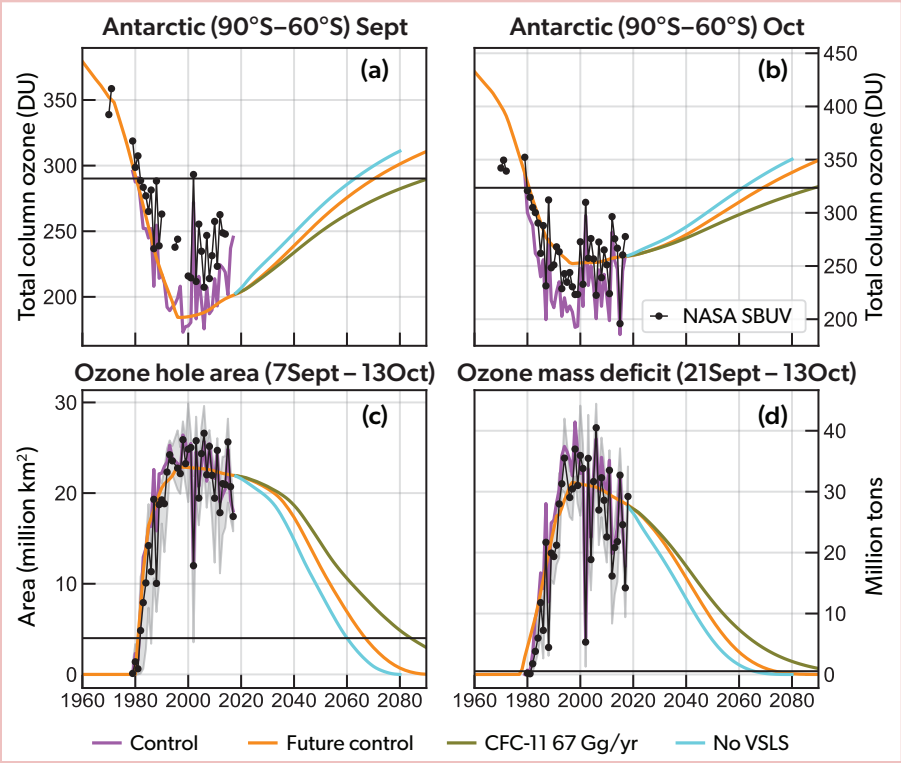


**Figure 4-25.** Antarctic ozone and metrics quantifying ozone loss as a function of additional CFC-11 and VSLS emissions. Mean column ozone (DU) averaged from 90–60°S for (a) September and (b) October from four TOMCAT 3-D model simulations: control (varying meteorology), future control (2000 meteorology), with constant 67 Gg $yr^{-1}$ emissions of CFC-11, and with no chlorinated very short-lived substances (VSLSs), as well as SBUV observations from 1960 to 2019 (black lines with dots). The horizontal black lines indicate the modeled 1980 values. (c) Estimates of the size of the Antarctic ozone hole under control, future control, 67 Gg $yr^{-1}$ CFC-11 emissions, no VSLSs, and as observed (based on ozonewatch.gsfc.nasa.gov) using the area contained within the 220 DU contour ($10^6$ $km^2$; averaged over the period 7 September–13 October). (d) As in (c) but for ozone mass deficit ($10^6$ metric tons; averaged over the period 21 September–13 October). The gray shading in panels (c) and (d) gives the maximum and minimum values for each year in the period analyzed. Additional emissions of CFC-11 at the level assumed would delay recovery of the Antarctic ozone hole, meaning a delay in the date of return to 1980 values, by around 17.5 years. Similarly, elimination of chlorinated VSLS emissions is projected to speed up the ozone return by around 7 years (for both September and October). [Adapted from Chipperfield et al., 2020, and Dhomse et al., 2019.]

ozone, offsetting the ozone increases driven by climate cooling acting to decrease the rate of the $NO_x$ catalytic ozone loss cycle. This result indicates that $NO_x$ production in the upper mesosphere and thermosphere will be an important factor for the future upper-stratospheric Antarctic ozone evolution and could potentially prevent a super-recovery (i.e., where ozone abundance is greater than the 1980 values) in that altitude region.

Therefore, the TCO recovery to a historical baseline (e.g., 1980 conditions) will depend strongly on the GHG scenario (**Box 3-4**), particularly in the Arctic. This is shown in **Figure 4-24** using projections from the CCMs used in the CMIP6 model ensemble. This figure shows results from five CCMs for the Antarctic and four CCMs for the Arctic (Keeble et al., 2021), as well as four different SSPs (SSP1-2.6, SSP2-4.5, SSP3-7.0, and SSP5-8.5). The TCO return date and range for each SSP is shown in **Figure 4-20**. As discussed in *Section 4.5.3.1*, the Arctic is more sensitive to GHG evolution than the Antarctic. The March MMM TCO recovery to 1980 conditions occurs around the year 2045 for the SSP1-2.6 (range of −24 and +16 DU in the 1σ deviation at that time) and SSP2-4.5 (range of −16 and +6 DU) simulations, with SSP2-4.5 having more of a super-recovery by the end of the 21st century (~35 DU above the 1980 baseline). The 1980 return dates for the SSP3-7.0 and SSP5-8.5 MMM simulations are earlier (~2035) than for the SSP1.2-6 and SSP2-4.5 scenarios, and they show a larger super-recovery by the end of the 21st century, with an increase in TCO above the baseline of ~70 DU. This is consistent with the results for the CCMI-1 assessment (Langematz, Tully et al., 2018).

In the Antarctic spring, there is less spread in the temporal evolution of the TCO across SSPs. The September return date to 1980 conditions is around the years 2063 and 2066 for SSP1-2.6 and SSP2-4.5, respectively. The 1980 return date is around 2052 and 2050 for SSP3-7.0 and SSP5-8.5, respectively. This is approximately 16 years earlier for SSP5-8.5 relative to the baseline SSP2-4.5 scenario. This new CMIP6 assessment result of a strong dependence of Antarctic ozone recovery on GHG scenario is not consistent with the CCMI-1 results discussed in Dhomse et al. (2018) and Langematz, Tully et al. (2018). This sensitivity of Antarctic recovery to climate change scenario may be due to the use of a smaller number of updated models (and model realizations) contained in the CMIP6 assessment (Keeble et al., 2021) relative to the larger CCMI-1 study. In addition, the evolution of GHGs could be different in these CMIP6 models (see discussion of uncertainty in polar ozone projections in *Section 4.5.4*).

### *4.5.3.5 The Role of VSLSs (Bromine and Chlorine)*

Results from simulations examining the effects of VSLS bromine emissions (e.g., bromoform [$CHBr_3$] and dibromomethane [$CH_2Br_2$]) on future polar ozone remain mixed, with no new information since the last Assessment (Langematz, Tully et al., 2018). Yang et al. (2014) and Oman et al. (2016) suggest that including VSLS bromine will extend the return date to 1980 conditions by

~10 years and 6–8 years, respectively, while Fernandez et al. (2017) do not see a change in the return date from inclusion of VSLS brominated species within the variability of the ensemble members. Thus, the magnitude of any potential impacts of VSLS bromine emissions on ozone recovery remains uncertain.

Total VSLS chlorine (e.g., chloroform [$CHCl_3$] and dichloromethane [$CH_2Cl_2$]) has a contribution of around 130 (100–160) ppt in the present-day stratosphere (*Chapter 1*; Hossaini et al., 2018; Fang et al., 2019). **Figure 4-25** shows the impact of keeping the VSLS chlorine flux constant at current conditions (Dhomse et al., 2019; Chipperfield et al., 2020). This contrasts with what was shown in Langematz, Tully et al. (2018), where a positive trend in VSLS chlorine abundance was assumed. **Figure 4-25** shows the 1980 return dates for both the Antarctic September and October polar cap TCO, along with two additional diagnostics, i.e., ozone hole area and ozone mass deficit. The "future" control case simulation includes present-day emissions of VSLS chlorine. The "no VSLS" case zeroes these emissions. Including VSLS chlorine emissions delays the TCO return date to 1980 conditions by approximately 7 years. For comparison, the more extreme noncompliant CFC-11 emissions scenario of 67 Gg $yr^{-1}$ (WMO, 2018) delays the TCO return date to 1980 conditions by ~17.5 years, although the impact will scale for smaller perturbations (see *Section 4.5.3.2*). The ozone hole area and ozone mass deficit diagnostics give the same return dates (within ±1 year) as the TCO for both the VSLS chlorine and 67 Gg $yr^{-1}$ noncompliant emissions scenarios.

## 4.5.4 Uncertainty in Polar Ozone Projections

Current CCMs, developed over the past 20 years, have similar representations of dynamical, transport, and chemical processes (e.g., SPARC, 2010; Morgenstern et al., 2017). Nevertheless, there are three types of uncertainties that still need to be considered (Box 3-3 of Braesicke, Neu et al., 2018). The first is internal variability, which arises from chaotic processes and can be minimized by running multiple realizations with different starting conditions and forming an ensemble average. The second is structural uncertainty, which arises from different representations of resolution (e.g., high-top models that include a well-resolved stratosphere versus low-top models that have an upper lid below the stratopause), including or not an interactive QBO, and/or representing a deep ocean. The choice of chemical mechanism and/or the choice of laboratory rate constant recommendations can also add to the overall uncertainty (e.g., Fleming et al., 2015). The third is scenario uncertainty, whereby the specification of ODS and GHG time series can have large impacts on a given ozone recovery diagnostic. The assumed ODS scenario, in particular, has a direct impact on the polar TCO return date, especially in the Antarctic, where changes in GHGs and climate have comparatively smaller impacts on ozone (Klobas et al., 2020).

### 4.5.4.1 Model Uncertainty

Ideally, the multi-model mean (MMM) ozone return date would be calculated using an ensemble of models that are fully independent. However, model components are shared amongst families of models, so they are not strictly independent. Amos et al. (2020) developed a procedure to use observations to assess and account for both model performance and model independence (**Figure 4-26**). Model performance was derived from comparison to observations and used to weight the CCMI-1 ensemble simulations to derive weighted-mean estimates of Antarctic ozone depletion and subsequent ozone recovery. The return to 1980 date from this weighted MMM was the year 2056 (95% confidence interval 2052–2060). While the ozone return date found in this work (2056) is different from that (2062) found by Dhomse et al. (2018), these two dates are not easily comparable, as they are created from different subsets of the same ensemble. For the subset of models in Amos et al. (2020), the simple MMM return date was three years earlier (2053) than the weighted mean. Amos et al. (2020) also argued that the weighted MMM showed a greater projective skill than the simple MMM. The construction of a weighted mean also provided insight into model performance and dependence between the models.

### 4.5.4.2 Uncertainty in Ozone Return Dates

Although ozone recovery is underway (see *Section 4.4*), uncertainty remains about how it will progress in the future and what metric is best to diagnose it. The date for the atmosphere to return to a specified state does not take account of variability in

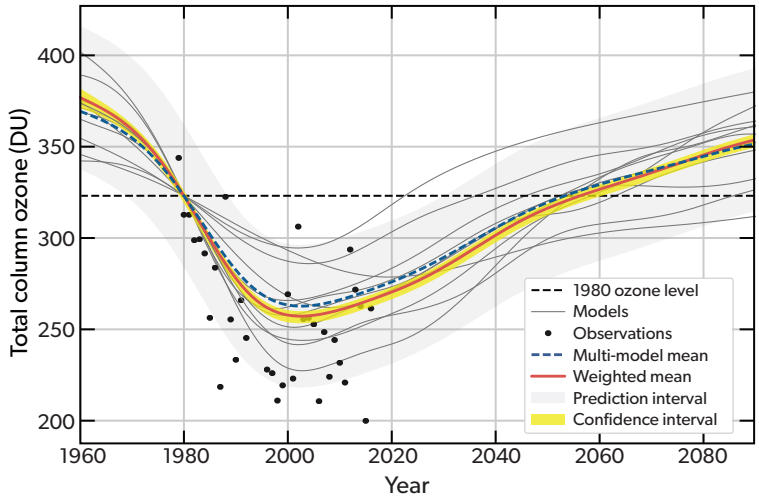


**Figure 4-26.** Simulated and observed Antarctic (60–90°S) October TCO. The weighted model mean is shown in red, the multi-model mean in blue, and individual model trends in gray lines. Observed TCO (black dots) are from NIWA-BS data. All model projections and ensemble projections are normalized to the observational 1979–1981 mean, shown as the black dashed line, and so they converge in the year 1980. The 95% confidence and prediction intervals for the weighted mean are also shown with yellow and light gray shading, respectively. [From Amos et al., 2020.]

that pathway or in the impact of other transient factors before the final return date. Pyle et al. (2022) discuss the use of integrated ozone depletion as a metric for ozone recovery both globally and in specific regions. This metric integrates the additional ozone depletion, based on model simulations, due to any emissions scenario over the full (possibly multi-decadal) duration of the impact, taking account of short-term perturbations and avoiding sensitivity to the date of a single return event. For this metric, a simple empirical expression exists for perturbations due to long-lived ODSs. For the Antarctic ozone hole in particular, other established measures of its size (e.g., ozone mass deficit, ozone hole area) may give a more robust perspective on recovery, especially when considered together and when applied to periods of greatest sensitivity to halogen-induced chemical loss (**Figure 4-25**; Dhomse et al., 2019).

***Sensitivity to ODS and GHG Scenarios.*** A direct influence on the ozone return date is the choice of the halogen recovery scenario. In **Figure 4-21**, the EESC based on Engel et al. (2018) is shown for a specific polar condition (i.e., mean age of 5.5 years). The evolution of EESC is shown for CCMI-1 and CMIP6 (different EESC for each SSP; SSP2-4.5 is the baseline scenario). Comparison of the CCMI-1 EESC (RCP6.0) to the CMIP6 EESC (SSP2-4.5) suggests that very little difference is expected in the return date, which is borne out in the return dates in **Figure 4-20**. However, the EESC for the currently ongoing CCMI-2022, based on Carpenter, Daniel et al. (2018), shows a five-to-seven-year extension in the halogen recovery relative to CCMI-1 and CMIP6 SSP2-4.5 (**Figure 4-21**). This change in EESC alone would translate to an extension of the Antarctic TCO return date as implied in **Figure 4-22**, but simulations based on this halogen scenario are not included in this Assessment.

***Sensitivity to VSLSs.*** Langematz, Tully et al. (2018) discussed the uncertainty in both bromine and chlorine future VSLS emissions and found that the uncertainty in the delay of the return date of Antarctic TCO to historical values was somewhere between several years and up to three decades. This uncertainty includes the unknown influence of climate change on the emissions of bromine-containing VSLSs, predominantly from oceanic emissions (e.g., Tegtmeier et al., 2015; Ziska et al., 2018). The chlorine-containing VSLSs (e.g., $CHCl_3$, $CH_2Cl_2$) are mainly produced by industry (*Chapter 1*). Hossaini et al. (2017) assumed a future impact on the return date to 1980 conditions from a continuous increase in $CH_2Cl_2$ with a mean emission rate observed for the 2004–2014 period. This increasing $CH_2Cl_2$ emissions rate delayed the ozone return date by approximately 20 years. In *Section 4.5.3.5*, this study was updated with a constant flux based on present-day conditions (**Figure 4-25**). The delay in the ozone return to 1980 values was approximately 7 years. There have not been any additional studies since the 2018 Assessment that have reduced projected VSLS return date uncertainty.

# REFERENCES


Adcock, K.E., P.J. Fraser, B.D. Hall, R.L. Langenfelds, G. Lee, S.A. Montzka, D.E. Oram, T. Röckmann, F. Stroh, W.T. Sturges, B. Vogel, and J.C. Laube, Aircraft-based observations of ozone-depleting substances in the upper troposphere and lower stratosphere in and above the Asian summer monsoon, ***J. Geophys. Res. Atmos.***, ***126*** (1), e2020JD033137, doi:10.1029/2020JD033137, 2021.

Albers, J.R., J. Perlwitz, A.H. Butler, T. Birner, G.N. Kiladis, Z.D. Lawrence, G.L. Manney, A.O. Langford, and J. Dias, Mechanisms governing interannual variability of stratosphere-to-troposphere ozone transport, ***J. Geophys. Res. Atmos.***, ***123*** (1), 234–260, doi:10.1002/2017JD026890, 2018.

Allen, D.R., M.D. Fromm, G.P. Kablick III, and G.E. Nedoluha, Smoke with induced rotation and lofting (SWIRL) in the stratosphere, ***J. Atmos. Sci.***, ***77*** (12), 4297–4316, doi:10.1175/JAS-D-20-0131.1, 2020.

Amos, M., P.J. Young, J.S. Hosking, J.-F. Lamarque, N.L. Abraham, H. Akiyoshi, A.T. Archibald, S. Bekki, M. Deushi, P. Jöckel, D. Kinnison, O. Kirner, M. Kunze, M. Marchand, D.A. Plummer, D. Saint-Martin, K. Sudo, S. Tilmes, and Y. Yamashita, Projecting ozone hole recovery using an ensemble of chemistry-climate models weighted by model performance and independence, ***Atmos. Chem. Phys.***, ***20***, 9961–9977, doi:10.5194/acp-20-9961-2020, 2020.

Ayarzagüena, B., A.J. Charlton-Perez, A.H. Butler, P. Hitchcock, I.R. Simpson, L.M. Polvani, N. Butchart, E.P. Gerber, L. Gray, B. Hassler, P. Lin, F. Lott, E. Manzini, R. Mizuta, C. Orbe, S. Osprey, D. Saint-Martin, M. Sigmond, M. Taguchi, E.M. Volodin, and S. Watanabe, Uncertainty in the response of sudden stratospheric warmings and stratosphere-troposphere coupling to quadrupled $CO_2$ concentrations in CMIP6 models, ***J. Geophys. Res. Atmos.***, ***125*** (6), e2019JD032345, doi:10.1029/2019JD032345, 2020.

Ayarzagüena, B., L.M. Polvani, U. Langematz, H. Akiyoshi, S. Bekki, N. Butchart, M. Dameris, M. Deushi, S.C. Hardiman, P. Jöckel, A. Klekociuk, M. Marchand, M. Michou, O. Morgenstern, F.M. O'Connor, L.D. Oman, D.A. Plummer, L. Revell, E. Rozanov, D. Saint-Martin, J. Scinocca, A. Stenke, K. Stone, Y. Yamashita, K. Yoshida, and G. Zeng, No robust evidence of future changes in major stratospheric sudden warmings: a multi-model assessment from CCMI, ***Atmos. Chem. Phys.***, ***18***, 11277–11287. doi:10.5194/acp-18-11277-2018, 2018.

Bahramvash Shams, S., V.P. Walden, J.W. Hannigan, W.J. Randel, I.V. Petropavlovskikh, A.H. Butler, and A. de la Cámara, Analyzing ozone variations and uncertainties at high latitudes during sudden stratospheric warming events using MERRA-2, ***Atmos. Chem. Phys.***, ***22*** (8), 5435–5458, doi:10.5194/acp-22-5435-2022, 2022.

Baldwin, M.P., B. Ayarzagüena, T. Birner, N. Butchart, A.H. Butler, A.J. Charlton-Perez, D.I.V. Domeisen, C.I. Garfinkel, H. Garny, E.P. Gerber, M.I. Hegglin, U. Langematz, and N.M. Pedatella, Sudden stratospheric warmings, ***Rev. Geophys.***, ***59*** (1), e2020RG000708, doi:10.1029/2020RG000708, 2021.

Barrera, J.A., R.P. Fernandez, F. Iglesias-Suarez, C.A. Cuevas, J.-F. Lamarque, and A. Saiz-Lopez, Seasonal impact of biogenic very short-lived bromocarbons on lowermost stratospheric ozone between 60°N and 60°S during the 21st century, ***Atmos. Chem. Phys.***, ***20***, 8083–8102, doi:10.5194/acp-20-8083-2020, 2020.

Bednarz, E.M., A.C. Maycock, N.L. Abraham, P. Braesicke, O. Dessens, and J.A. Pyle, Future Arctic ozone recovery: The importance of chemistry and dynamics, ***Atmos. Chem. Phys.***, ***16***, 12,159–12,176, doi:10.5194/acp-16-12159-2016, 2016.

Bernath, P., C. Boone, and J. Crouse, Wildfire smoke destroys stratospheric ozone, ***Science***, ***375***, 1292–1295, doi:10.1126/science.abm5611, 2022.

Bernhard, G.H., V.E. Fioletov, J.-U. Grooß, I. Ialongo, B. Johnsen, K. Lakkala, G.L. Manney, and R. Müller, Ozone and UV radiation [in "State of the Climate in 2018"], ***Bull. Amer. Meteor. Soc.***, ***100,*** S274–S277, doi:10.1175/2019BAMSStateoftheClimate.1, 2019.

Bernhard, G.H., V.E. Fioletov, J.-U. Grooß, I. Ialongo, B. Johnsen, K. Lakkala, G.L. Manney, R. Müller, and T. Svendby, Record-breaking increases in Arctic solar ultraviolet radiation caused by exceptionally large ozone depletion in 2020, ***Geophys. Res. Lett.***, ***47*** (24), e2020GL090844, doi:10.1029/2020GL090844, 2020.

Bodeker, G.E., and D.W. Waugh (Lead Authors), H. Akiyoshi, P. Braesicke, V. Eyring, D.W. Fahey, E. Manzini, M.J. Newchurch, R.W. Portmann, A. Robock, K.P. Shine, W. Steinbrecht, and E.C. Weatherhead, The Ozone Layer in the 21st Century, Chapter 6 in ***Scientific Assessment of Ozone Depletion: 2007***, Global Ozone Research and Monitoring Project–Report No. 50, World Meteorological Organization, Geneva, Switzerland, 2007.

Bodeker, G.E., and S. Kremser, Indicators of Antarctic ozone depletion: 1979 to 2019, ***Atmos. Chem. Phys.***, ***21***, 5289–5300, doi:10.5194/acp-21-5289-2021, 2021.

Bodeker, G.E., J. Nitzbon, J.S. Tradowsky, S. Kremser, A. Schwertheim, and J. Lewis, A global total column ozone climate data record, ***Earth Syst. Sci. Data***, ***13*** (8), 3885–3906, doi:10.5194/essd-13-3885-2021, 2021.

Bognar, K., R. Alwarda, K. Strong, M.P. Chipperfield, S.S. Dhomse, J.R. Drummond, W. Feng, V. Fioletov, F. Goutail, B. Herrera, G.L. Manney, E.M. McCullough, L.F. Millán, A. Pazmino, K.A. Walker, T. Wizenberg, and X. Zhao, Unprecedented spring 2020 ozone depletion in the context of 20 years of measurements at Eureka, Canada, ***J. Geophys. Res. Atmos.***, ***126*** (8), e2020JD034365, doi:10.1029/2020JD034365, 2021.

Bond, N.A., J.E. Overland, M. Spillane, and P. Stabeno, Recent shifts in the state of the North Pacific, ***Geophys. Res. Lett.***, ***30*** (23), doi:10.1029/2003GL018597, 2003.

Braesicke, P., and J. Neu et al. (Lead Authors), V. Fioletov, S. Godin-Beekmann, D. Hubert, I. Petropavlovskikh, M. Shiotani, and B.-M Sinnhuber, Update on Global Ozone: Past, Present, and Future, Chapter 3 in ***Scientific Assessment of Ozone Depletion: 2018***, Global Ozone Research and Monitoring Project–Report No. 58, World Meteorological Organization, Geneva, Switzerland, 2018.

Braun, M., J.-U. Grooß, W. Woiwode, S. Johansson, M. Höpfner, F. Friedl-Vallon, H. Oelhaf, P. Preusse, J. Ungermann, B.-M. Sinnhuber, H. Ziereis, and P. Braesicke, Nitrification of the lowermost stratosphere during the exceptionally cold Arctic winter 2015–2016, ***Atmos. Chem. Phys.***, ***19***, 13681–13699, doi:10.5194/acp-19-13681-2019, 2019.

Breeden, M.L., A.H. Butler, J.R. Albers, M. Sprenger, and A.O. Langford, The spring transition of the North Pacific jet and its relation to deep stratosphere-to-troposphere mass transport over western North America, ***Atmos. Chem. Phys.***, ***21***, 2781–2794, doi:10.5194/acp-21-2781-2021, 2021.

Brenna, H., S. Kutterolf, and K. Krüger, Global ozone depletion and increase of UV radiation caused by pre-industrial tropical volcanic eruptions, ***Sci. Rep.,*** ***9*** (1), 9435, doi:10.1038/s41598-019-45630-0, 2019.

Bushra, N., and R.V. Rohli, Relationship between atmospheric teleconnections and the northern hemisphere's circumpolar vortex, ***Earth Space Sci.***, ***8*** (9), e2021EA001802, doi:10.1029/2021EA001802, 2021.

Butchart, N., and E.E. Remsberg, The area of the stratospheric polar vortex as a diagnostic for tracer transport on an isentropic surface, ***J. Atmos. Sci.***, ***43***, 1319–1339, doi:10.1175/1520-0469(1986)043<1319:TAOTSP>2.0.CO;2, 1986.

Butler, A.H., J.P. Sjoberg, D.J. Seidel, and K.H. Rosenlof, A sudden stratospheric warming compendium, ***Earth Syst. Sci. Data***, ***9*** (1), 63–76, doi:10.5194/essd-9-63-2017, 2017.

Butler, A.H., A. Charlton-Perez, D.I.V. Domeisen, I.R. Simpson, and J. Sjoberg, Predictability of northern hemisphere final stratospheric warmings and their surface impacts, ***Geophys. Res. Lett.***, ***46*** (17-18), 10578–10588, doi:10.1029/2019GL083346, 2019.

Butler, A.H., Z.D. Lawrence, S.H. Lee, S.P. Lillo, and C.S. Long, Differences between the 2018 and 2019 stratospheric polar vortex split events, ***Q. J. R. Meteorol. Soc.***, ***146***, 3503–3521, doi:10.1002/qj.3858, 2020.

Butler, A.H., and D.I.V. Domeisen, The wave geometry of final stratospheric warming events, ***Weather Clim. Dynam.***, ***2,*** 453–474, doi:10.5194/wcd-2-453-2021, 2021.

Carpenter, L.J., and J.S. Daniel (Lead Authors), E.L. Fleming, T. Hanaoka, J. Hu, A.R. Ravishankara, M.N. Ross, S. Tilmes, T.J. Wallington, and D.J. Wuebbles, Scenarios and Information for Policymakers, Chapter 6 in ***Scientific Assessment of Ozone Depletion: 2018***, Global Ozone Research and Monitoring Project–Report No. 58, World Meteorological Organization, Geneva, Switzerland, 2018.

Cellitti, M.P., J.E. Walsh, R.M. Rauber, and D.H. Portis, Extreme cold air outbreaks over the United States, the polar vortex, and the large-scale circulation, ***J. Geophys. Res. Atmos.***, ***111*** (D2), doi:10.1029/2005JD006273, 2006.

Charlton, A.J., and L.M. Polvani, A new look at stratospheric sudden warmings: Part I: Climatology and modeling benchmarks, ***J. Clim.***, ***20*** (3), 449–469, doi:10.1175/JCLI3996.1, 2007.

Chipperfield, M.P., S.S. Dhomse, W. Feng, R.L. McKenzie, G. Velders, and J.A. Pyle, Quantifying the ozone and UV benefits already achieved by the Montreal Protocol, ***Nat. Commun.***, ***6***, 7233, doi:10.1038/ncomms8233, 2015.

Chipperfield, M.P., R. Hossaini, S.A. Montzka, S. Reimann, D. Sherry, and S. Tegtmeier, Renewed and emerging concerns over the production and emission of ozone-depleting substances, ***Nat. Rev. Earth Environ.***, ***1*** (5), 251–263, doi:10.1038/s43017-020-0048-8, 2020.

Claxton, T., R. Hossaini, C. Wilson, S.A. Montzka, M.P. Chipperfield, O. Wild, E.M. Bednarz, L.J. Carpenter, S.J. Andrews, S.C. Hackenberg, J. Mühle, D. Oram, S. Park, M.-K. Park, E. Atlas, M. Navarro, S. Schauffler, D. Sherry, M. Vollmer, T. Schuck, A. Engel, P.B. Krummel, M. Maione, J. Arduini, T. Saito, Y. Yokouchi, S. O'Doherty, D. Young, and C. Lunder, A synthesis inversion to constrain global emissions of two very short lived chlorocarbons: dichloromethane, and perchloroethylene, ***J. Geophys. Res. Atmos.***, ***125*** (12), e2019JD031818, doi:10.1029/2019JD031818, 2020.

Cohen, J., X. Zhang, J. Francis, T. Jung, R. Kwok, J. Overland, T.J. Ballinger, U.S. Bhatt, H.W. Chen, D. Coumou, S. Feldstein, H. Gu, D. Handorf, G. Henderson, M. Ionita, M. Kretschmer, F. Laliberte, S. Lee, H.W. Linderholm, W. Maslowski, Y. Peings, K. Pfeiffer, I. Rigor, T. Semmler, J. Stroeve, P.C. Taylor, S. Vavrus, T. Vihma, S. Wang, M. Wendisch, Y. Wu, and J. Yoon, Divergent consensuses on Arctic amplification influence on midlatitude severe winter weather, ***Nat. Clim. Change***, ***10*** (1), 20–29, doi:10.1038/s41558-019-0662-y, 2020.

Cohen, J.L., L. Agel, M. Barlow, C.I. Garfinkel, and I. White, Linking Arctic variability and change with extreme winter weather in the United States, ***Science***, ***373*** (6559), 1116–1121, doi:10.1126/science.abi9167, 2021.

Cuevas, C.A., R.P. Fernandez, D.E. Kinnison, Q. Li., J.-F. Lamarque, T. Trabelsi, J.S. Francisco, S. Solomon, and A. Saiz-Lopez, The influence of iodine on the Antarctic stratospheric ozone hole, ***Proc. Natl. Acad. Sci.***, ***119*** (7), e2110864119, doi:10.1073/pnas.e2110864119, 2022.

Dai, G., C. Li, Z. Han, D. Luo, and Y. Yao, The nature and predictability of the East Asian extreme cold events of 2020/21, ***Adv. Atmos. Sci.***, doi:10.1007/s00376-021-1057-3, 2021.

Dameris, D., V. Grewe, I. Köhler, R. Sausen, C. Brühl, J.-U. Grooß, and B. Steil, Impact of aircraft $NO_x$ emissions on tropospheric and stratospheric ozone, part II: 3-D model results, ***Atmos. Environ.***, ***32***, 3185–3199, doi:10.1016/S1352-2310(97)00505-0, 1998.

Dameris, M., and S. Godin-Beekmann (Lead Authors), S. Alexander, P. Braesicke, M. Chipperfield, A.T.J. de Laat, Y. Orsolini, M. Rex, and M.L. Santee, Polar Stratospheric Ozone: Past, Present, and Future, Chapter 3 in ***Scientific Assessment of Ozone Depletion: 2014***, Global Ozone Research and Monitoring Project–Report No. 55, World Meteorological Organization, Geneva, Switzerland, 2014.

Dameris, M., P. Jöckel, and M. Nützel, Possible implications of enhanced chlorofluorocarbon-11 concentrations on ozone, ***Atmos. Chem. Phys.***, ***19*** (22), 13759–13771, doi:10.5194/acp-19-13759-2019, 2019.

Dameris, M., D.G. Loyola, M. Nützel, M. Coldewey-Egbers, C. Lerot, F. Romahn, and M. van Roozendael, Record low ozone values over the Arctic in boreal spring 2020, ***Atmos. Chem. Phys.***, ***21***, 617–633, doi:10.5194/acp-21-617-2021, 2021.

Davis, S.M., M.I. Hegglin, M. Fujiwara, R. Dragani, Y. Harada, C. Kobayashi, C. Long, G.L. Manney, E.R. Nash, G.L. Potter, S. Tegtmeier, T. Wang, K. Wargan, and J.S. Wright, Assessment of upper tropospheric and stratospheric water vapor and ozone in reanalyses as part of S-RIP, ***Atmos. Chem. Phys.***, ***17***, 12743–12778, doi:10.5194/acp-17-12743-2017, 2017.

de la Cámara, A., M. Abalos, P. Hitchcock, N. Calvo, and R.R. Garcia, Response of Arctic ozone to sudden stratospheric warmings, ***Atmos. Chem. Phys.***, ***18***, 16499–16513, doi:10.5194/acp-18-16499-2018, 2018.

de Laat, A.T.J., M. van Weele, and R.J. van der A, Onset of stratospheric ozone recovery in the Antarctic ozone hole in assimilated daily total ozone columns, ***J. Geophys. Res. Atmos.***, ***122***, 11,880–11,899, doi:10.1002/2016JD025723, 2017.

DeLand, M.T., P.K. Bhartia, N. Kramarova, and Z. Chen, OMPS LP observations of PSC variability during the NH 2019–2020 season, ***Geophys. Res. Lett.***, ***47*** (20), e2020GL090216, doi:10.1029/2020GL090216, 2020.

Dhomse, S.S., D. Kinnison, M.P. Chipperfield, R.J. Salawitch, I. Cionni, M.I. Hegglin, N.L. Abraham, H. Akiyoshi, A.T. Archibald, E.M. Bednarz, S. Bekki, P. Braesicke, N. Butchart, M. Dameris, M. Deushi, S. Frith, S.C. Hardiman, B. Hassler, L.W. Horowitz, R.-M. Hu, P. Jöckel, B. Josse, O. Kirner, S. Kremser, U. Langematz, J. Lewis, M. Marchand, M. Lin, E. Mancini, V. Marécal, M. Michou, O. Morgenstern, F.M. O'Connor, L. Oman, G. Pitari, D.A. Plummer, J.A. Pyle, L.E. Revell, E. Rozanov, R. Schofield, A. Stenke, K. Stone, K. Sudo, S. Tilmes, D. Visioni, Y. Yamashita, and G. Zeng, Estimates of ozone return dates from Chemistry-Climate Model Initiative simulations, ***Atmos. Chem. Phys.***, ***18*** (11), 8409–8438, doi:10.5194/acp-18-8409-2018, 2018.

Dhomse, S.S., W. Feng, S.A. Montzka, R. Hossaini, J. Keeble, J.A. Pyle, J.S. Daniel, and M.P. Chipperfield, Delay in recovery of the Antarctic ozone hole from unexpected CFC-11 emissions, ***Nat. Commun.***, ***10*** (1), ***5781***, doi:10.1038/s41467-019-13717-x, 2019.

Domeisen, D.I.V., and A.H. Butler, Stratospheric drivers of extreme events at the Earth's surface, ***Comm. Earth Environ.***, ***1*** (1), 59, doi:10.1038/s43247-020-00060-z, 2020.

Douglass, A., and V. Fioletov (Coordinating Lead Authors), S. Godin-Beekmann, R. Müller, R.S. Stolarski, A. Webb, A. Arola, J.B. Burkholder, J.P. Burrows, M.P. Chipperfield, R. Cordero, C. David, P.N. den Outer, S.B. Diaz, L.E. Flynn, M. Hegglin, J.R. Herman, P. Huck, S. Janjai, I.M. Jánosi, J.W. Krzyścin, Y. Liu, J. Logan, K. Matthes, R.L. McKenzie, N.J. Muthama, I. Petropavlovskikh, M. Pitts, S. Ramachandran, M. Rex, R.J. Salawitch, B.-M. Sinnhuber, J. Staehelin, S. Strahan, K. Tourpali, J. Valverde-Canossa, and C. Vigouroux, Stratospheric Ozone and Surface Ultraviolet Radiation, Chapter 2 in ***Scientific Assessment of Ozone Depletion: 2010***, Global Ozone Research and Monitoring Project–Report No. 52, World Meteorological Organization, Geneva, Switzerland, 2011.

Duderstadt, K.A., C.-L. Huang, H.E. Spence, S. Smith, J.B. Blake, A.B. Crew, A.T. Johnson, D.M. Klumpar, D.R. Marsh, J.G. Sample, M. Shumko, and F.M. Vitt, Estimating the impacts of radiation belt electrons on atmospheric chemistry using FIREBIRD II and Van Allen Probes observations, ***J. Geophys. Res. Atmos.***, ***126*** (7), e2020JD033098, doi:10.1029/2020JD033098, 2021.

Engel, A., H. Bönisch, J. Ostermöller, M.P. Chipperfield, S. Dhomse, and P. Jöckel, A refined method for calculating equivalent effective stratospheric chlorine, ***Atmos. Chem. Phys.***, ***18***, 601–619, doi:10.5194/acp-18-601-2018, 2018.

Eyring, V., J.M. Arblaster, I. Cionni, J. Sedláček, J. Perlwitz, P.J. Young, S. Bekki, D. Bergmann, P. Cameron-Smith, W.J. Collins, G. Faluvegi, K.-D. Gottschaldt, L.W. Horowitz, D.E. Kinnison, J.-F. Lamarque, D.R. Marsh, D. Saint-Martin, D.T. Shindell, K. Sudo, S. Szopa, and S. Watanabe, Long-term ozone changes and associated climate impacts in CMIP5 simulations, ***J. Geophys. Res. Atmos.***, ***118***, 5029–5060, doi:10.1002/jgrd.50316, 2013.

Fang, X., S. Park, T. Saito, R. Tunnicliffe, A.L. Ganesan, M. Rigby, S. Li, Y. Yokouchi, P.J. Fraser, C.M. Harth, P.B. Krummel, J. Mühle, S. O'Doherty, P.K. Salameh, P.G. Simmonds, R.F. Weiss, D. Young, M.F. Lunt, A.J. Manning, A. Gressent, and R.G. Prinn, Rapid increase in ozone-depleting chloroform emissions from China, ***Nat. Geosci.***, ***12*** (2), 89–93, doi:10.1038/s41561-018-0278-2, 2019.

Fernandez, R.P., D.E. Kinnison, J-F. Lamarque, S. Times, and A. Saiz-Lopez, Impact of biogenic very short-lived bromine on the Antarctic ozone hole during the 21st century, ***Atmos. Chem. Phys.***, ***17***, 1673–1688, doi:10.5194/acp-17-1673-2017.

Feng, W., S.S. Dhomse, C. Arosio, M. Weber, J.P. Burrows, M.L. Santee, and M.P. Chipperfield, Arctic ozone depletion in 2019/20: Roles of chemistry, dynamics and the Montreal Protocol, ***Geophys. Res. Lett.***, ***48*** (4), e2020GL091911, doi:10.1029/2020GL091911, 2021.

Fiehn, A., B. Quack, C.A. Marandino, and K. Krüger, Transport variability of very short lived substances from the West Indian Ocean to the stratosphere, ***J. Geophys. Res. Atmos.***, ***123*** (10), 5720–5738, doi:10.1029/2017JD027563, 2018.

Filus, M.T., E.L. Atlas, M.A. Navarro, E. Meneguz, D. Thomson, M.J. Ashfold, L.J. Carpenter, S.J. Andrews, and N.R.P. Harris, Transport of short-lived halocarbons to the stratosphere over the Pacific Ocean, ***Atmos. Chem. Phys.***, ***20***, 1163–1181, doi:10.5194/acp-20-1163-2020, 2020.

Fleming, E.L., C. George, D.E. Heard, C.H. Jackman, M.J. Kurylo, W. Mellouki, V.L. Orkin, W.H. Swartz, T.J. Wallington, P.H. Wine, and J.B. Burkholder, The impact of current $CH_4$ and $N_2O$ atmospheric loss process uncertainties on calculated ozone abundances and trends, ***J. Geophys. Res.***, ***120***, 5267–5293, doi:10.1002/2014JD022067, 2015.

Fleming, E.L., P.A. Newman, Q. Liang, and J.S. Daniel, The impact of continuing CFC-11 emissions on stratospheric ozone, ***J. Geophys. Res.***, ***125*** (3), e2019JD031849, doi:10.1029/2019JD031849, 2020.

Fu, Q., S. Solomon, H.A. Pahlavan, and P. Lin, Observed changes in Brewer–Dobson circulation for 1980–2018, ***Environ. Res. Lett., 14*** (11), 114026, doi:10.1088/1748-9326/ab4de7, 2019.

Fujiwara, M., J.S. Wright, G.L. Manney, L.J. Gray, J. Anstey, T. Birner, S. Davis, E.P. Gerber, V.L. Harvey, M.I. Hegglin, C.R. Homeyer, J.A. Knox, K. Krüger, A. Lambert, C.S. Long, P. Martineau, A. Molod, B.M. Monge-Sanz, M.L. Santee, S. Tegtmeier, S. Chabrillat, D.G.H. Tan, D.R. Jackson, S. Polavarapu, G.P. Compo, R. Dragani, W. Ebisuzaki, Y. Harada, C. Kobayashi, W. McCarty, K. Onogi, S. Pawson, A. Simmons, K. Wargan, J.S. Whitaker, and C-Z. Zou, Introduction to the SPARC Reanalysis Intercomparison Project (S-RIP) and overview of the reanalysis systems, ***Atmos. Chem. Phys.***, ***17***, 1417–1452, doi:10.5194/acp-17-1417-2017, 2017.

Funke, B., M. López-Puertas, G.P. Stiller, and T. von Clarmann, Mesospheric and stratospheric $NO_y$ produced by energetic particle precipitation during 2002–2012, ***J. Geophys. Res.***, ***119***, 4429–4446, doi:10.1002/2013JD021404, 2014.

Gelaro, R., W. McCarty, M.J. Suárez, R. Todling, A. Molod, L. Takacs, C.A. Randles, A. Darmenov, M.G. Bosilovich, R. Reichle, K. Wargan, L. Coy, R. Cullather, C. Draper, S. Akella, V. Buchard, A. Conaty, A.M. da Silva, W. Gu, G.-K. Kim, R. Koster, R. Lucchesi, D. Merkova, J.E. Nielsen, G. Partyka, S. Pawson, W. Putman, M. Rienecker, S.D. Schubert, M. Sienkiewicz, and B. Zhao, The modern-era retrospective analysis for research and applications, version 2 (MERRA-2), ***J. Clim.***, ***30***, 5419–5454, doi:10.1175/JCLI-D-16-0758.1, 2017.

Gordon, E.M., A. Seppälä, and J. Tamminen, Evidence for energetic particle precipitation and quasi-biennial oscillation modulations of the Antarctic $NO_2$ springtime stratospheric column from OMI observations, ***Atmos. Chem. Phys.***, ***20***, 6259–6271, doi:10.5194/acp-20-6259-2020, 2020.

Gordon, E.M., A. Seppälä, B. Funke, J. Tamminen, and K.A. Walker, Observational evidence of energetic particle precipitation $NO_x$ (EPP-$NO_x$) interaction with chlorine curbing Antarctic ozone loss, ***Atmos. Chem. Phys.***, ***21***, 2819–2836, doi:10.5194/acp-21-2819-2021, 2021.

Griffin, D., K.A. Walker, I. Wohltmann, S.S. Dhomse, M. Rex, M.P. Chipperfield, W. Feng, G.L. Manney, J. Liu, and D. Tarasick, Stratospheric ozone loss in the Arctic winters between 2005 and 2013 derived with ACE-FTS measurements, ***Atmos. Chem. Phys.***, ***19***, 577–601, doi:10.5194/acp-19-577-2019, 2019.

Grooß, J.-U., R. Müller, R. Spang, I. Tritscher, T. Wegner, M.P. Chipperfield, W. Feng, D.E. Kinnison, and S. Madronich, On the discrepancy of HCl processing in the core of the wintertime polar vortices, ***Atmos. Chem. Phys.***, ***18***, 8647–8666, doi:10.5194/acp-18-8647-2018, 2018.

Grooß, J.-U., and R. Müller, Simulation of record Arctic stratospheric ozone depletion in 2020, ***J. Geophys. Res. Atmos.***, ***126*** (12), e2020JD033339, doi:10.1029/2020JD033339, 2021.

Haigh, J.D., and H.K. Roscoe, The final warming date of the Antarctic polar vortex and influences on its interannual variability, ***J. Clim.***, ***22***, 5809–5819, doi:10.1175/2009JCLI2865.1, 2009.

Harrison, J.J., M.P. Chipperfield, R. Hossaini, C.D. Boone, S. Dhomse, W. Feng, and P.F. Bernath, Phosgene in the upper troposphere and lower stratosphere: A marker for product gas injection due to chlorine-containing very short-lived substances, ***Geophys. Res. Lett.***, ***46***, 1032–1039, doi:10.1029/2018GL079784, 2019.

Hauchecorne, A., C. Claud, P. Keckhut, and A. Mariaccia, Stratospheric Final Warmings fall into two categories with different evolution over the course of the year, ***Commun. Earth Environ., 3*** (1), doi:10.1038/s43247-021-00335-z, 2022.

Hendon, H.H., D.W. Thompson, E.-P. Lim, A.H. Butler, P.A. Newman, L. Coy, and A. Scaife, Rare forecasted climate event under way in the Southern Hemisphere, ***Nature***, ***573*** (7775), 495–495, doi:10.1038/d41586-019-02858-0, 2019.

Hersbach, H., B. Bell, P. Berrisford, S. Hirahara, A. Horányi, J. Muñoz-Sabater, J. Nicolas, C. Peubey, R. Radu, D. Schepers, A. Simmons, C. Soci, S. Abdalla, X. Abellan, G. Balsamo, P. Bechtold, G. Biavati, J. Bidlot, M. Bonavita, G. De Chiara, P. Dahlgren, D. Dee, M. Diamantakis, R. Dragani, J. Flemming, R. Forbes, M. Fuentes, A. Geer, L. Haimberger, S. Healy, R.J. Hogan, E. Hólm, M. Janisková, S. Keeley, P. Laloyaux, P. Lopez, C. Lupu, G. Radnoti, P. de Rosnay, I. Rozum, F. Vamborg, S. Villaume, and J.-N. Thépaut, The ERA5 global reanalysis, ***Q. J. R. Meteorol. Soc.***, ***146***, 1999–2049, doi:10.1002/qj.3803, 2020.

Hong, H.-J., and T. Reichler, Local and remote response of ozone to Arctic stratospheric circulation extremes, ***Atmos. Chem. Phys.***, ***21***, 1159–1171, doi:10.5194/acp-21-1159-2021, 2021.

Höpfner, M., T. Deshler, M. Pitts, L. Poole, R. Spang, G. Stiller, and T. von Clarmann, The MIPAS/Envisat climatology (2002–2012) of polar stratospheric cloud volume density profiles, ***Atmos. Meas. Tech.***, ***11***, 5901–5923, doi:10.5194/amt-11-5901-2018, 2018.

Hoshi, K., J. Ukita, M. Honda, T. Nakamura, K. Yamazaki, Y. Miyoshi, and R. Jaiser, Weak stratospheric polar vortex events modulated by the Arctic sea-ice loss, ***J. Geophys. Res. Atmos***, ***124***, 858–869, doi:10.1029/2018JD029222, 2019.

Hossaini, R., M.P. Chipperfield, S.A. Montzka, A.A. Leeson, S.S. Dhomse, and J.A. Pyle, The increasing threat to stratospheric ozone from dichloromethane, ***Nat. Commun.***, ***8***, 186–190, doi:10.1038/ncomms15962, 2017.

Hossaini, R., E. Atlas, S.S. Dhomse, M.P. Chipperfield, P.F. Bernath, A.M. Fernando, J. Mühle, A.A. Leeson, S.A. Montzka, W. Feng, J.J. Harrison, P. Krummel, M.K. Vollmer, S. Reimann, S. O'Doherty, D. Young, M. Maione, J. Arduini, and C.R. Lunder, Recent trends in stratospheric chlorine from very short-lived substances, ***J. Geophys. Res. Atmos***, ***124*** (4), 2318–2335, doi:10.1029/2018JD029400, 2019.

Hu, D., Z. Guan, W. Tian, and R. Ren, Recent strengthening of the stratospheric Arctic vortex response to warming in the central North Pacific, ***Nat. Commun.***, ***9*** (1), 1697, doi:10.1038/s41467-018-04138-3, 2018.

Hu, D., Z. Guan, M. Liu, and W. Feng, Dynamical mechanisms for the recent ozone depletion in the Arctic stratosphere linked to North Pacific sea surface temperatures, ***Clim. Dyn., 58*** (9), 2663–2679, doi:10.1007/s00382-021-06026-x, 2022.

Hu, J.G., R.C. Ren, and H.M. Xu, Occurrence of winter stratospheric sudden warming events and the seasonal timing of spring stratospheric final warming, ***J. Atmos. Sci.***, ***71***, 2319–2334, doi:10.1175/JAS-D-13-0349.1, 2014.

Huang, J., P. Hitchcock, A.C. Maycock, C.M. McKenna, and W. Tian, Northern Hemisphere cold air outbreaks are more likely to be severe during weak polar vortex conditions, ***Comm. Earth Env.***, ***2*** (1), 147, doi:10.1038/s43247-021-00215-6, 2021.

Hurwitz, M.M., P.A. Newman, and C.I. Garfinkel, On the influence of North Pacific sea surface temperature on the Arctic winter climate, ***J. Geophys. Res.***, ***117*** (D19), doi:10.1029/2012JD017819, 2012.

Ingenito, A., Impact of hydrogen fueled hypersonic airliners on the $O_3$ layer depletion, ***Int. J. Hydrog. Energy***, ***43***, 22694–22704, doi:10.1016/j.ijhydene.2018.09.208, 2018.

Inness, A., M. Ades, A. Agustí-Panareda, J. Barré, A. Benedictow, A.-M. Blechschmidt, J.J. Dominguez, R. Engelen, H. Eskes, J. Flemming, V. Huijnen, L. Jones, Z. Kipling, S. Massart, M. Parrington, V.-H. Peuch, M. Razinger, S. Remy, M. Schulz, and M. Suttie, The CAMS reanalysis of atmospheric composition, ***Atmos. Chem. Phys.***, ***19***, 3515–3556, doi:10.5194/acp-19-3515-2019, 2019.

Inness, A., S. Chabrillat, J. Flemming, V. Huijnen, B. Langenrock, J. Nicolas, I. Polichtchouk, and M. Razinger, Exceptionally low Arctic stratospheric ozone in spring 2020 as seen in the CAMS reanalysis, ***J. Geophys. Res. Atmos.***, ***125*** (23), e2020JD033563, doi:10.1029/2020JD033563, 2020.

IPCC (Intergovenmental Panel on Climate Change), ***Climate Change 2021: The Physical Science Basis. Contribution of Working Group I to the Sixth Assessment Report of the Intergovernmental Panel on Climate Change***, edited by V. Masson-Delmotte, P. Zhai, A. Pirani, S.L. Connors, C. Péan, S. Berger, N. Caud, Y. Chen, L. Goldfarb, M.I. Gomis, M. Huang, K. Leitzell, E. Lonnoy, J.B.R. Matthews, T.K. Maycock, T. Waterfield, O. Yelekçi, R. Yu, and B. Zhou, Cambridge University Press, Cambridge, United Kingdom, 2021.

Jackman, C.H., E.L. Fleming, and F.M. Vitt, Influence of extremely large solar proton events in a changing stratosphere, ***J. Geophys. Res.***, ***105***, 11659–11670, doi:10.1029/2000JD900010, 2000.

James, A.D., J.S.A. Brooke, T.P. Mangan, T.F. Whale, J.M.C. Plane, and B.J. Murray, Nucleation of nitric acid hydrates in polar stratospheric clouds by meteoric material, ***Atmos. Chem. Phys.***, ***18***, 4519–4531, doi:10.5194/acp-18-4519-2018, 2018.

Jesswein, M., H. Bozem, H.-C. Lachnitt, P. Hoor, T. Wagenhäuser, T. Keber, T. Schuck, and A. Engel, Comparison of inorganic chlorine in the Antarctic and Arctic lowermost stratosphere by separate late winter aircraft measurements, ***Atmos. Chem. Phys.***, ***21*** (23), 17225–17241, doi:10.5194/acp-21-17225-2021, 2021.

Johansson, S., M.L. Santee, J.-U. Grooß, M. Höpfner, M. Braun, F. Friedl-Vallon, F. Khosrawi, O. Kirner, E. Kretschmer, H. Oelhaf, J. Orphal, B.-M. Sinnhuber, I. Tritscher, J. Ungermann, K.A. Walker, and W. Woiwode, Unusual chlorine partitioning in the 2015/16 Arctic winter lowermost stratosphere: observations and simulations, ***Atmos. Chem. Phys.***, ***19***, 8311–8338, doi:10.5194/acp-19-8311-2019, 2019.

Kablick, G.P., D.R. Allen, M.D. Fromm, and G.E. Nedoluha, Australian PyroCb smoke generates synoptic-scale stratospheric anticyclones, ***Geophys. Res. Lett.***, ***47*** (13), e2020GL088101, doi:10.1029/2020GL088101, 2020.

Kalakoski, N., P.T. Verronen, A. Seppälä, M.E. Szeląg, A. Kero, and D.R. Marsh, Statistical response of middle atmosphere composition to solar proton events in WACCM-D simulations: the importance of lower ionospheric chemistry, ***Atmos. Chem. Phys.***, ***20***, 8923–8938, doi:10.5194/acp-20-8923-2020, 2020.

Karpechko, A.Y., and A.C. Maycock (Lead Authors), M. Abalos, H. Akiyoshi, J.M. Arblaster, C.I. Garfinkel, K.H. Rosenlof, and M. Sigmond, Stratospheric Ozone Changes and Climate, Chapter 5 in ***Scientific Assessment of Ozone Depletion: 2018***, Global Ozone Research and Monitoring Project–Report No. 58, World Meteorological Organization, Geneva, Switzerland, 2018.

Kawa, S.R., J.G. Anderson, S.L. Baughcum, C.A. Brock, W.H. Brune, R.C. Cohen, D.E. Kinnison, P.A. Newman, J.M. Rodriguez, R.S. Stolarski, D. Waugh, and S.C. Wofsy, ***Assessment of the Effects of High-Speed Aircraft in the Stratosphere: 1998***, NASA Technical Paper TP-1999-209237, Washington, DC: National Aeronautics and Space Administration, 1999.

Keeble, J., N.L. Abraham, A.T. Archibald, M.P. Chipperfield, S. Dhomse, P.T. Griffiths, and J.A. Pyle, Modelling the potential impacts of the recent, unexpected increase in CFC-11 emissions on total column ozone recovery, ***Atmos. Chem. Phys., 20***, 7153–7166, doi:10.5194/acp-20-7153-2020, 2020.

Keeble, J., B. Hassler, A. Banerjee, R. Checa-Garcia, G. Chiodo, S. Davis, V. Eyring, P.T. Griffiths, O. Morgenstern, P. Nowack, G. Zeng, J. Zhang, G. Bodeker, S. Burrows, P. Cameron-Smith, D. Cugnet, C. Danek, M. Deushi, L.W. Horowitz, A. Kubin, L. Li, G. Lohmann, M. Michou, M.J. Mills, P. Nabat, D. Olivié, S. Park, Ø. Seland, J. Stoll, K.-H. Wieners, and T. Wu, Evaluating stratospheric ozone and water vapor changes in CMIP6 models from 1850 to 2100, ***Atmos. Chem. Phys.***, ***21***, 5015–5061, doi:10.5194/acp-21-5015-2021, 2021.

Khaykin, S., B. Legras, S. Bucci, P. Sellitto, L. Isaksen, F. Tencé, S. Bekki, A. Bourassa, L. Rieger, D. Zawada, J. Jumelet, and S. Godin-Beekmann, The 2019/20 Australian wildfires generated a persistent smoke-charged vortex rising up to 35 km altitude, ***Commun. Earth Environ., 1*** (1), 22, doi:10.1038/s43247-020-00022-5, 2020.

Kim, B.-M., S.-W. Son, S.-K. Min, J.-H. Jeong, S.-J. Kim, X. Zhang, T. Shim, and J.-H. Yoon, Weakening of the stratospheric polar vortex by Arctic sea-ice loss, ***Nat. Commun.***, ***5***, 4646, doi:10.1038/ncomms5646, 2014.

Kinnison, D., G.P. Brasseur, S.L. Baughcum, J. Zhang, and D. Wuebbles, The impact on the ozone layer of a potential fleet of civil hypersonic aircraft, ***Earth's Future***, ***8*** (10), e2020EF001626, doi:10.1029/2020EF001626, 2020.

Klekociuk A.R., M.B. Tully, P.B. Krummel, S.I. Henderson, D. Smale, R. Querel, S. Nichol, S.P. Alexander, P.J. Fraser, and G. Nedoluha, The Antarctic ozone hole during 2018 and 2019, ***J. South. Hemisphere Earth Syst. Sci.***, ***71***, 66–91, doi:10.1071/ES20010, 2021.

Klekociuk, A.R., M. Tully, P. Krummel, S. Henderson, D. Smale, R. Querel, S. Nichol, S.P. Alexander, P. Fraser, and G. Nedoluha, The Antarctic Ozone Hole during 2020, ***J. South. Hemisphere Earth Syst. Sci., 72***, doi:10.1071/ES21015, 2022.

Klobas, J.E., D.M. Wilmouth, D.K. Weisenstein, J.G. Anderson, and R.J. Salawitch, Ozone depletion following future volcanic eruptions, ***Geophys. Res. Lett.***, ***44*** (14), 7490–7499, doi:10.1002/2017GL073972, 2017.

Klobas, J.E., D.K. Weisenstein, R.J. Salawitch, and D.M. Wilmouth, Reformulating the bromine alpha factor and equivalent effective stratospheric chlorine (EESC): evolution of ozone destruction rates of bromine and chlorine in future climate scenarios, ***Atmos. Chem. Phys.***, ***20***, 9459–9471, doi:10.5194/acp-20-9459-2020, 2020.

Koenig, T.K., S. Baidar, P. Campuzano-Jost, C.A. Cuevas, B. Dix, R.P. Fernandez, H. Guo, S.R. Hall, D. Kinnison, B.A. Nault, K. Ullmann, J.L. Jimenez, A. Saiz-Lopez, and R. Volkamer, Quantitative detection of iodine in the stratosphere, ***Proc. Natl. Acad. Sci.***, ***117*** (4), 1860–1866; doi:10.1073/pnas.1916828117, 2020.

Kömüşcü, A.Ü., and K. Oğuz, Analysis of cold anomalies observed over Turkey during the 2018/2019 winter in relation to polar vortex and other atmospheric patterns, ***Meteorol. Atmos. Phys.***, ***133***, 1327–1354, doi:10.1007/s00703-021-00806-0, 2021.

Kramarova, N., P.A. Newman, E.R. Nash, S.E. Strahan, C.S. Long, B. Johnson, M. Pitts, M.L. Santee, I. Petropavlovskikh, G.O. Braathen, L. Coy, and J. de Laat, 2018 Antarctic ozone hole [in ''State of the Climate in 2018''], ***Bull. Amer. Meteor. Soc.***, ***100***, S185–S187, doi:10.1175/2019BAMSStateoftheClimate.1, 2019.

Kramarova, N., P.A. Newman, E.R. Nash, S.E. Strahan, C.S. Long, B. Johnson, M. Pitts, M.L. Santee, I. Petropavlovskikh, L. Coy, and J. de Laat, 2019 Antarctic ozone hole [in "State of the Climate in 2019"], ***Bull. Amer. Meteor. Soc.***, ***101***, S310–S312, doi:10.1175/BAMS-D-20-0090.1, 2020.

Kramarova, N., P.A. Newman, E.R. Nash, S.E. Strahan, C.S. Long, B. Johnson, M. Pitts, M.L. Santee, I. Petropavlovskikh, L. Coy, J. de Laat, G.H. Bernhard, S. Stierle, and K. Lakkala, 2020 Antarctic ozone hole [in "State of the Climate in 2020"], ***Bull. Amer. Meteor. Soc.***, ***102***, S345–S349, doi:10.1175/BAMS-D-21-0081.1, 2021.

Kretschmer, M., J. Cohen, V. Mattias, J. Runge, and D. Coumou, The different stratospheric influence on cold-extremes in Eurasia and North America, ***npj Clim. Atmos. Sci.***, ***1*** (1), doi:10.1038/s41612-018-0054-4, 2018.

Kretschmer, M., G. Zappa, and T.G. Shepherd, The role of Barents–Kara sea ice loss in projected polar vortex changes, ***Weather Clim. Dynam.***, ***1***, 715–730, doi:10.5194/wcd-1-715-2020, 2020.

Kunze, M., T. Kruschke, U. Langematz, M. Sinnhuber, T. Reddmann, and K. Matthes, Quantifying uncertainties of climate signals in chemistry climate models related to the 11-year solar cycle – Part 1: Annual mean response in heating rates, temperature, and ozone, ***Atmos. Chem. Phys.***, ***20***, 6991–7019, doi:10.5194/acp-20-6991-2020, 2020.

Kuttippurath, J., P. Kumar, P.J. Nair, and P.C. Pandey, Emergence of ozone recovery evidenced by reduction in the occurrence of Antarctic ozone loss saturation, ***npj Clim. Atmos. Sci., 1*** (1), 42, doi:10.1038/s41612-018-0052-6, 2018.

Kuttippurath, J., W. Feng, R. Müller, P. Kumar, S. Raj, G.P. Gopikrishnan, and R. Roy, Exceptional loss in ozone in the Arctic winter/spring of 2019/2020, ***Atmos. Chem. Phys.***, ***21***, 14019–14037, doi:10.5194/acp-21-14019-2021, 2021.

Langematz, U., S. Meul, K. Grunow, E. Romanowsky, S. Oberländer, J. Abalichin, and A. Kubin, Future Arctic temperature and ozone, The role of stratospheric composition changes, ***J. Geophys. Res. Atmos.***, ***119***, 2092–2112, doi:10.1002/2013JD021100, 2014.

Langematz, U., F. Schmidt, M. Kunze, G.E. Bodeker, and P. Braesicke, Antarctic ozone depletion between 1960 and 1980 in observations and chemistry–climate model simulations, ***Atmos. Chem. Phys.***, ***16***, 15619–15627, doi:10.5194/acp-16-15619-2016, 2016.

Langematz, U., and M. Tully (Lead Authors), N. Calvo, M. Dameris, A.T.J. de Laat, A. Klekociuk, R. Müller, and P. Young, Polar Stratospheric Ozone: Past, Present, and Future, Chapter 4 in ***Scientific Assessment of Ozone Depletion: 2018***, Global Ozone Research and Monitoring Project–Report No. 58, World Meteorological Organization, Geneva, Switzerland, 2018.

Lawrence, Z.D., and G.L. Manney, Characterizing stratospheric polar vortex variability with computer vision techniques, ***J. Geophys. Res. Atmos.***, ***123***, 1510–1535, doi:10.1002/2017JD027556, 2018.

Lawrence, Z.D., G.L. Manney, and K. Wargan, Reanalysis intercomparisons of stratospheric polar processing diagnostics, ***Atmos. Chem. Phys.***, ***18***, 13547–13579, doi:10.5194/acp-18-13547-2018, 2018.

Lawrence, Z.D., J. Perlwitz, A.H. Butler, G.L. Manney, P.A. Newman, S.H. Lee, and E.R. Nash, The remarkably strong Arctic stratospheric polar vortex of winter 2020: Links to record-breaking Arctic Oscillation and ozone loss, ***J. Geophys. Res.***, ***125*** (22), e2020JD033271, doi:10.1029/2020JD033271, 2020.

Lecouffe, A., S. Godin-Beekmann, A. Pazmiño, and A. Hauchecorne, Evolution of the intensity and duration of the Southern Hemisphere stratospheric polar vortex edge for the period 1979–2020, ***Atmos. Chem. Phys.***, 22, 4187–4200, doi:10.5194/acp-22-4187-2022, 2022.

Lee, S.H., J.C. Furtado, and A.J. Charlton-Perez, Wintertime North American weather regimes and the Arctic stratospheric polar vortex, ***Geophys. Res. Lett.***, ***46***, 14,892–14,900, doi:10.1029/2019GL085592, 2019.

Lee, S.H., and A.H. Butler, The 2018–2019 Arctic stratospheric polar vortex, ***Weather***, ***75*** (2), 52–57, doi:10.1002/wea.3643, 2020.

Lee, S.H., Z.D. Lawrence, A.H. Butler, and A.Y. Karpechko, Seasonal forecasts of the exceptional Northern Hemisphere winter of 2020, ***Geophys. Res. Lett.***, ***47*** (21), e2020GL090328, doi:10.1029/2020GL090328, 2020.

Lee, S.H., The January 2021 sudden stratospheric warming, ***Weather***, ***76***, 135–136, doi:10.1002/wea.3966, 2021.

Li, Y., W. Tian, F. Xie, Z. Wen, J. Zhang, D. Hu, and Y. Han, The connection between the second leading mode of the winter North Pacific sea surface temperature anomalies and stratospheric sudden warming events, ***Clim. Dyn. 51***, 581–595, doi:10.1007/s00382-017-3942-0, 2018.

Lickley M., S. Solomon, S. Fletcher, G.J.M. Velders, J. Daniel, M. Rigby, S.A. Montzka, L.J.M. Kuijpers, and K. Stone, Quantifying contributions of chlorofluorocarbon banks to emissions and impact on the ozone layer and climate, ***Nat. Commun.***, ***11*** (1), doi:10.1038/s41467-020-15162-7, 2020.

Lillo, S.P., S.M. Cavallo, D.B. Parsons, and C. Riedel, The role of a tropopause polar vortex in the generation of the January 2019 extreme Arctic outbreak, ***J. Atmos. Sci.***, ***78***, 2801–2821, doi:10.1175/JAS-D-20-0285.1, 2021.

Lim, E.P., H.H. Hendon, G. Boschat, D. Hudson, D.W.J. Thompson, A.J. Dowdy, and J.M. Arblaster, Australian hot and dry extremes induced by weakenings of the stratospheric polar vortex, ***Nat. Geosci.***, ***12***, 896–901, doi:10.1038/s41561-019-0456-x, 2019.

Lim, E., H.H. Hendon, A.H. Butler, D.W.J. Thompson, Z.D. Lawrence, A.A. Scaife, T.G. Shepherd, I. Polichtchouk, H. Nakamura, C. Kobayashi, R. Comer, L. Coy, A. Dowdy, R.D. Garreaud, P.A. Newman, and G. Wang, The 2019 Southern Hemisphere stratospheric polar vortex weakening and its impacts, ***Bull. Amer. Meteor. Soc***, ***102*** (6), E1150–E1171, doi:10.1175/BAMS-D-20-0112.1, 2021.

Liu, G., T. Hirooka, N. Eguchi, and K. Krüger, Dynamical evolution of a minor sudden stratospheric warming in the Southern Hemisphere in 2019, ***Atmos. Chem. Phys.***, ***22***, 3493–3505, doi:10.5194/acp-22-3493-2022, 2022.

Livesey, N.J., M.L. Santee, and G.L. Manney, A Match-based approach to the estimation of polar stratospheric ozone loss using Aura Microwave Limb Sounder observations, ***Atmos. Chem. Phys.***, ***15***, 9945–9963, doi:10.5194/acp-15-9945-2015, 2015.

Lyons, B.A., A. Hasell, and N.J. Stroud, Enduring extremes? Polar vortex, drought, and climate change beliefs, ***Environ. Commun.***, ***12*** (7), 876–894, doi:10.1080/17524032.2018.1520735, 2018.

Maliniemi, V., D.R. Marsh, H.N. Tyssøy, and C. Smith-Johnsen, Will climate change impact polar $NO_x$ produced by energetic particle precipitation?, ***Geophys. Res. Lett.***, ***47*** (9), e2020GL087041, doi:10.1029/2020GL087041, 2020.

Maliniemi, V., H.N. Tyssøy, C. Smith-Johnsen, P. Arsenovic, and D.R. Marsh, Effects of enhanced downwelling of NOx on Antarctic upper-stratospheric ozone in the 21st century, ***Atmos. Chem. Phys.***, ***21***, 11,041–11,052, 2021, doi:10.5194/acp-21-11041-2021, 2021.

Manney, G.L., M.L. Santee, M. Rex, N.J. Livesey, M.C. Pitts, P. Veefkind, E.R. Nash, I. Wohltmann, R. Lehmann, L. Froidevaux, L.R. Poole, M.R. Schoeberl, D.P. Haffner, J. Davies, V. Dorokhov, H. Gernandt, B. Johnson, R. Kivi, E. Kyrö, N. Larsen, P.F. Levelt, A. Makshtas, C.T. McElroy, H. Nakajima, M.C. Parrondo, D.W. Tarasick, P. von der Gathen, K.A. Walker, and N.S. Zinoviev, Unprecedented Arctic ozone loss in 2011, ***Nature***, ***478*** (7370), 469–475, doi:10.1038/nature10556, 2011a.

Manney, G.L., M.I. Hegglin, W.H. Daffer, M.L. Santee, E.A. Ray, S. Pawson, M.J. Schwartz, C.D. Boone, L. Froidevaux, N.J. Livesey, W.G. Read, and K.A. Walker, Jet characterization in the upper troposphere/lower stratosphere (UTLS): Applications to climatology and transport studies, ***Atmos. Chem. Phys.***, ***11*** (12), 6115–6137, doi:10.5194/acp-11-6115-2011, 2011b.

Manney, G.L., M.I. Hegglin, W.H. Daffer, M.J. Schwartz, M.L. Santee, and S. Pawson, Climatology of upper tropospheric-lower stratospheric (UTLS) jets and tropopauses in MERRA, ***J. Clim.***, ***27***, 3248–3271, doi:10.1175/JCLI-D-13-00243.1, 2014.

Manney, G.L., Z.D. Lawrence, M.L. Santee, W.G. Read, N.J. Livesey, A. Lambert, L. Froidevaux, H.C. Pumphrey, and M.J. Schwartz, A minor sudden stratospheric warming with a major impact: Transport and polar processing in the 2014/2015 Arctic winter, ***Geophys. Res. Lett.***, ***42***, 7808–7816, doi:10.1002/2015GL065864, 2015.

Manney, G.L., N.J. Livesey, M.L. Santee, L. Froidevaux, A. Lambert, Z.D. Lawrence, L.F. Millán, J.L. Neu, W.G. Read, M.J. Schwartz, and R.A. Fuller, Record-low Arctic stratospheric ozone in 2020: MLS observations of chemical processes and comparisons with previous extreme winters, ***Geophys. Res. Lett.***, ***47*** (16), e2020GL089063, doi:10.1029/2020GL089063, 2020.

Manney, G.L., A.H. Butler, Z.D. Lawrence, K. Wargan, and M.L. Santee, What's in a name? On the use and significance of the term "polar vortex", ***Geophys. Res. Lett.***, e2021GL097617, doi:10.1029/2021GL097617, 2022.

Manzini, E., A.Y. Karpechko, and L. Kornblueh, Nonlinear response of the stratosphere and the North Atlantic-European climate to global warming, ***Geophys. Res. Lett.***, ***45***, 4255–4263, doi:10.1029/2018GL077826, 2018.

Marsing, A., T. Jurkat-Witschas, J.-U. Grooß, S. Kaufmann, R. Heller, A. Engel, P. Hoor, J. Krause, and C. Voigt, Chlorine partitioning in the lowermost Arctic vortex during the cold winter 2015/2016, ***Atmos. Chem. Phys.***, ***19***, 10757–10772, doi:10.5194/acp-19-10757-2019, 2019.

Matthes, K., B. Funke, M.E. Andersson, L. Barnard, J. Beer, P. Charbonneau, M.A. Clilverd, T. Dudok de Wit, M. Haberreiter, A. Hendry, C.H. Jackman, M. Kretzschmar, T. Kruschke, M. Kunze, U. Langematz, D.R. Marsh, A.C. Maycock, S. Misios, C.J. Rodger, A.A. Scaife, A. Seppälä, M. Shangguan, M. Sinnhuber, K. Tourpali, I. Usoskin, M. van de Kamp, P.T. Verronen, and S. Versick, Solar forcing for CMIP6 (v3.2), ***Geosci. Model Dev.***, ***10***, 2247–2302, doi:10.5194/gmd-10-2247-2017, 2017.

Matthias, V., A. Dörnbrack, and G. Stober, The extraordinarily strong and cold polar vortex in the early northern winter 2015/2016, ***Geophys. Res. Lett.***, ***43***, 287–294, doi:10.1002/2016GL071676, 2016.

McPeters, R., M. Kroon, G. Labow, E. Brinksma, D. Balis, I. Petropavlovskikh, J.P. Veefkind, P.K. Bhartia, and P.F. Levelt, Validation of the Aura Ozone Monitoring Instrument total column ozone product, ***J. Geophys. Res.***, ***113***, D15S14, doi:10.1029/2007JD008802, 2008.

McPeters, R.D., S. Frith, and G.J. Labow, OMI total column ozone: extending the long-term data record, ***Atmos. Meas. Tech.***, ***8***, 4845–4850, doi:10.5194/amt-8-4845-2015, 2015.

Meinshausen, M., E. Vogel, A. Nauels, K. Lorbacher, N. Meinshausen, D.M. Etheridge, P.J. Fraser, S.A. Montzka, P.J. Rayner, C.M. Trudinger, P.B. Krummel, U. Beyerle, J.G. Canadell, J.S. Daniel, I.G. Enting, R.M. Law, C.R. Lunder, S. O'Doherty, R.G. Prinn, S. Reimann, M. Rubino, G.J.M. Velders, M.K. Vollmer, R.H.J. Wang, and R. Weiss, Historical greenhouse gas concentrations for climate modelling (CMIP6), ***Geosci. Model Dev.***, ***10***, 2057–2116, doi:10.5194/gmd-10-2057-2017, 2017.

Meinshausen, M., Z.R.J. Nicholls, J. Lewis, M.J. Gidden, E. Vogel, M. Freund, U. Beyerle, C. Gessner, A. Nauels, N. Bauer, J.G. Canadell, J.S. Daniel, A. John, P.B. Krummel, G. Luderer, N. Meinshausen, S.A. Montzka, P.J. Rayner, S. Reimann, S.J. Smith, M. van den Berg, G.J.M. Velders, M.K. Vollmer, and R.H.J. Wang, The shared socioeconomic pathway (SSP) greenhouse gas concentrations and their extensions to 2500, ***Geosci. Model Dev.***, ***13***, 3571–3605, doi:10.5194/gmd-13-3571-2020, 2020.

Mironova, I.A., K.L. Aplin, F. Arnold, G.A. Bazilevskaya, R.G. Harrison, A.A. Krivolutsky, K.A. Nicoll, E.V. Rozanov, E. Turunen, and I.G. Usoskin, Energetic particle influence on the Earth's atmosphere, ***Space Sci. Rev.***, ***194***, 1–96, doi:10.1007/s11214-015-018-4, 2015.

Mironova, I.A., A.A. Artamonov, G. Bazilevskaya, E. Rozanov, G.A. Kovaltsov, V.S. Makhmutov, L. Mishev, and A.V. Karagodin, Ionization of the polar atmosphere by energetic electron precipitation retrieved from balloon measurements, ***Geophys. Res. Lett.***, ***46*** (2), 990–996, doi:10.1029/2018GL079421, 2019.

Montzka, S., G. Dutton, P. Yu, E. Ray, R. Portmann, J. Daniel, L. Kuijpers, B. Hall, D. Mondeel, C. Siso, J. Nance, M. Rigby, A. Manning, L. Hu, F. Moore, B. Miller, and J. Elkins, An unexpected and persistent increase in global emissions of ozone-depleting CFC-11, ***Nature, 557***, 413–417, doi:10.1038/s41586-018-0106-2, 2018.

Montzka, S.A., G.S. Dutton, R.W. Portmann, M.P. Chipperfield, S. Davis, W. Feng, A.J. Manning, E. Ray, M. Rigby, B.D. Hall, C. Siso, J.D. Nance, P.B. Krummel, J. Mühle, D. Young, S. O'Doherty, P.K. Salameh, C.M. Harth, R.G. Prinn, R.F. Weiss, J.W. Elkins, H. Walter-Terrinoni, and C. Theodoridi, A decline in global CFC-11 emissions during 2018–2019, ***Nature, 590***, 428–432, doi:10.1038/s41586-021-03260-5, 2021.

Morgenstern, O., M. Giorgetta, K. Shibata, V. Eyring, D. Waugh, T. Shepherd, H. Akiyoshi, J. Austin, A.J.G. Baumgaertner, S. Bekki, P. Braesicke, C. Brühl, M.P. Chipperfield, D. Cugnet, M. Dameris, S. Dhomse, S.M. Frith, H. Garny, A. Gettelman, S.C. Hardiman, M.I. Hegglin, P. Jöckel, D.E. Kinnison, J.-F. Lamarque, E. Mancini, E. Manzini, M. Marchand, M. Michou, T. Nakamura, J.E. Nielsen, D. Olivié, G. Pitari, D.A. Plummer, E. Rozanov, J.F. Scinocca, D. Smale, H. Teyssèdre, M. Toohey, W. Tian, and Y. Yamashita, Review of the formulation of present-generation stratospheric chemistry-climate models and associated external forcings, ***J. Geophys. Res.***, ***115*** (D3), doi:10.1029/2009JD013728, 2010.

Morgenstern, O., M.I. Hegglin, E. Rozanov, F.M. O'Connor, N.L. Abraham, H. Akiyoshi, A.T. Archibald, S. Bekki, N. Butchart, M.P. Chipperfield, M. Deushi, S.S. Dhomse, R.R. Garcia, S.C. Hardiman, L.W. Horowitz, P. Jöckel, B. Josse, D. Kinnison, M. Lin, E. Mancini, M.E. Manyin, M. Marchand, V. Marécal, M. Michou, L.D. Oman, G. Pitari, D.A. Plummer, L.E. Revell, D. Saint-Martin, R. Schofield, A. Stenke, K. Stone, K. Sudo, T.Y. Tanaka, S. Tilmes, Y. Yamashita, K. Yoshida, and G. Zeng, Review of the global models used within phase 1 of the Chemistry–Climate Model Initiative (CCMI), ***Geosci. Model Dev.***, ***10***, 639–671, doi:10.5194/gmd-10-639-2017, 2017.

Mori, M., Y. Kosaka, M. Watanabe, H. Nakamura, and M. Kimoto, A reconciled estimate of the influence of Arctic sea-ice loss on recent Eurasian cooling, ***Nat. Clim. Change***, ***9***, 123–129, doi:10.1038/s41558-018-0379-3, 2019.

Müller, R., J.-U. Grooß, C. Lemmen, D. Heinze, M. Dameris, and G. Bodeker, Simple measures of ozone depletion in the polar stratosphere, ***Atmos. Chem. Phys.***, ***8***, 251–264, doi:10.5194/acp-8-251-2008, 2008.

Müller, R., J.-U. Grooß, A.M. Zafar, S. Robrecht, and R. Lehmann, The maintenance of elevated active chlorine levels in the Antarctic lower stratosphere through HCl null cycles, ***Atmos. Chem. Phys.***, ***18***, 2985–2997, doi:10.5194/acp-18-2985-2018, 2018.

Nakamura, T., K. Yamazaki, K. Iwamoto, M. Honda, Y. Miyoshi, Y. Ogawa, Y. Tomikawa, and J. Ukita, The stratospheric pathway for Arctic impacts on midlatitude climate, ***Geophys. Res. Lett.***, ***43***, 494–3501, doi:10.1002/2016GL068330, 2016.

Nash, E.R., P.A. Newman, J.E. Rosenfeld, and M.R. Schoeberl, An objective determination of the polar vortex using Ertel's potential vorticity, ***J. Geophys. Res., 101***, 9471–9478, doi:10.1029/96JD00066, 1996.

Nesse Tyssøy, H., A. Haderlein, M.I. Sandanger, and J. Stadsnes, Intercomparison of the POES/MEPED loss cone electron fluxes with the CMIP6 parametrization, ***J. Geophys. Res. Space Phys.***, ***124***, 628–642, doi:10.1029/2018JA025745, 2019.

Newman, P.A., S.R. Kawa, and E.R. Nash, On the size of the Antarctic ozone hole, ***Geophys. Res. Lett.***, ***31***, L21104, doi:10.1029/2004GL020596, 2004.

Newman, P.A., J.S. Daniel, D.W. Waugh, and E.R. Nash, A new formulation of equivalent effective stratospheric chlorine (EESC), ***Atmos. Chem. Phys.***, ***7***, 4537–4552, doi:10.5194/acp-7-4537-2007, 2007.

Newman, P.A. and M. Rex (Lead Authors), P.O. Canziani, K.S. Carslaw, K. Drdla, S. Godin-Beekmann, C.H. Jackman, K. Kreher, U. Langematz, R. Müller, H. Nakane, Y.J. Orsolini, R.J. Salawitch, M.L. Santee, M. von Hobe, and S. Yoden, Polar Ozone: Past and Present, Chapter 4 in ***Scientific Assessment of Ozone Depletion: 2007***, Global Ozone Research and Monitoring Project–Report No. 50, World Meteorological Organization, Geneva, Switzerland, 2007.

Newman, P.A., E.R. Nash, N. Kramarova, and A. Butler, The 2019 southern stratospheric warming [in ''State of the Climate in 2019''], ***Bull. Amer. Meteor. Soc.***, ***101***, S297–S298, doi: 0.1175/BAMS-D-20-0090.1, 2020.

Oberländer, S., U. Langematz, and S. Meul, Unraveling impact factors for future changes in the Brewer-Dobson circulation, ***J. Geophys. Res. Atmos.***, ***118***, 10,296–10,312, doi:10.1002/jgrd.50775, 2013.

Olsen, M.A., G.L. Manney, and J. Liu, The ENSO and QBO impact on ozone variability and stratosphere-troposphere exchange relative to the subtropical jets, ***J. Geophys. Res.***, ***124***, doi:10.1029/2019JD030435, 2019.

Oman, L.D., D.A. Plummer, D.W. Waugh, J. Austin, J.F. Scinocca, A.R. Douglass, R.J. Salawitch, T. Canty, H. Akiyoshi, S. Bekki, P. Braesicke, N. Butchart, M.P. Chipperfield, D. Cugnet, S. Dhomse, V. Eyring, S. Frith, S.C. Hardiman, D.E. Kinnison, J.-F. Lamarque, E. Mancini, M. Marchand, M. Michou, O. Morgenstern, T. Nakamura, J.E. Nielsen, D. Olivié, G. Pitari, J. Pyle, E. Rozanov, T.G. Shepherd, K. Shibata, R.S. Stolarski, H. Teyssèdre, W. Tian, Y. Yamashita, and J.R. Ziemke, Multimodel assessment of the factors driving stratospheric ozone evolution over the 21st century, ***J. Geophys. Res. Atmos.***, ***115*** (D24), doi:10.1029/2010JD014362, 2010.

Oman, L.D., A.R. Douglass, R.J. Salawitch, T.P. Canty, J.R. Ziemke, and M. Manyin, The effect of representing bromine from VSLS on the simulation and evolution of Antarctic ozone, ***Geophys. Res. Lett.***, ***43***, 9869–9876, doi:10.1002/2016GL070471, 2016.

O'Neill, B.C., E. Kriegler, K. Riahi, K.L. Ebi, S. Hallegatte, T.R. Carter, R. Mathur, and D.P. van Vuuren, A new scenario framework for climate change research: the concept of shared socioeconomic pathways, ***Clim. Change, 122*** (3)**,** 387–400, doi:10.1007/s10584-013-0905, 2014.

Pazmiño, A., S. Godin-Beekmann, A. Hauchecorne, C. Claud, S. Khaykin, F. Goutail, E. Wolfram, J. Salvador, and E. Quel, Multiple symptoms of total ozone recovery inside the Antarctic vortex during austral spring, ***Atmos. Chem. Phys.***, ***18***, 7557–7572, doi:10.5194/acp-18-7557-2018, 2018.

Pérot, K., and Y. Orsolini, Impact of the major SSWs of February 2018 and January 2019 on the middle atmospheric nitric oxide abundance, ***J. Atmos. Sol. Terr. Phys.***, ***218***, 105586, doi:10.1016/j.jastp.2021.105586, 2021.

Pettit, J.M., C.E. Randall, E.D. Peck, D.R. Marsh, M. van de Kamp, X. Fang, V.L. Harvey, C.J. Rodger, and B. Funke, Atmospheric effects of >30-keV energetic electron precipitation in the southern hemisphere winter during 2003, ***J. Geophys. Res. Space Phys.***, ***124*** (10), 8138–8153, doi:10.1029/2019JA026868, 2019.

Pitts, M.C., L.R. Poole, and R. Gonzalez, Polar stratospheric cloud climatology based on CALIPSO spaceborne lidar measurements from 2006 to 2017, ***Atmos. Chem. Phys.***, ***18***, 10881–10913, doi:10.5194/acp-18-10881-2018, 2018.

Plummer D., T. Nagashima, S. Tilmes, A. Archibald, G. Chiodo, S. Fadnavis, H. Garny, B. Josse, J. Kim, J.-F. Lamarque, O. Morgenstern, L. Murray, C. Orbe, A. Tai, M. Chipperfield, B. Funke, M. Juckes, D. Kinnison, M. Kunze, B. Luo, K, Matthes, P.A. Newman, C. Pascoe, and T. Peter, CCMI-2022: A new set of Chemistry-Climate Model Initiative (CCMI) community simulations to update the assessment of models and support upcoming Ozone Assessment activities, ***SPARC newsletter***, (57), [available at: https://www.sparc-climate.org/wp-content/uploads/sites/5/2021/07/SPARCnewsletter_Jul2021_web.pdf#page=22], 2021.

Polvani, L.M., M. Abalos, R. Garcia, D. Kinnison, and W.J. Randel, Significant weakening of Brewer-Dobson circulation trends over the 21st century as a consequence of the Montreal Protocol, ***Geophys. Res. Lett.***, ***45***, 401–409, doi:10.1002/2017GL075345, 2017.

Polvani, L.M., L. Wang, M. Abalos, N. Butchart, M.P. Chipperfield, M. Dameris, M. Deushi, S.S. Dhomse, P. Jöckel, D. Kinnison, M. Michou, O. Morgenstern, L.D. Oman, D.A. Plummer, and K.A. Stone, Large impacts, past and future, of ozone-depleting substances on Brewer-Dobson circulation trends: A multimodel assessment, ***J. Geophys. Res. Atmos.***, ***124*** (13), 6669–6680, doi:10.1029/2018JD029516, 2019.

Poole, L.R., and M.C. Pitts, Polar stratospheric cloud climatology based on Stratospheric Aerosol Measurement II observations from 1978 to 1989, ***J. Geophys. Res. Atmos.***, ***99***, 13,083–13,089, doi:10.1029/94JD00411, 1994.

Prignon, M., S. Chabrillat, M. Friedrich, D. Smale, S.E. Strahan, P.F. Bernath, M.P. Chipperfield, S.S. Dhomse, W. Feng, D. Minganti, C. Servais, and E. Mahieu, Stratospheric fluorine as a tracer of circulation changes: Comparison between infrared remote-sensing observations and simulations with five modern reanalyses, ***J. Geophys. Res.***, ***126*** (19), e2021JD034995, doi:10.1029/2021JD034995, 2021.

Pyle, J.A., J. Keeble, N.L. Abraham, M.P. Chipperfield, and P.T. Griffiths, Integrated ozone depletion as a metric for ozone recovery, ***Nature***, ***608***, 719–723, doi:10.1038/s41586-022-04968-8, 2022.

Rao, J., R. Ren, H. Chen, Y. Yu, and Y. Zhou, The stratospheric sudden warming event in February 2018 and its prediction by a climate system model, ***J. Geophys. Res. Atmos.***, ***123***, 13,332–13,345, doi:10.1029/2018JD028908, 2018.

Rao, J., C.I. Garfinkel, H. Chen, and I.P. White, The 2019 New Year stratospheric sudden warming and its real-time predictions in multiple S2S models, ***J. Geophys. Res. Atmos.***, ***124***, 11155–11174, doi:10.1029/2019JD030826, 2019.

Rao, J., and C.I. Garfinkel, Arctic ozone loss in March 2020 and its seasonal prediction in CFSv2: A comparative study with the 1997 and 2011 cases, ***J. Geophys. Res. Atmos.***, ***125*** (21), e2020JD033524, doi:10.1029/2020JD033524, 2020.

Rao, J., C.I. Garfinkel, I.P. White, and C. Schwartz, The Southern Hemisphere minor sudden stratospheric warming in September 2019 and its predictions in S2S models, ***J. Geophys. Res. Atmos.***, ***125*** (14), e2020JD032723, doi:10.1029/2020JD032723, 2020.

Rao, J., and C.I. Garfinkel, The strong stratospheric polar vortex in March 2020 in sub-seasonal to seasonal models: Implications for empirical prediction of the low Arctic total ozone extreme, ***J. Geophys. Res. Atmos.***, ***126*** (9), e2020JD034190, doi:10.1029/2020JD034190, 2021.

Rex, M., R.J. Salawitch, H. Deckelmann, P. von der Gathen, N.R.P. Harris, M.P. Chipperfield, B. Nau- jokat, E. Reimer, M. Allaart, S.B. Andersen, R. Bevilacqua, G.O. Braathen, H. Claude, J. Davies, H. De Backer, H. Dier, V. Dorokhov, H. Fast, M. Gerding, S. Godin-Beekmann, K. Hoppel, B. Johnson, E. Kyrö, Z. Litynska, D. Moore, H. Nakane, M.C. Parrondo, A.D. Risley Jr., P. Skrivankova, R. Stübi, P. Viatte, V. Yushkov, and C. Zerefos, Arctic winter 2005: Implications for stratospheric ozone loss and climate change, ***Geophys. Res. Lett.***, ***33***, L23808, doi:10.1029/2006GL026731, 2006.

Rieger, L.A., W.J. Randel, A.E. Bourassa, and S. Solomon, Stratospheric temperature and ozone anomalies associated with the 2020 Australian New Year fires, ***Geophys. Res. Lett.***, ***48*** (24), e2021GL095898, doi:10.1029/2021GL095898, 2021.

Rotermund, M.K., V. Bense, M.P. Chipperfield, A. Engel, J.-U. Grooß, P. Hoor, T. Hüneke, T. Keber, F. Kluge, B. Schreiner, T. Schuck, B. Vogel, A. Zahn, and K. Pfeilsticker, Organic and inorganic bromine measurements around the extratropical tropopause and lowermost stratosphere: Insights into the transport pathways and total bromine, ***Atmos. Chem. Phys.***, ***21*** (20), 15,375–15,407, doi:10.5194/acp-21-15375-2021, 2021.

Safieddine, S., M. Bouillon, A.-C. Paracho, J. Jumelet, F. Tencé, A. Pazmiño, F. Goutail, C. Wespes, S. Bekki, A. Boynard, J. Hadji-Lazaro, P.-F. Coheur, D. Hurtmans, and C. Clerbaux, Antarctic ozone enhancement during the 2019 sudden stratospheric warming event, ***Geophys. Res. Lett.***, ***47*** (14), e2020GL087810, doi:10.1029/2020GL087810, 2020.

Saha, S., S. Moorthi, H. Pan, X. Wu, J. Wang, S. Nadiga, P. Tripp, R. Kistler, J. Woollen, D. Behringer, H. Liu, D. Stokes, R. Grumbine, G. Gayno, J. Wang, Y. Hou, H. Chuang, H.H. Juang, J. Sela, M. Iredell, R. Treadon, D. Kleist, P. van Delst, D. Keyser, J. Derber, M. Ek, J. Meng, H. Wei, R. Yang, S. Lord, H. van den Dool, A. Kumar, W. Wang, C. Long, M. Chelliah, Y. Xue, B. Huang, J. Schemm, W. Ebisuzaki, R. Lin, P. Xie, M. Chen, S. Zhou, W. Higgins, C. Zou, Q. Liu, Y. Chen, Y. Han, L. Cucurull, R.W. Reynolds, G. Rutledge, and M. Goldberg, The NCEP climate forecast system reanalysis, ***Bull. Am. Meteorol. Soc.***, ***91***, 1015–1058, doi:10.1175/2010BAMS3001.1, 2010.

Santee, M.L., A. Lambert, G.L. Manney, N.J. Livesey, L. Froidevaux, J.L. Neu, M.J. Schwartz, L.F. Millán, F. Werner, W.G. Read, M. Park, R.A. Fuller, and B.M. Ward, Prolonged and pervasive perturbations in the composition of the Southern Hemisphere midlatitude lower stratosphere from the Australian New Year's fires, ***Geophys. Res. Lett.***, ***49*** (4), e2021GL096270, doi:10.1029/2021GL096270, 2022.

Schneider, J., R. Weigel, T. Klimach, A. Dragoneas, O. Appel, A. Hünig, S. Molleker, F. Köllner, H.-C. Clemen, O. Eppers, P. Hoppe, P. Hoor, C. Mahnke, M. Krämer, C. Rolf, J.-U. Grooß, A. Zahn, F. Obersteiner, F. Ravegnani, A. Ulanovsky, H. Schlager, M. Scheibe, G.S. Diskin, J.P. DiGangi, J.B. Nowak, M. Zöger, and S. Borrmann, Aircraft-based observation of meteoric material in lower-stratospheric aerosol particles between 15 and 68°N, ***Atmos. Chem. Phys.***, ***21***, 989–1013, doi:10.5194/acp-21-989-2021, 2021.

Schwartz, M.J., M.L. Santee, H.C. Pumphrey, G.L. Manney, A. Lambert, N.J. Livesey, L. Millán, J.L. Neu, W.G. Read, and F. Werner, Australian New Year's pyroCb impact on stratospheric composition, ***Geophy. Res. Lett.***, ***47*** (24), e2020GL090831, doi:10.1029/2020GL090831, 2020.

Screen, J.A., Simulated atmospheric response to regional and Pan-Arctic sea-ice loss, ***J. Clim.***, ***30*** (11), 3945–3962, doi:10.1175/JCLI-D-16-0197.1, 2017.

Screen, J.A., C. Deser, and L. Sun, Reduced risk of North American cold extremes due to continued Arctic sea ice loss, ***Bull. Amer. Meteor. Soc.***, ***96*** (9), 1489–1503, doi:10.1175/BAMS-D-14-00185.1, 2015.

Shen, X., L. Wang, and S. Osprey, Tropospheric forcing of the 2019 Antarctic sudden stratospheric warming, ***Geophys. Res. Lett.***, ***47*** (20), e2020GL089343, doi:10.1029/2020GL089343, 2020.

Shepherd, M., 12 weather and climate concepts that confuse the public, ***Forbes,*** [available at: https://www.forbes.com/sites/marshallshepherd/2016/12/13/12-weather-and-climate-concepts-that-confuse-the-public/?sh=2943e192350b], 2016.

Sinnhuber, M., H. Nieder, and N. Wieters, Energetic particle precipitation and the chemistry of the mesosphere/lower thermosphere, ***Surv. Geophys.***, ***33*** (6), 1281–1334, doi:10.1007/s10712-012-9201-3, 2012.

Sinnhuber, M., U. Berger, B. Funke, H. Nieder, T. Reddmann, G. Stiller, S. Versick, T. von Clarmann, and J.M. Wissing, $NO_y$ production, ozone loss and changes in net radiative heating due to energetic particle precipitation in 2002–2010, ***Atmos. Chem. Phys.***, ***18*** (2), 1115–1147, doi:10.5194/acp-18-1115-2018, 2018.

Smale, D., S.E. Strahan, R. Querel, U. Frieß, G.E. Nedoluha, S.E. Nichol, J. Robinson, I. Boyd, M. Kotkamp, R.M. Gomez, M. Murphy, H. Tran, and J. McGaw, Evolution of observed ozone, trace gases, and meteorological variables over Arrival Heights, Antarctica (77.8°S, 166.7°E) during the 2019 Antarctic stratospheric sudden warming, ***Tellus B: Chem. Phys. Meteorol.***, ***73*** (1), 1–18, doi:10.1080/16000889.2021.1933783, 2021.

Snels, M., A. Scoccione, L. Di Liberto, F. Colao, M. Pitts, L. Poole, T. Deshler, F. Cairo, C. Cagnazzo, and F. Fierli, Comparison of Antarctic polar stratospheric cloud observations by ground-based and space-borne lidar and relevance for chemistry–climate models, ***Atmos. Chem. Phys.***, ***19***, 955–972, doi:10.5194/acp-19-955-2019, 2019.

Snels, M., F. Colao, F. Cairo, I. Shuli, A. Scoccione, M. De Muro, M. Pitts, L. Poole, and L. Di Liberto, Quasi-coincident observations of polar stratospheric clouds by ground-based lidar and CALIOP at Concordia (Dome C, Antarctica) from 2014 to 2018, ***Atmos. Chem. Phys.***, ***21***, 2165–2178, doi:10.5194/acp-21-2165-2021, 2021.

Solomon, S., J. Haskins, D.J. Ivy, and F. Min, Fundamental differences between Arctic and Antarctic ozone depletion, ***Proc. Natl. Acad. Sci.***, ***111*** (17), 6220–6225, doi:10.1073/pnas.1319307111, 2014.

Solomon, S., D.J. Ivy, D. Kinnison, M.J. Mills, R.R. Neely III, and A. Schmidt, Emergence of healing in the Antarctic ozone layer, ***Science***, ***353*** (6296), 269–274, doi:10.1126/science.aae0061, 2016.

Spang, R., L. Hoffmann, R. Müller, J.-U. Grooß, I. Tritscher, M. Höpfner, M. Pitts, A. Orr, and M. Riese, A climatology of polar stratospheric cloud composition between 2002 and 2012 based on MIPAS/Envisat observations, ***Atmos. Chem. Phys.***, ***18***, 5089–5113, doi:10.5194/acp-18-5089-2018, 2018.

SPARC CCMVal (Stratosphere-troposphere Processes And their Role in Climate), ***SPARC Report on the Evaluation of Chemistry-Climate Models***, edited by V. Eyring, T.G. Shepherd, and D.W. Waugh, SPARC Report No. 5, WCRP-132, WMO/TD-No. 1526, 478 pp., [available at: http://www.atmosp.physics.utoronto.ca/SPARC/ccmval_final/index.php], 2010.

SPARC (Stratosphere-troposphere Processes And their Role in Climate), ***SPARC Reanalysis Intercomparison Project (S-RIP) Final Report***, edited by M. Fujiwara, G.L. Manney, L.J. Gray, and J.S. Wright, SPARC Report No. 10, WCRP-17/2020, doi:10.17874/800dee57d13, 2022.

Stecher, L., F. Winterstein, M. Dameris, P. Jockel, M. Ponater, and M. Kunze, Slow feedbacks resulting from strongly enhanced atmospheric methane mixing ratios in a chemistry–climate model with mixed-layer ocean, ***Atmos. Chem. Phys.***, ***21***, 731–754, doi:10.5194/acp-21-731-2021, 2021.

Stone, K.A., S. Solomon, D.E. Kinnison, M.C. Pitts, L.R. Poole, M.J. Mills, A. Schmidt, R.R. Neely III, D. Ivy, M.J. Schwartz, J.-P. Vernier, B.J. Johnson, M.B. Tully, A.R. Klekociuk,G. König-Langlo, and S. Hagiya, Observing the impact of Calbuco volcanic aerosols on South Polar ozone depletion in 2015, ***J. Geophys. Res. Atmos.***, ***122***, 11862–11879, doi:10.1002/2017JD026987, 2017.

Stone, K.A., S. Solomon, and D.E. Kinnison, On the identification of ozone recovery, ***Geophys. Res. Lett.***, ***45***, 5158–5165, doi:10.1029/2018GL077955, 2018.

Stone, K.A., S. Solomon, D.E. Kinnison, and M.J. Mills, On recent large Antarctic ozone holes and ozone recovery metrics, ***Geophys. Res. Lett.***, ***48*** (22), e2021GL095232, doi:10.1029/2021GL095232, 2021.

Strahan, S.E., A.R. Douglass, and S.D. Steenrod, Chemical and dynamical impacts of stratospheric sudden warmings on Arctic ozone variability, ***J. Geophys. Res. Atmos.***, ***121***, 11,836–11,851, doi:10.1002/2016JD025128, 2016.

Strahan, S.E., A.R. Douglass, and M.R. Damon, Why do Antarctic ozone recovery trends vary?, ***J. Geophys. Res. Atmos., 124***, 8837–8850, doi:10.1029/2019JD030996, 2019.

Strahan, S.E., D. Smale, A.R. Douglass, T. Blumenstock, J.W. Hannigan, F. Hase, N.B. Jones, E. Mahieu, J. Notholt, L.D. Oman, I. Ortega, M. Palm, M. Prignon, J. Robinson, M. Schneider, R. Sussmann, and V.A. Velazco, Observed hemispheric asymmetry in stratospheric transport trends from 1994 to 2018, ***Geophys. Res. Lett.***, ***47*** (17), e2020GL088567, doi:10.1029/2020GL088567, 2020.

Tegtmeier, S., M. Rex, I. Wohltmann, and K. Krüger, Relative importance of dynamical and chemical contributions to Arctic wintertime ozone, ***Geophys. Res. Lett.***, ***35***, L17801, doi:10.1029/2008GL034250, 2008.

Tegtmeier, S., F. Ziska, I. Pisso, B. Quack, G.J.M. Velders, X. Yang, and K. Krüger, Oceanic bromoform emissions weighted by their ozone depletion potential, ***Atmos. Chem. Phys.***, ***15***, 13,647–13,663, doi:10.5194/acp-15-13647-2015, 2015.

Tritscher, I., M.C. Pitts, L.R. Poole, S.P. Alexander, F. Cairo, M.P. Chipperfield, J.-U. Grooß, M. Höpfner, A. Lambert, B. Luo, S. Molleker, A. Orr, R. Salawitch, M. Snels, R. Spang, W. Woiwode, and T. Peter, Polar stratospheric clouds: Satellite observations, processes, and role in ozone depletion, ***Rev. Geophys.***, ***59*** (2), e2020RG000702, doi:10.1029/2020RG000702, 2021.

Tully, M.B., P.B. Krummel, and A.R. Klekociuk, Trends in Antarctic ozone hole metrics 2001–17, ***J. South. Hemisph. Earth Syst. Sci., 69*** (1), 52–56, doi:10.1071/ES19020, 2019.

UCAR, Why the polar vortex keeps breaking out of the Arctic, ***University Corporation for Atmospheric Research***, [available at: https://scied.ucar.edu/learning-zone/climate-change-impacts/why-polar-vortex-keeps-breaking-out-arctic], 2021.

UC Davis, What is the polar vortex?, ***University of California, Davis,*** [available at: https://climatechange.ucdavis.edu/climate-change-definitions/what-is-the-polar-vortex], 2019.

Vargin, P.N., S.V. Kostrykin, E.M. Volodin, A.I. Pogoreltsev, and K. Wei, Arctic stratosphere circulation changes in the 21st century in simulations of INM CM5, ***Atmosphere***, ***13*** (1), 25, doi:10.3390/atmos13010025, 2022.

van de Kamp, M., A. Seppälä, M.A. Clilverd, C.J. Rodger, P.T. Verronen, and I.C. Whittaker, A model providing long-term data sets of energetic electron precipitation during geomagnetic storms, ***J. Geophys. Res. Atmos.***, ***121*** (20), 12,520–12,540, doi:10.1002/2015jd024212, 2016.

van der A, R.J., M.A.F. Allaart, and H.J. Eskes, Multi-Sensor Reanalysis (MSR) of total ozone, version 2. Dataset, ***Royal Netherlands Meteorological Institute (KNMI)***, doi:10.21944/temis-ozone-msr2, 2015.

von der Gathen, P., R. Kivi, I. Wohltmann, R.J. Salawitch, and M. Rex, Climate change favours large seasonal loss of Arctic ozone, ***Nat. Commun., 12*** (1)**,** 3886, doi:10.1038/s41467-021-24089-6, 2021.

Wallace, J.M., I.M. Held, D.W.J. Thompson, K.E. Trenberth, and J.E. Walsh, Global warming and winter weather, ***Science***, ***343*** (6172), 729–730, doi:10.1126/science.343.6172.729, 2014.

Wang, S., D. Kinnison, S.A. Montzka, E.C. Apel, R.S. Hornbrook, A.J. Hills, D.R. Blake, B. Barletta, S. Meinardi, C. Sweeney, F. Moore, M. Long, A. Saiz-Lopez, R.P. Fernandez, S. Tilmes, L.K. Emmons, and J.-F. Lamarque, Ocean biogeochemistry control on the marine emissions of brominated very short-lived ozone-depleting

substances: a machine-learning approach, ***J. Geophys. Res. Atmos.***, ***124*** (22), 12319–12339, doi:10.1029/2019JD031288, 2019.

Wang, S.-Y., L. Hipps, R.R. Gillies, and J.-H. Yoon, Probable causes of the abnormal ridge accompanying the 2013–2014 California drought: ENSO precursor and anthropogenic warming footprint, ***Geophys. Res. Lett.***, ***41***, 3220–3226, doi:10.1002/2014GL059748, 2014.

Wargan, K., G. Labow, S. Frith, S. Pawson, N. Livesey, and G. Partyka, Evaluation of the ozone fields in NASA's MERRA-2 reanalysis, ***J. Clim.***, ***30*** (8), 2961–2988, doi:10.1175/JCLI-D-16-0699.1, 2017.

Wargan, K., B. Weir, G.L. Manney, S.E. Cohn, and N.J., Livesey, The anomalous 2019 Antarctic ozone hole in the GEOS Constituent Data Assimilation System with MLS observations, ***J. Geophys. Res. Atmos., 125*** (18), e2020JD033335, doi:10.1029/2020JD033335, 2020.

Waugh, D.W., A.H. Sobel, and L.M. Polvani, What is the polar vortex and how does it influence weather?, ***Bull. Am. Meteor. Soc.***, ***98*** (1), 37–44, doi:10.1175/BAMS-D-15-00212.1, 2017.

Weber, M., S. Dikty, J.P Burrows, H. Garny, M. Dameris, A. Kubin, J. Abalichin, and U. Langematz, The Brewer-Dobson circulation and total ozone from seasonal to decadal time scales, ***Atmos. Chem. Phys.***, ***11***, 11221–11235, doi:10.5194/acp-11-11221-2011, 2011.

Weber, M., M. Coldewey-Egbers, V.E. Fioletov, S.M. Frith, J.D. Wild, J.P. Burrows, C.S. Long, and D. Loyola, Total ozone trends from 1979 to 2016 derived from five merged observational datasets – the emergence into ozone recovery, ***Atmos. Chem. Phys.***, ***18*** (3), 2097–2117, doi:10.5194/acp-18-2097-2018, 2018.

Weber, M., C. Arosio, W. Feng, S.S. Dhomse, M.P. Chipperfield, A. Meier, J.P. Burrows, K.-U. Eichmann, A. Richter, and A. Rozanov, The unusual stratospheric Arctic winter 2019/20: Chemical ozone loss from satellite observations and TOMCAT chemical transport model, ***J. Geophys. Res. Atmos.***, ***126*** (6), e2020JD034386, doi:10.1029/2020JD034386, 2021.

Weber, M., C. Arosio, M. Coldewey-Egbers, V. Fioletov, S.M. Frith, J.D. Wild, K. Tourpali, J.P. Burrows, and D. Loyola, Global total ozone recovery trends attributed to ODS changes derived from five merged ozone datasets, ***Atmos. Chem. Phys.***, ***22*** (10), 6843–6859, doi:10.5194/acp-22-6843-2022, 2022.

Westbrook, C.D., The fall speeds of sub-100 µm ice crystals, ***Q. J. Roy. Meteor. Soc.***, ***134***, 1243–1251, doi:10.1002/qj.290, 2008.

Wilka, C., S. Solomon, D. Kinnison, and D. Tarasick, An Arctic ozone hole in 2020 if not for the Montreal Protocol, ***Atmos. Chem. Phys., 21,*** 15771–15781, doi:10.5194/acp-21-15771, 2021.

Winterstein, F., F. Tanalski, P. Jockel, M. Dameris, and M. Ponater, Implication of strongly increased atmospheric methane concentrations for chemistry-climate connections, ***Atmos. Chem. Phys.***, ***19***, 7151–7163, doi:10.5194/acp-19-7151-2019, 2019.

WMO (World Meteorological Organization), ***Scientific Assessment of Ozone Depletion: 2006***, Global Ozone Research and Monitoring Project–Report No. 50, 572 pp., Geneva, Switzerland, 2007.

WMO (World Meteorological Organization), ***Scientific Assessment of Ozone Depletion: 2010***, Global Ozone Research and Monitoring Project–Report No. 52, 516 pp., Geneva, Switzerland, 2010.

WMO (World Meteorological Organization), ***Scientific Assessment of Ozone Depletion: 2014***, Global Ozone Research and Monitoring Project–Report No. 55, 416 pp., Geneva, Switzerland, 2014.

WMO (World Meteorological Organization***), Scientific Assessment of Ozone Depletion: 2018***, Global Ozone Research and Monitoring Project–Report No. 58, 588 pp., Geneva, Switzerland, 2018.

WMO (World Meteorological Organization), ***Report on Unexpected Emissions of CFC-11***, Ozone Research and Monitoring, A Report of the Scientific Assessment Panel of the Montreal Protocol on Substance that Deplete the Ozone Layer–No. 1268, Geneva, Switzerland, 2021.

Wohltmann, I., P. von der Gathen, R. Lehmann, M. Maturilli, H. Deckelmann, G.L. Manney, J. Davis, D. Tarasick, N. Jepsen, R. Kivi, N. Lyall, and M. Rex, Near complete local reduction of Arctic stratospheric ozone by severe chemical loss in spring 2020, ***Geophys. Res. Lett.***, ***47***, e2020GL089547, doi:10.1029/2020GL089547, 2020.

Wohltmann, I., P. von der Gathen, R. Lehmann, H. Deckelmann, G.L. Manney, J. Davies, D. Tarasick, N. Jepsen, R. Kivi, N. Lyall, and M. Rex, Chemical evolution of the exceptional Arctic stratospheric winter 2019/2020 compared to previous Arctic and Antarctic winters, ***J. Geophys. Res. Atmos.***, ***126*** (18), e2020JD034356, doi:10.1029/2020JD034356, 2021.

Woiwode, W., M. Höpfner, L. Bi, F. Khosrawi, and M.L. Santee, Vortex-wide detection of large aspherical NAT particles in the Arctic winter 2011/12 stratosphere, ***Geophys. Res. Lett.***, ***46***, 13420–13429, doi:10.1029/2019GL084145, 2019.

Wright, C.J., R.J. Hall, T.P. Banyard, N.P. Hindley, I. Krisch, D.M. Mitchell, and W.J.M. Seviour, Dynamical and surface impacts of the January 2021 sudden stratospheric warming in novel Aeolus wind observations, MLS and ERA5, ***Weather Clim. Dynam., 2,*** 1283–1301, doi:10.5194/wcd-2-1283-2021, 2021.

Xia, Y., W. Xu, Y. Hu, and F. Xi, Southern-Hemisphere high-latitude stratospheric warming revisit, ***Clim. Dyn., 54,*** 1671–1682, doi:10.1007/s00382-019-05083-7, 2020.

Yamazaki, Y., V. Matthias, Y. Miyoshi, C. Stolle, T. Siddiqui, G. Kervalishvili, J. Laštovička, M. Kozubek, W. Ward, D.R. Themens, S. Kristoffersen, and P. Alken, September 2019 Antarctic sudden stratospheric warming: Quasi-6-day wave burst and ionospheric effects, ***Geophys. Res. Lett.***, ***47*** (1), e2019GL086577, doi:10.1029/2019GL086577, 2020.

Yanes, J., Hypersonic: The future of aviation, ***OpenMind BBVA***, [available at: https://www.bbvaopenmind.com/en/technology/future/hypersonic-the-future-of-aviation], 2020.

Yang, X., N.L. Abraham, A.T. Archibald, P. Braesicke, J. Keeble, P.J. Telford, N.J. Warwick, and J.A. Pyle, How sensitive is the recovery of stratospheric ozone to changes in concentrations of very shortlived bromocarbons?, ***Atmos. Chem. Phys.***, ***14***, 10,431–10,438, doi:10.5194/acp-14- 10431-2014, 2014.

Yook, S., D.W.J. Thompson, and S. Solomon, Climate impacts and potential drivers of the unprecedented Antarctic ozone holes of 2020 and 2021, ***Geophys. Res. Lett.***, ***49*** (10), e2022GL098064, doi:10.1029/2022GL098064, 2022.

Yu, B., and X. Zhang, A physical analysis of the severe 2013/2014 cold winter in North America, ***J. Geophys. Res. Atmos.***, ***120***, 10,149–10,165, doi:10.1002/2015JD023116, 2015.

Yu, P., S.M. Davis, O.B. Toon, R.W. Portmann, C.G. Bardeen, J.E. Barnes, H. Telg, C. Maloney, and K.H. Rosenlof, Persistent stratospheric warming due to 2019–2020 Australian wildfire smoke, ***Geophys. Res. Lett.***, ***48*** (7), e2021GL092609, doi:10.1029/2021GL092609, 2021.

Zafar, A.M., R. Müller, J.-U. Grooß, S. Robrecht, B. Vogel, and R. Lehmann, The relevance of reactions of the methyl peroxy radical ($CH_3O_2$) and methylhypochlorite ($CH_3OCl$) for Antarctic chlorine activation and ozone loss, ***Tellus B: Chem. Phys. Meteorol.***, ***70*** (1), 1–18, doi:10.1080/16000889.2018.1507391, 2018.

Zhang, P., Y. Wu, I.R. Simpson, K.L. Smith, X. Zhang, B. De, and P. Callaghan, A stratospheric pathway linking a colder Siberia to Barents–Kara sea ice loss, ***Sci. Adv., 4*** (7), doi:10.1126/sciadv.aat6025, 2018.

Zhang, J., D. Wuebbles, D. Kinnison, and S.L. Baughcum, Potential impacts of supersonic aircraft emissions on ozone and resulting forcing on climate: An update on historical analysis, ***J. Geophys. Res. Atmos.***, ***126*** (6), e2020JD034130, doi:10.1029/2020JD034130, 2021.

Ziska, F., B. Quack, I. Stemmler, S. Tegtmeier, and K. Krüger, Future emissions of marine halogenated very short-lived substances under climate change, ***J. Atmos. Chem.***, ***74*** (2), 245–260, doi:10.1007/s10874-016-9355-3, 2017.

Zhu, Y., O.B. Toon, D. Kinnison, V.L. Harvey, M.J. Mills, C.G. Bardeen, M. Pitts, N. Bègue, J.-B. Renard, G. Berthet, and F. Jégou, Stratospheric aerosols, polar stratospheric clouds, and polar ozone depletion after the Mount Calbuco eruption in 2015, ***J. Geophys. Res. Atmos.***, ***123*** (21), 12,308–12,331, doi:10.1029/2018JD028974, 2018.